UNIVERSITÀ DEGLI STUDI DI PADOVA

DIPARTIMENTO DI INGEGNERIA CIVILE EDILE ED AMBIENTALE

ICEA

Tesi di laurea magistrale

"Groundwater flow through the test dike constructed with dredged materials"

RELATORE: Ing. Giampaolo Cortellazzo

LAUREANDA: Irene Pasetto

Anno Accademico 2013-2014

Alla mia famiglia

Index

INDEX **1**

ABSTRACT **5**

SOMMARIO **7**

INTRODUCTION **11**

GDAŃSK 11

Climate *12*

The Vistula River *13*

FLOODS 15

LEVEE 17

DREDGED MATERIAL AND PROJECT DREDGDIKES **21**

TEST DIKE DESCRIPTION 24

Geometry *24*

Materials *26*

Tephra 28

Coal ashes 28

Core of the test dike *30*

Mechanical parameters: Mohr-Coulomb soil model *41*

STEADY-STATE ANALYSIS **45**

DIFFERENT SLOPES 54

DIFFERENT THICKNESS 55

DIFFERENT CONDUCTIVITY COEFFICIENT AT SATURATION 57

TOE-DRAIN 59

SLOPE STABILITY ANALYSIS **63**

METHODS OF SLICES 64

Ordinary method (1927) 64

Bishop simplified (1955) 65

Janbu's simplified method (1954, 1973) 66

Spencer method (1967,1973) 67

Morgenstern-Price method (1965) 67

General limit equilibrium method (GLE) (1981) 68
RESULTS 70
DIFFERENT SLOPES 73
DIFFERENT MATERIALS 74
DIFFERENT COHESION 75
DIFFERENT FRICTION ANGLE 76
TRANSIENT ANALYSIS 79
Volumetric Water Content (VWC) Function 80
Material property function: VWC function 83
Hydraulic conductivity 87
Material property function: Hydraulic Conductivity function 88
TRANSIENT SEEPAGE PROBLEM. FILL OF THE RESERVOIR 94
Initial conditions 95
Boundary conditions 95
Time steps 96
Results 96
Different speed of the reservoir filling 98
Different thickness of the tephra and sand layer 99
Different riverside layer 100
Insertion of a drain 101
Monitoring 102
TRANSIENT SEEPAGE PROBLEM. RAINFALL 106
DRAWDOWN 112
Slow drawdown 114
Rapid drawdown 127
Instantaneous drawdown analysis 134
TRANSIENT FLOW THROUGH THE DIKE: COMPARISON BETWEEN FEM SOFTWARE 138
FIELD TESTS 143
MEASUREMENTS 143
SEEPAGE EXPERIMENTS 145
FEM ANALYSIS 149
Groundwater analysis 149
Slope Stability 159
CONCLUSION 167

FIGURE INDEX **171**

TABLE INDEX **176**

REFERENCES **177**

Abstract

The Vistula is the Poland's largest River. It flows from the south to the north and has its mouth in the Baltic Sea. In coastal areas large amounts of sediments accrue, so, to maintain the mouth navigable, it is necessary to remove them from the bottom of the river. This operation is called "dredging".

Dredged materials consist of different fractions of mineral and organic components. They do not have common application, because their utilization is expensive: the not contaminated materials are re-used in agriculture, landscape construction and in the recultivation of landfills. The use of dredged materials in dike construction is a new possibility.

DredgDikes Project, realized within "South Baltic Cross-border Co-operation Program", deals with implementation of dredged materials in dike construction.

Part of the project, executed in Poland, focuses on checking the application of dredged material as a dike's core material.

In this thesis, a model of the test dike in Trzcińsko (Gdańsk) is developed, to simulate the behavior of a three-layer embankment, constructed with dredged material and coal ashes. Because of the lack of studies dealing with changes in parameters of dredged materials, due to fly ash addition, the creation of the model is connected with hydraulic analysis based on laboratory research.

The results of the analysis have been compared to field test executed on the test dike.

Sommario

L'esigenza di mantenere un franco adeguato per la navigazione, comporta la necessità di asportare i sedimenti depositati dalle correnti nei porti e allo sbocco dei fiumi. L'operazione di scavo per asportare terreno da fondo subacqueo, dragaggio, produce materiale di scarto che viene utilizzato per il recupero ambientale di aree agricole o per scopi edilizi.

Nella Polonia settentrionale, nella baia di Danzica, sfocia il fiume Vistola, il più grande della nazione. Questo fiume è navigabile e collega molte città importanti, quindi ha una rilevante importanza economica e commerciale. Le correnti marine tendono a depositare una grande quantità di materiale allo sbocco della Vistola, quindi, per garantire la navigabilità, sono necessarie periodiche operazioni di dragaggio.

Le Università di Rostock e Danzica hanno dato vita al Progetto DredgDike. In questo progetto viene studiata la possibilità di utilizzare il materiale dragato come materiale per la costruzione di dighe e argini.

Il progetto prevede che la sabbia prelevata dal letto della Vistola e mescolata con delle ceneri venga utilizzata nella costruzione di un argine sperimentale situato a Wiślinka/Trzcińsko a circa 20 km da Danzica. Per creare questa nuova miscela vengono impiegate le ceneri ottenute dalla combustione del carbone. Scopo della ricerca è valutare la loro efficacia nel sostituire l'argilla nella costruzione di rilevati fluviali. Infatti, oggigiorno si riscontra una crescente carenza di questo tipo di terreno e la sua estrazione, oltre ad essere costosa, causa pesanti effetti negativi sull'ambiente.

L'argine sperimentale costruito in Polonia presenta un nucleo costituito dal 70% di cenere e dal 30% di sabbia dragata (percentuali ottimali stabilite dopo diverse prove in laboratorio) e da uno strato esterno costituito da argilla verso il lato campagna e da una miscela di tephra e sabbia dragata verso il lato fiume. Lo strato esterno ha una più bassa permeabilità rispetto a quella del nucleo: il coefficiente di permeabilità saturo

dell'argilla e della miscela di sabbia e tephra ($k_s = 10^{-7}$ [m/s]) è minore di quello del nucleo di un ordine di grandezza ($k_s = 10^{-6}$ [m/s]).

Per stimare il comportamento idraulico e la stabilità del rilevato sono state condotte molteplici analisi agli elementi finiti.

La prima analisi riguarda la filtrazione in condizioni stazionarie, assumendo la soluzione indipendente dal tempo. Se il livello dell'acqua nel serbatoio si mantenesse costante per un tempo infinito, l'acqua uscirebbe dal paramento verso lato campagna ad un'altezza pari a 1,32 m. Visto l'elevata altezza della linea di saturazione si è valutata la possibilità che le pressioni sviluppatesi al piede nello strato di sabbia potessero scalzare il sovrastante strato di argilla, ma questo non avviene e la stabilità al piede è garantita.

Sono state compiute delle modifiche nella geometria del rilevato e nelle caratteristiche dei materiali utilizzati atte a tentare di abbassare il livello di fuoriuscita dell'acqua, ma si ottengono risultati significativi solo se si ipotizza di utilizzare materiali più impermeabili a formare il nucleo o lo strato esterno verso fiume. In questo caso si riesce ad ottenere un abbassamento dell'altezza piezometrica di oltre un metro.

Per evitare che il flusso d'acqua giunga a toccare il paramento esterno, si può valutare l'ipotesi di inserire un dreno al piede verso lato campagna.

È stata successivamente verificata la stabilità dell'argine (ancora in condizioni stazionarie), ed è stata poi eseguita un'analisi di sensibilità per valutare quale parametro (e la sua variazione) la influenzasse maggiormente. La variazione dell'angolo di attrito comporta una variazione del fattore di sicurezza, ma le differenze maggiori si riscontrano nel caso in cui si faccia variare il valore della coesione, che risulta quindi essere la proprietà più influente nella verifica di stabilità. Quest'ultimo punto giustifica l'utilizzo della grande quantità di tephra nella miscela costituente il nucleo del rilevato.

Conclusa l'analisi stazionaria, si è effettuata quella non stazionaria. Si sono anzitutto determinate le curve di suzione e di permeabilità di tutti i materiali, e si è poi passati all'analisi vera e propria, che considera il riempimento del serbatoio e il suo svuotamento.

Nel primo caso si è osservato che, se il livello dell'acqua nel serbatoio impiegasse 24 ore a riempirsi, la linea di saturazione nel rilevato impiegherebbe 14 giorni a raggiungere il paramento esterno. Poiché ad un rilevato arginale è richiesto di evitare la fuoriuscita dell'acqua per tutto il periodo di piena, e questo è stimato corrispondente a circa 14 giorni, si può affermare che l'argine sperimentale così ottenuto soddisfa i requisiti richiesti.

Si sono poi valutati gli effetti conseguenti all'introduzione di un dreno, alla modifica di alcuni parametri geometrici (quali lo spessore dello strato verso fiume) e al riempimento del serbatoio in modo più o meno veloce di quello considerato. Si è successivamente ipotizzato un piano di monitoraggio del livello del serbatoio (sia in fase di riempimento, che in fase di svuotamento) per valutare quando si potrebbe avere fuoriuscita d'acqua in diverse condizioni.

Infine è stata inserita nell'analisi l'infiltrazione dell'acqua piovana e si è osservato che in questo caso la falda impiega meno tempo a raggiungere il paramento esterno dell'argine. La presenza di terreno saturo o con elevati contenuti d'acqua nel rilevato comporta cioè un aumento di permeabilità.

Lo svuotamento del serbatoio è stato analizzato nel caso di svuotamento lento e svaso rapido, e per entrambi è stata poi valutata la stabilità del paramento lato fiume.

Nel primo caso il livello piezometrico nel rilevato verso fiume è considerato coincidente con il livello dell'acqua nel serbatoio. In questo caso si perde l'effetto stabilizzante dell'acqua sul terreno, quindi il coefficiente di sicurezza diminuisce, ma in modo graduale poiché non si creano pressioni eccessive nel rilevato.

Nel caso di svaso rapido il coefficiente diminuisce bruscamente perché si creano delle pressioni eccessive dovute al fatto che l'acqua nel serbatoio diminuisce in poco tempo e l'acqua nei pori non riesce a drenare velocemente a causa dello strato di copertura di bassa permeabilità. Nonostante la brusca diminuzione del coefficiente di sicurezza, la stabilità del rilevato è assicurata anche in questa fase.

Si sono poi confrontati i risultati delle analisi con i dati piezometrici raccolti durante una campagna di indagine.

I risultati dell'analisi di filtrazione sono risultati del tutto dissimili dai dati misurati. Questo può essere dovuto a molteplici fattori, quali ad esempio il fatto che la permeabilità valutata mediante prove in laboratorio può essere diversa da quella effettiva, oppure dal fatto che condizioni metereologiche potrebbero aver comportato l'alterazione di alcune caratteristiche dei materiali, oppure, ancora, da discrepanze tra caso reale e modellazione tramite elementi finiti.

Introduction

Nowadays, there is an increasing shortage of clay, which is usually used as a dike's core material. The extraction of clay from natural deposit causes negative effects on the environment, and is also very expensive. Considering both economic and ecological reasons the DredgDikes project aims to replace these materials with dredged materials.

Dredged materials are obtained from dredging works on rivers and harbors. They do not have common application, because their utilization is expensive.

DredgDikes Project, realized within "South Baltic Cross-border Co-operation Program", deals with implementation of dredged materials in dike construction.

The aim of this master thesis is to study the full scale test dike constructed in Gdańsk. The dike's core was built using a mixture of dredged materials and fly ash, so a model of the dike was created to check the application of dredged material as a dike's core material.

The results of the analysis have been compared to field tests executed on the embankment, in order to check if the application of dredged materials meets the requirements of dike structures.

There have not been many studies dealing with changes in parameters of dredged materials, due to fly ash addition, so the creation of model is connected with advanced hydraulic analysis based on external laboratory research.

Gdańsk

Gdańsk is a Polish city on the Baltic coast, the capital of the Pomeranian Voivodeship, Poland's principal seaport, the largest city of Kashubia, and the center of the country's fourth-largest metropolitan area.

The city lies on the southern edge of Gdańsk Bay(of the Baltic Sea), and, together with the city of Gdynia, Sopot, and suburban communities, forms a metropolitan area called the *Trójmiasto*, with a population near 1.400.000.

Climate

Gdańsk enjoys a temperate climate, with cold, cloudy, moderate winters and mild summers with frequent showers and thunderstorms. Average temperatures range from −1.0 to 17.2°C, but in winter they can drop as low as -15°C and in summer they can reach as high as 30-35°C. Rainfall varies from 31.0 mm/month to 84.0 mm/month. Total annual precipitation averages 499 mm. In general it is a maritime climate and therefore damp, variable and mild.

Table 1: Environmental average parameters in Gdansk

Gdansk	Season				Year
	Winter	Spring	Summer	Autumn	
Average max temperature	2,1	10,4	20,4	11,6	11,2
Average min	-2,7	3,2	12,5	5,7	4,7
Average	76,2	100,8	186,0	144,3	507,3
Number of wet days	44	36	38	44	162

Figure 1 shows a diagram of climatic parameters, such as precipitation, temperatures (max, min and average), wind speed, humidity, sunlight hours and days.

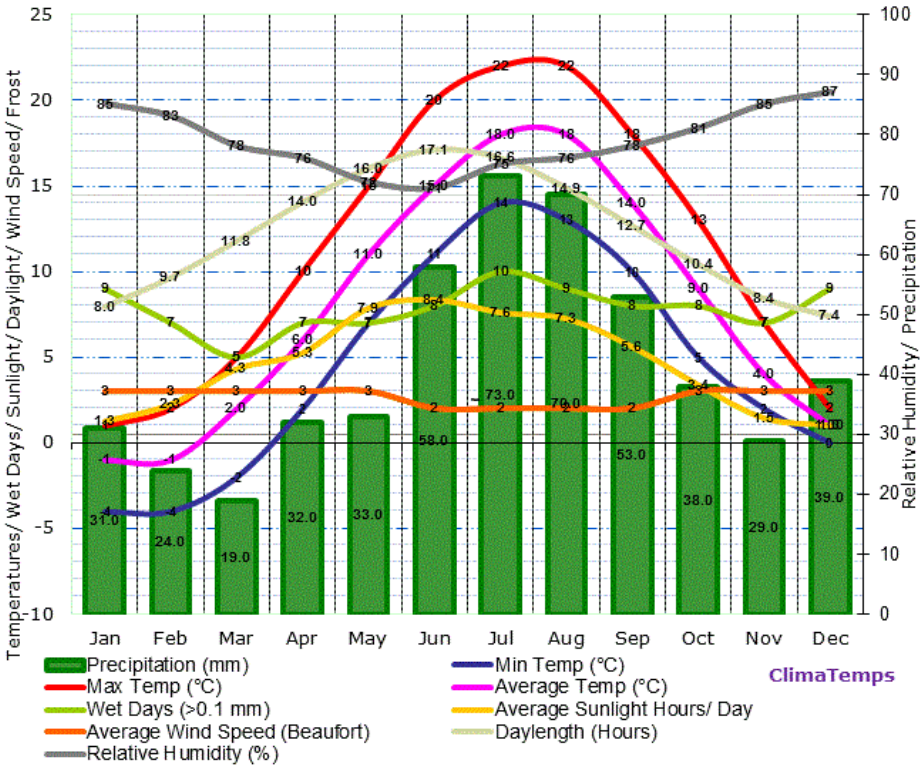

Figure 1: Gdansk, Poland climate graph (altitude 12m)

The Vistula River

Gdańsk is situated at the mouth of the MotławaRiver, connected to the Leniwka, a branch in the delta of the nearby Vistula River (*Wojciech Majewski*, 2013). The Vistula is the largest Polish river. Its sources are in the mountains in the south of Poland and it discharges in the north to the Baltic Sea (Bay of Gdańsk).

The Vistula river basin measures 194 000 km^2 from which 87% (169 000 km^2) is within Polish boundaries. The catchment of the Vistula occupies 54% of Polish territory and encloses important cities and industrial centers. The total length of the Vistula is 1047 km from its sources in the mountains to its outlet to the sea.

Hydrographically the Vistula is divided into three distinctly different river sections and river basins. These are: the Upper Vistula, the Middle Vistula and the Lower Vistula. The division of the Vistula basin into three subcatchments is presented in Figure 2.

Figure 2: Division of Vistula basin into 3 subcatchments (source IMGW-PIB)

The Upper Vistula encompasses the section from the source to the right hand San tributary. The length of this section is 399 km and the catchment mounts to 45.900 km^2 and makes up about 30% of Polish water resources.

The Middle Vistula encompasses river section from the San tributary to the Narew tributary. The length of this section is 256 km and its catchment (within Polish boundaries)amounts to 88.800 km^2.

The Lower Vistula constitutes the 391 km long river section from the confluence of the Narew to its mouth in Gdańsk Bay. The catchment of the Lower Vistula amounts to 34.300 km^2. It is presented in Figure 3.

Figure 3: The catchment of the Lower Vistula

The Vistula supplies about 7% of fresh water to the Baltic Sea. The discharge of the Vistula into the sea is now through an artificially formed (in 1895) direct channel (Przekop in Polish), because the previous layout of the final Vistula section resulted in frequent and numerous winter floods, such as the ones resulted in 1829 in the city of Gdańsk where inundation reached the second floor of buildings, causing significant economic and social losses.

The Lower Vistula has always presented a considerable flood hazard. This has mainly been due to the formation of ice jams, formed either of ice floes or large amounts of frazil ice. These floods have occurred either at the beginning of winter or at the beginning of spring during ice break-up and ice-run.

Floods

The European Union (EU) Floods Directive defines a flood as "a covering by water of land not normally covered by water".

Heavy rain can cause flooding when the rate of rainfall exceeds the drainage capacity of the area, or if water falls on an impermeable surface, such as concrete or frozen ground, and cannot rapidly dissipate into the ground.

Flat or low-lying areas can be inundated when the ground is saturated and water cannot run off quickly enough to stop accumulating. In this case, water can move away from the plain and cover the lands nearby. If homes and businesses are in the natural flood plains of rivers, damages will occur.

The flood can also occurs in estuarine and coastal areas. Flooding in estuaries is mostly caused by a combination of sea tidal surges caused by winds and low barometric pressure. Coastal areas may be inundated by storm events at sea, resulting in waves over-topping defenses.

Figure 4 shows a table with the principal natural causes of floods.

	Factors leading to causes of flood	
Causes	**Natural factors**	**Man-made factors**
Silting of the river bed	Due to bank erosion Earthquake loosening the soil	Due to dams, embankments and bunds
Inadequate capacity within the banks	High runoff or rise in the water level Silting of river bed due to bank erosion	High discharge from the river due to silting Decrease in bank height – deforestation
River bank erosion	High discharge of water due to rain Shifting river courses	Decrease in vegetative cover due to deforestation
Flow obstruction and change in river course	Landslides Falling of the trees	Construction activities in the river bed
Common floods in the main and tributary rivers	Flash flood due to high discharge in the main river	Breaking of bunds constructed on the tributary rivers for irrigation purposes
Poor natural drainage	Obstruction of the natural drainage Absorbing capacity of the soil	High rate of urbanization – pressure on the drainage system
Cyclones	High precipitation Absorbing capacity of the soil	
Retardation of flow and back water effect	High runoff Topography and obstruction of the natural drainage	Inadequate drainage capacity and; Urbanization in the low lying areas
Heavy rainfall	Same as above	Decreasing vegetative cover High urbanization leads to high runoff

Figure 4: Natural causes of floods

Some floods develop slowly, while others can develop by localized heavy rain from a series of storms moving over the same area in just a few minutes (flash flooding). Floods can also be local, impacting a neighborhood or community, or very large, affecting entire river basins, destroying everything on its way. Catastrophic inundation is usually associated with major infrastructure failures such as the collapse of a levee.

Levee

A levee is an embankment raised to preserve the water filtration for the time of flood (typically about 14 days), to regulate water levels or to prevent a river from overflowing: the stability of the dike is endangered during fast changes in water level (as well as during dike's overflowing).

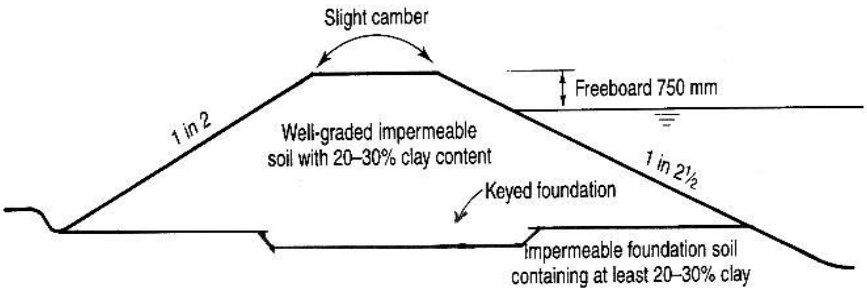

Figure 5: Typical embankment

The levee is commonly grass-covered, but may need additional protection against erosion by swiftly flowing water, waves or overtopping, so geogrids and geotextiles can be used to reinforce grass on flood embankments. Trees should not be planted on flood embankments as they accelerate drying out and cracking, and a breach of the bank may result if they are blown down in a storm.

If the foundation is highly permeable it may be necessary to take steps to cut off the seepage path through the foundation.

The width of the crest is normally from 2 m to 5 m. The embankment side slopes are between 1:2 (vertical to horizontal) and 1:3.

The levee can be constructed from a variety of earth materials. Wherever possible, locally won material should be used, to reduce costs and lessen the environmental impact. The required strength is achieved by constructing the embankment in layers and compacting each layer using mechanical plant appropriate to the type of soil.

Soils with high plastic clay content are best avoided because these crack when they dry out, and such cracks can extend into the bank. Cracks in embankments can create seepage paths, compromising its function as a flood defense.

Soils with a high sand or gravel content can be used, but may have to incorporate some form of cutoff to reduce seepage in flood conditions. Granular soils are less resistant to erosion than cohesive soils once the topsoil layer has been eroded.

There are different kind of flood embankments, as it is shown in Figure 5, and different materials can be used.

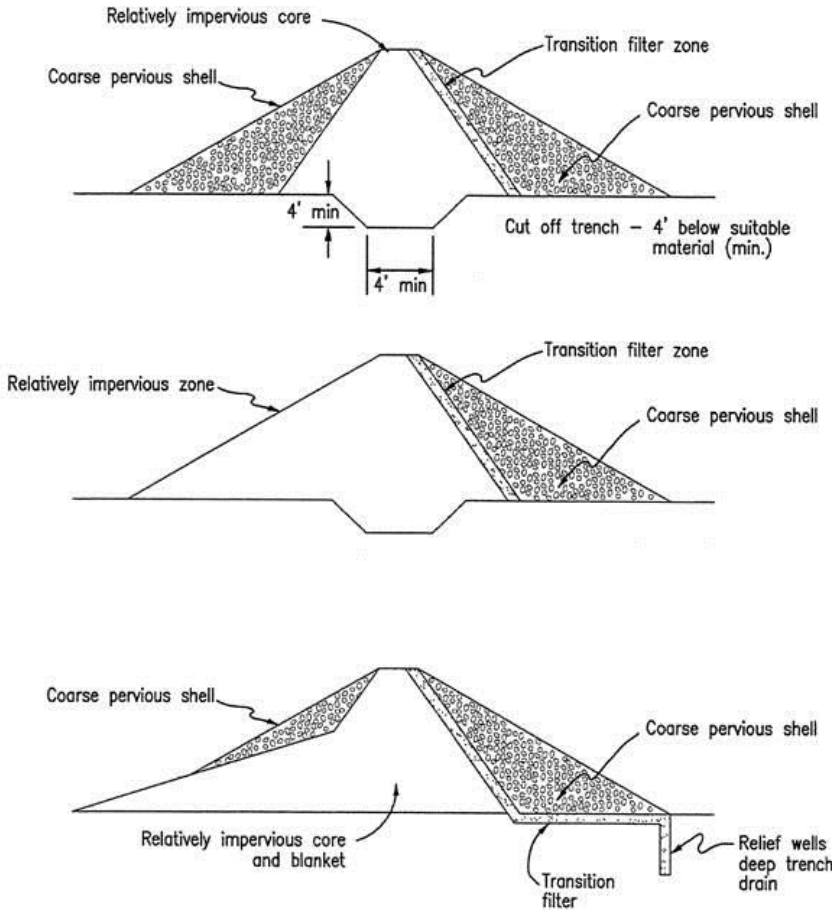

Figure 6: Different kinds of embankment

In Poland, in Pomerania, a region extremely endangered due to close vicinity to Vistula river and its outlet to the Baltic sea, a total length of 650 km of dikes protect over 140.000 ha of coast and lowland areas. Most of the embankment in this region requires immediate repair or reconstruction. In the next two decades, an investment of 160 million euro is planned for improving the protection against flooding, with the construction, improvement and reconstruction of dikes.

Dredged material and Project DredgDikes

Dredging is the removal of sediments from the bottom of lakes, rivers, harbors and other water bodies. Most dredging is done to maintain or deepen navigation channels, anchorages or berthing areas for the safe passage of boats and ships. Particularly in coastal areas large amounts of these dredged materials accrue. Sediments also often need to be removed due to construction works or in ecological revitalization projects. The dredged materials consist of different fractions of mineral and organic components.

The characteristics of dredged materials are widely different.

In the majority of dredging works the relocation of dredged materials is chosen. However, if the material characteristics do not allow relocation (e.g. due to a high content of fines) the dredged materials need to be removed from the water body.

Figure 7: Dredged material pumped onto a spoil field

A large portion of the uncontaminated materials is dredged directly into containment areas on shore (as shown in the figure below). These materials may be used as soil or construction material after sedimentation, dewatering and ripening.

Figure 8: Rostock deposition side

If the sediments contain contaminations that exceed the precaution values of soil and water protection jurisdiction so that the re-use is excepted, they may only be deposited.

The not contaminated materials are re-used in agriculture, landscape construction and in the recultivation of landfills. The use of dredged materials in dike construction is a new and promising possibility.

The project ***DredgDikes*** was initiated to investigate the application of dredged materials, geosynthetics and different ash-composites in dike construction.

Figure 9: DredgDikes Project logo

The international cooperation project is part-financed by the EU South Baltic Cross-border Co-operation Program 2007-2013.

Coordinated by the chair of *Geotechnics and Coastal Engineering at the University of Rostock*, Germany, it incorporates five eligible partners from Germany and Poland,

namely the *Technical University of Gdansk*, the water and soil association "*Untere Warnow – Küste*", the *Hanseatic City of Rostock* and the *Steinbeis Innovation gGmbH*, as well as 15 associated organizations from Poland, Lithuania, Germany and Latvia.

Besides the overall project coordination, the *University of Rostock* is responsible for the Rostock lab and field tests and the scientific evaluation of the pilot dike. That was built under the authority of the water and soil association „*Untere Warnow - Küste*". The *Civil Engineering and Harbor Construction Office of the Hanseatic City of Rostock* is responsible for the construction of the German test dike. The chair of *Geotechnics, Geology and Coastal Engineering at the Gdansk Polytechnica* is the main research partner and responsible for the Polish lab and field tests.

The *Department of Applied Landscape Planning (Steinbeis Innovation gGmbH)* is dealing with quality control, ecological and vegetation issues.

A high quantity of dredged materials was obtained by clearing the entrance to the port in Germany (mostly silts and clayey silts), and by clearing the outflow of Vistula river in Poland (sands): the DredgDike project born from the need to dispose of the overabundance of these materials.

In order to investigate the different dredged materials and material combinations, both in Rostock and Gdansk two full scale test dikes have been built.

In Gdansk, sand-ash composites are investigated with respect to their applicability in embankment construction. Sandy dredged material is improved with particular ashes, so it can be used as dike's cover material. Ash-sand mixtures can also be used to build stable dike's cores.

Figure 10: Test dike localization

Test dike description

Geometry

The three meters high test dike located in Wiślinka/Trzcińsko on the bank of Vistula River ca. 20 km away from the City of Gdańsk was completed in Summer 2012.

The 4-meter wide test segment of the 24-meter long dike has been separated by sheet pile walls to obtain 2D plane conditions for seepage and overtopping with a controlled water level.

Figure 11: Test dikes and sheet-pile wall

Both slopes have inclination of 1:2 and the dike is 3.0 m high with a 3.0 m wide crest.

The ground under the test dike was extensively explored with the use of CPTU penetrometer. Under a shallow sandy crust, some fine grained soft deposits interbedded by sandy layers are probed. Due to good drainage conditions the consolidation of the soft deposits under additional loading is quite fast and it occurs almost entirely during the earth works.

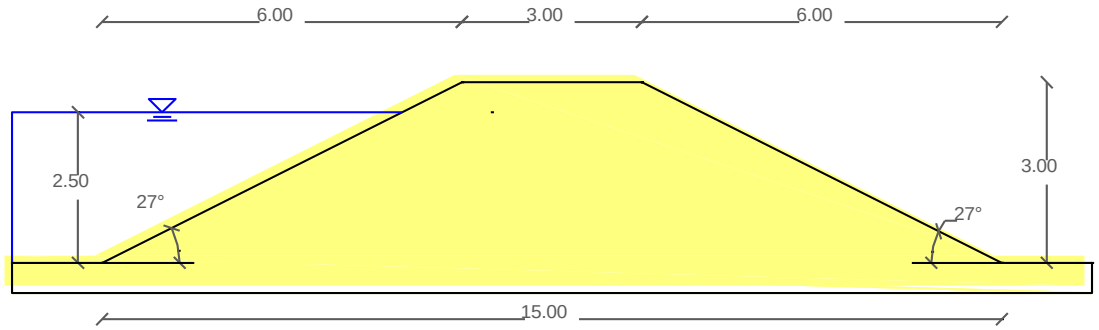

Figure 12: Geometry

To focus the attention on the seepage within the dike its bottom has been isolated from the permeable ground by 0,5 m thick impermeable liner. A high-water level of 2.5 m is planned to be maintained until the steady flow within the dike body is achieved. The greening was realized with rolled sod and now the sods need to connect by root penetration before overflowing experiments can be performed.

In the dike core 24 soil moisture probes have been installed to measure the seepage line. The dense sensor raster allows the comparison with numerical simulations. Four piezometers are used to verify the sensor data.

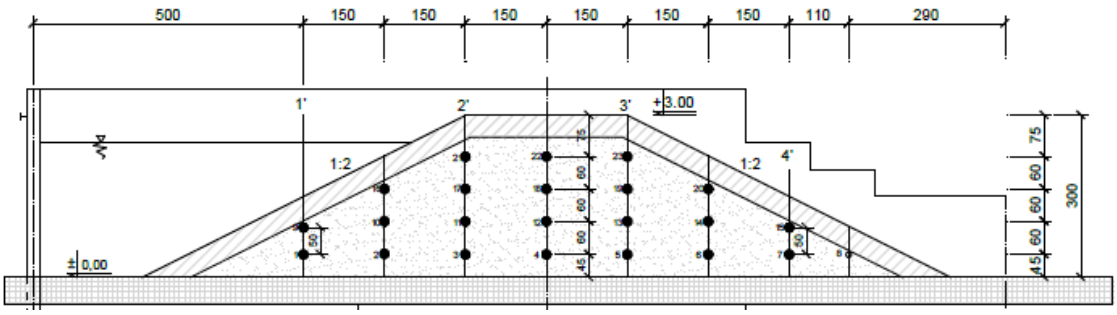

Figure 13: Positions of moisture probes and piezometers

Additionally, sampling and laboratory testing of the physical and mechanical parameters of the applied sand-ash mixture were carried out during the test.

Materials

The levee is composed from three different materials:

- the dike's core is made of a mixture of ash and sand;
- the top layer is divided in two material:
  - a mixture of Tephra, which is a special fluid ash mixture, and dredged sand in 50 cm layer thickness in upstream side;
  - clay in 30 cm layer thickness in the downstream side;

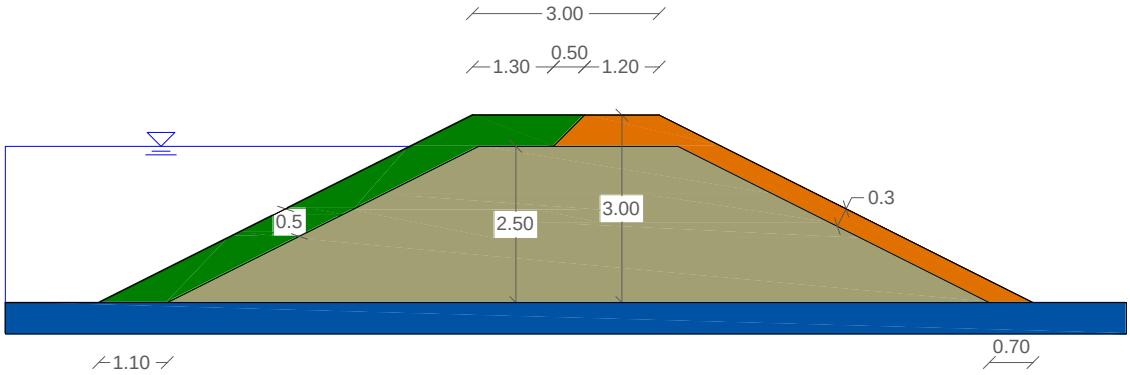

Figure 14: Geometry and thickness of materials

shows the geometry and the position of the different materials.

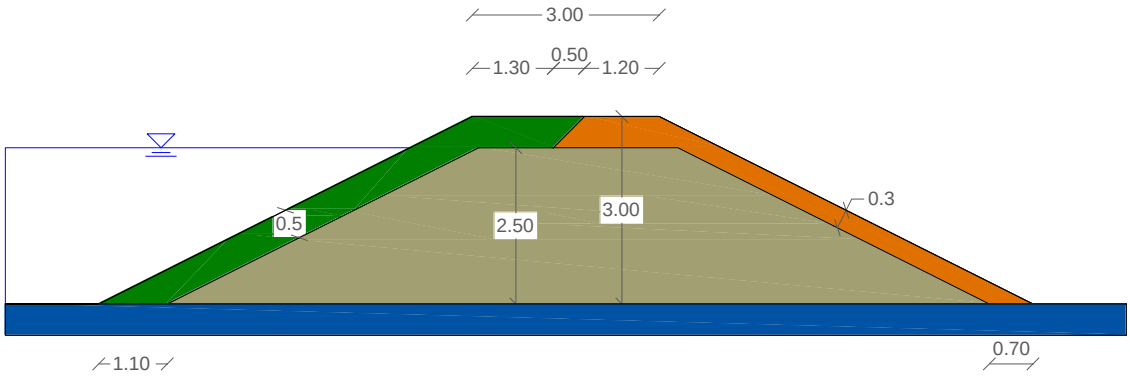

Figure 14: Geometry and thickness of materials

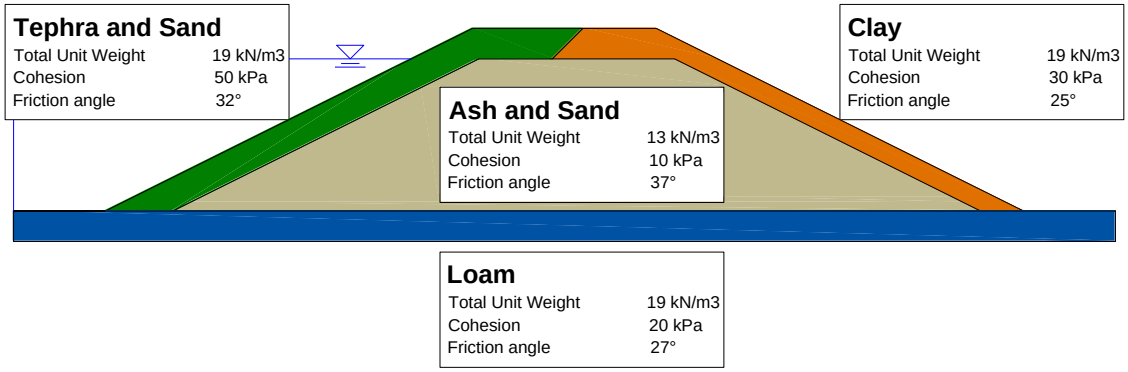

Figure 15: Materials

The bottom layer is made of hard compacted loam in order to provide cut-off layer for test conditions.

Tephra

Tephra is a collective term for fragments of volcanic rock and lava regardless of size that are blasted into the air by explosions or carried upward by hot gases in eruption columns or lava fountains. Tephra includes large dense blocks and bombs, and small light rock debris such as scoria, pumice, reticulite, and ash. Volcanic ash is a part of tephra and ranges in size between 6 and 4 mm. Cindar is a general term to define a partly vesiculated lava fragment ejected during an explosive eruption, equivalent to scoria; it typically consist of basaltic or andesitic composition. In geotechnical engineering, volcanic ash and Cindar are frequently used in construction: their principal uses are for secondary road surfaces, foundation materials, or protection of embankment slopes.

In this case, tephra (in form of ash) has been mixed with dredged sand and this mixture has been used on the surface layer.

Coal ashes

The core of the dike is made of mixture containing dredged materials and ashes.

Coal ashes are the by-products obtained from coal-fired thermal power plants, and are produced in large quantities all over the world (over 700 million tons a year): that calls for their utilization in bulk, without endangering the ecosystem. Geotechnical engineering practice provides such an opportunity for the bulk utilization of coal ashes, for the construction of embankments, mine filling, backfilling, road construction and foundation base materials.

Coal ashes can be of three types:

1. the very fine, very light noncombustible portion of the coal collected in the dry form through electrostatic precipitators and/or mechanical dust collectors is known as ***fly ash***;
2. the coarser, unburned granular material collected at the bottom of the boiler furnace is called ***bottom ash***.
3. If the thermal power plants have a wet disposal system, then the fly ash and the bottom ash are mixed with water to form a slurry, which is then pumped to nearby storage ponds known as ash ponds. The ash deposited in these ponds is known as ***pond ash***.

Coal ashes and fine-grained soils have essentially similar chemical composition (**Errore. L'origine riferimento non è stata trovata.**): fly ashes consist primarily of silt-size particles of uniform gradation; bottom ashes and pond ashes are predominantly sand-size particles, well graded or poorly graded.

Table 2: Chemical composition of coal ashes and soils

Compound	Fly ash: %	Sand ash: %	Bottom ash: %	Soil: %
SiO_2	38–65	37–75	23–73	43–61
Al_2O_3	16–44	11–54	13–27	12–39
TiO_2	0·4–1·8	0·2–1·4	0·2–1·8	0·2–2
Fe_2O_3	3–20	3–35	3–11	1–14
MnO	0–0·5	◆–0·6	◆–0·3	0–0·2
MgO	0·01–1·53	0·1–0·8	0·1–0·7	0·5–4
CaO	0·2–8	0·2–0·6	0·1–0·8	0–7
K_2O	0·04–0·9	0·1–0·7	◆–0·56	0·3–2
Na_2O	0·09–0·43	0·05–0·31	◆–0·3	0·2–3
LOI†	0·2–3·4	0·1–7·91	0·61–12·8	5–17

* Data from authors' files.
† Loss on ignition at 950°C.
◆: Trace.

From the viewpoint of bulk utilization in various geotechnical applications, the coal ashes have favorable properties:

- coal ashes are free-draining materials. Their permeability is in the same range as that of silts and sands.
- the compressibility of coal ashes is less than that of fine-grained soils.
- coal ashes exhibit very good frictional shear strength under almost all drainage conditions.
- coal ashes are relatively water-insensitive during compaction.

In addition to these advantageous properties, the ashes derived from lignite coal, bituminous and sub-bituminous coals have pozzolanic properties (i.e. lime reactivity), which soils do not possess. However, the lime reactivity of pond ashes and bottom ashes is relatively low compared with that of fly ashes. With the use of self-cementing and pozzolanic fly ashes in various geotechnical applications, the engineering properties of such systems will improve with time. Improvements achieved include, for example:

- decreased permeability with time,
- less pore pressure build-up on addition of load,
- reduced compressibility,
- increased shear strength.

Core of the test dike

Bottom ashes were used in the core of the test dike in Gdansk. Figure 16 shows the ashes grading curve from the particle size analysis.

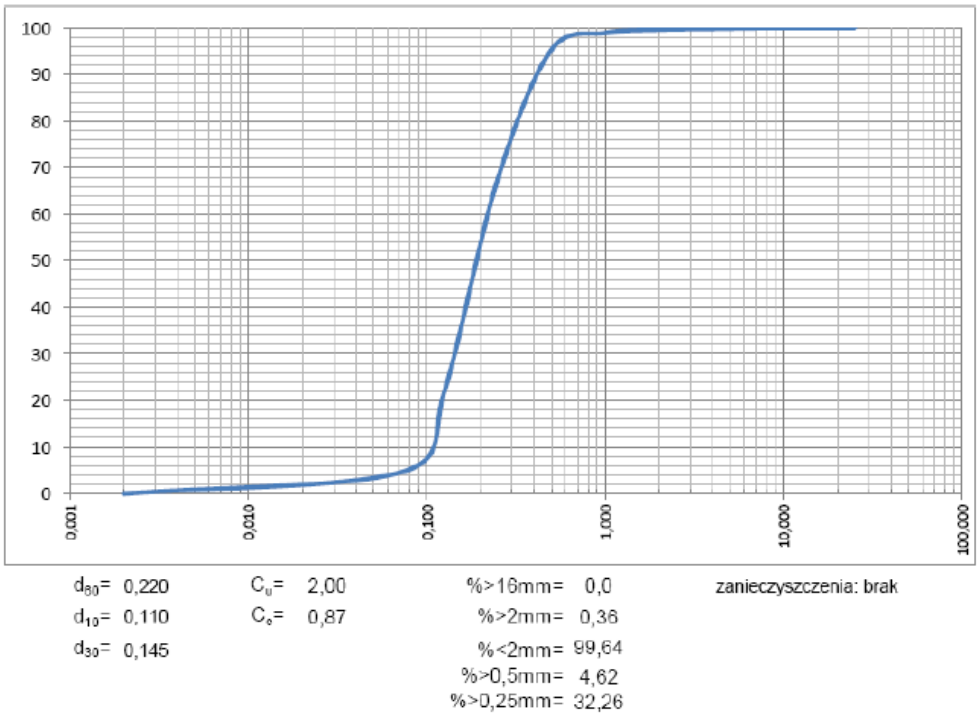

Figure 16: Grading curve of bottom ash

To classify the material, the "Geotechnical classification system for coal ashes" (*Prakash K. and Sridharan A.*, 2006), was utilized.

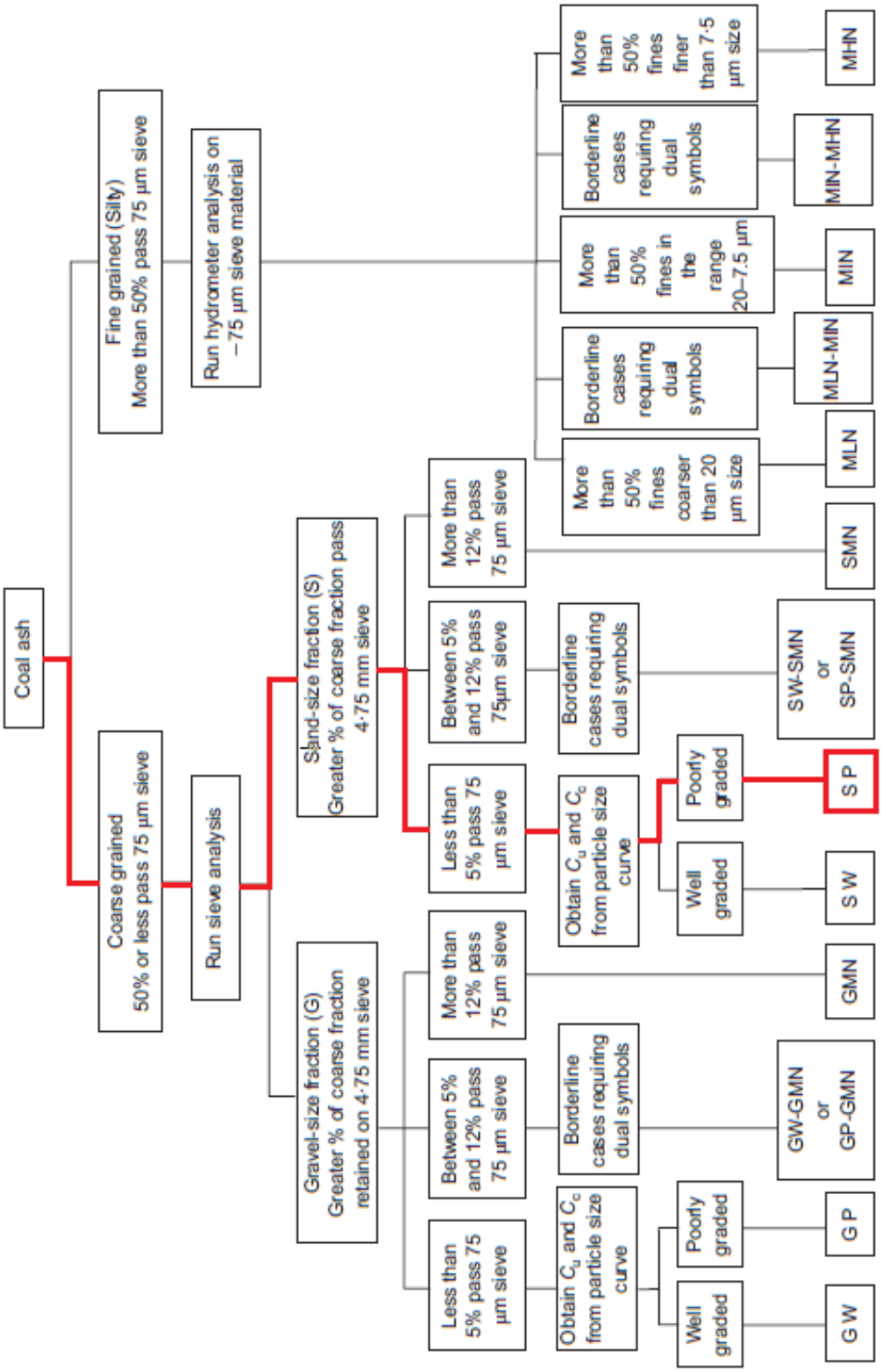

Figure 17: Flowchart for classifying coal ashes

Table 3: Coal ash classification system

Division		Subdivision		Group symbol	Typical description
Coarse-grained coal ashes (more than half of the material is larger than 0·075 mm sieve)	Gravel-size fraction (more than half of coarse fraction is larger than 4·75 mm sieve)	Clean gravel-size fraction (few or no fines)	Wide range in grain sizes and substantial amounts of all intermediate particle sizes	GW	Well-graded gravel-size fractions (gravel-size fraction–sand-size fraction) mixtures, few or no fines
			Predominantly of one size or of a range of sizes with some intermediate sizes missing	GP	Poorly graded gravel-size fractions (gravel-size fraction–sand-size fraction) mixtures, few or no fines
		Gravel-size fraction with appreciable amount of non-plastic fines	Non-plastic fines	GMN	Non-plastic silty gravel-size fractions, poorly graded mixture of (gravel–sand–silt) size fractions
	Sand-size fraction (more than half of coarse fraction is smaller than 4·75mm sieve)	Clean sand-size fraction (few or no fines)	Wide range in grain sizes and substantial amounts of all intermediate particle sizes	SW	Well-graded sand-size fractions, gravelly sand-size fractions, few or no fines
			Predominantly of one size or of a range of sizes with some intermediate sizes missing	SP	Poorly graded sand-size fractions, gravelly sand-size fractions, few or no fines
		Sand-size fraction with appreciable amount of non-plastic fines	Non-plastic fines	SMN	Non-plastic silt-size fractions, poorly graded mixture or (sand–silt) size fractions
Fine-grained coal ashes (more than half of material is smaller than 0·075 mm sieve)	Hydrometer analysis on fraction smaller than 75 μm size	More than 50% of fines is in particle size range 20 μm < particle size ⩽ 75 μm		MLN	Non-plastic inorganic coarse silt-size fractions
		More than 50% of fines is in particle size range 7·5 μm < particle size ⩽ 20 μm		MIN	Non-plastic inorganic medium silt-size fractions
		More than 50% of fines is in particle size range particle size ⩽ 7·5 μm		MHN	Non-plastic inorganic (fine silt + clay) size fractions

Table 4 shows the beneficial engineering properties of coal ashes, as described before.

Table 4: Beneficial engineering properties of coal ashes

Description of coal ash group	Group symbol	Engineering properties		
		Permeability when compacted*[14]	Shear strength when compacted and saturated†	Compressibility when compacted and saturated‡
Well-graded gravel-size fractions, (gravel-size fraction–sand-size fraction) mixtures, little or no fines	GW	High	Excellent	Negligible
Poorly graded gravel-size fractions, (gravel-size fraction–sand-size fraction) mixtures, little or no fines	GP	High	Very good	Negligible
Non-plastic silty gravel-size fractions, poorly graded mixture of (gravel–sand-silt) size fractions	GMN	Medium	Good	Negligible
Well-graded sand-size fractions, gravelly sand-size fractions, little or no fines	SW	High	Excellent	Negligible
Poorly graded sand-size fractions, gravelly sand-size fractions, few or no fines	SP	High	Good	Very low
Non-plastic silty sand-size fractions, poorly graded mixture of (sand-silt) size fractions	SMN	Medium	Good—fair	Low
Non-plastic inorganic coarse silt-size fractions	MLN	Low	Good—fair	Medium—low
Non-plastic inorganic medium silt-size fractions	MIN	Low	Fair	Medium—low
Non-plastic inorganic (fine silt + clay) size fractions	MHN	Low to very low	Fair	Medium—low

The bottom ash was mixed with the dredged material from the mouth of Vistula. The grading curve of the sand is shown in Figure 18.

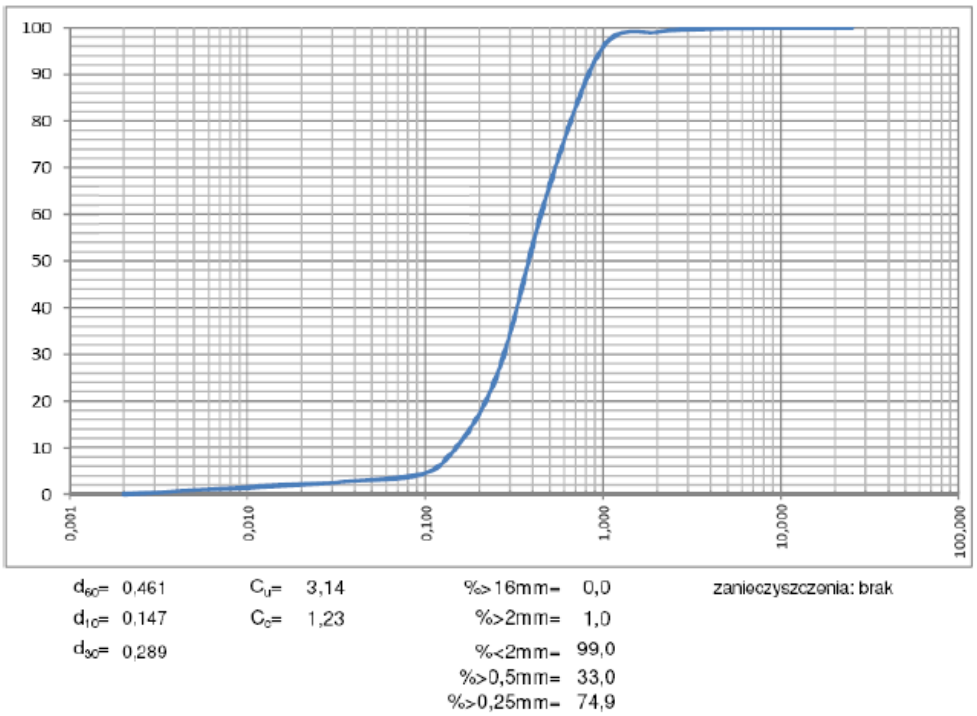

Figure 18: Grading curve of dredged material (sand)

The proportion of components in the test dike was chosen based on initial tests on the dredged materials: it was examined, how the properties of the mixture are influenced by the variation of the percentage of ash.

Bottom ash – dredged sand mixture								
Percentage	0/100	40/60	50/50	60/40	70/30	80/20	90/10	100/0

The graphs in Figure 19 and Figure 20 show as the maximum dry density decreases, and the optimum water content increases with ash content.

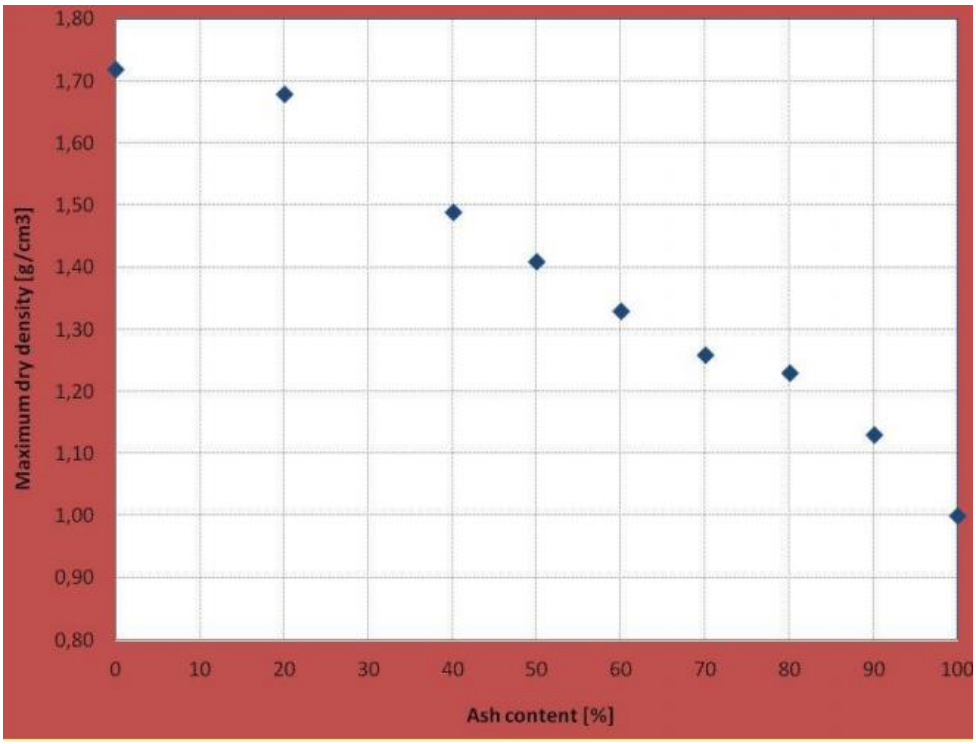

Figure 19: Proctor compaction test: maximum dry density

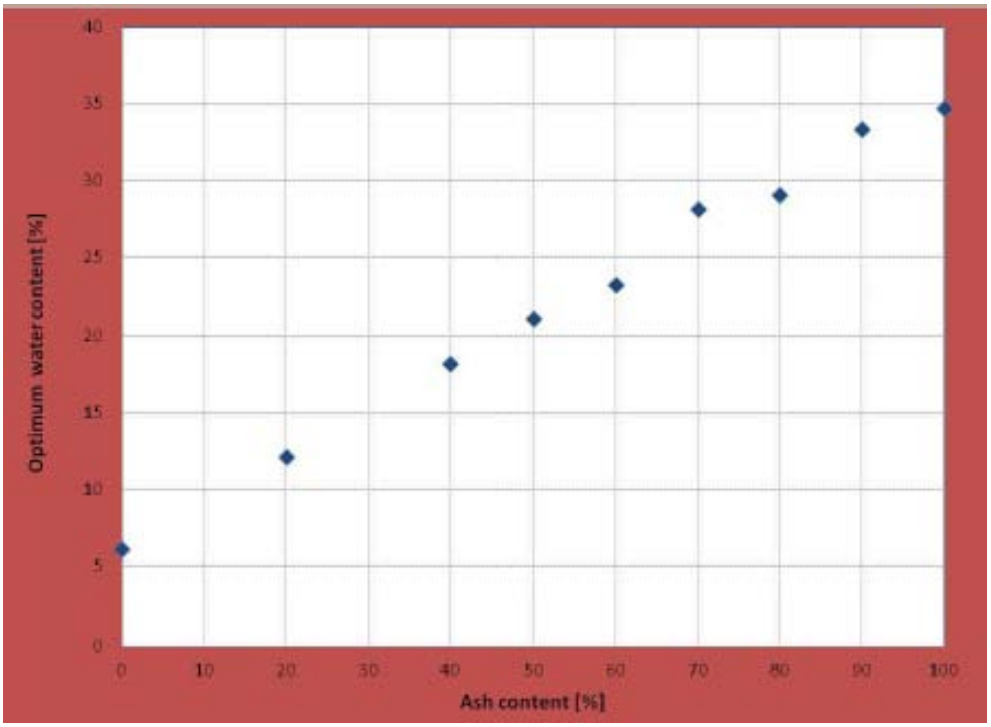

Figure 20: Proctor compaction test: optimum water content

The void ratio was obtained as result of the oedometric test. It grows with the increase of the ash percentage in the mixture.

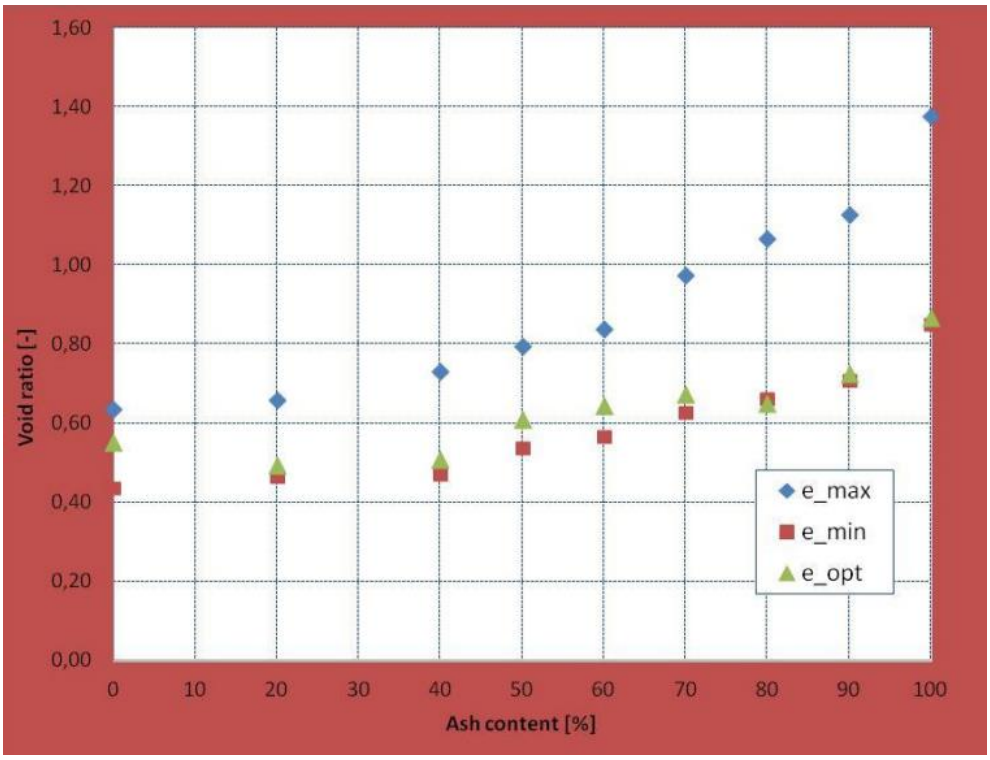

Figure 21: Oedometric test

The direct shear test allowed to determine the angle of internal friction and cohesion. The first one generally decrease with ash content; the cohesion found is small, especially for higher percentage of ash in the mixture.

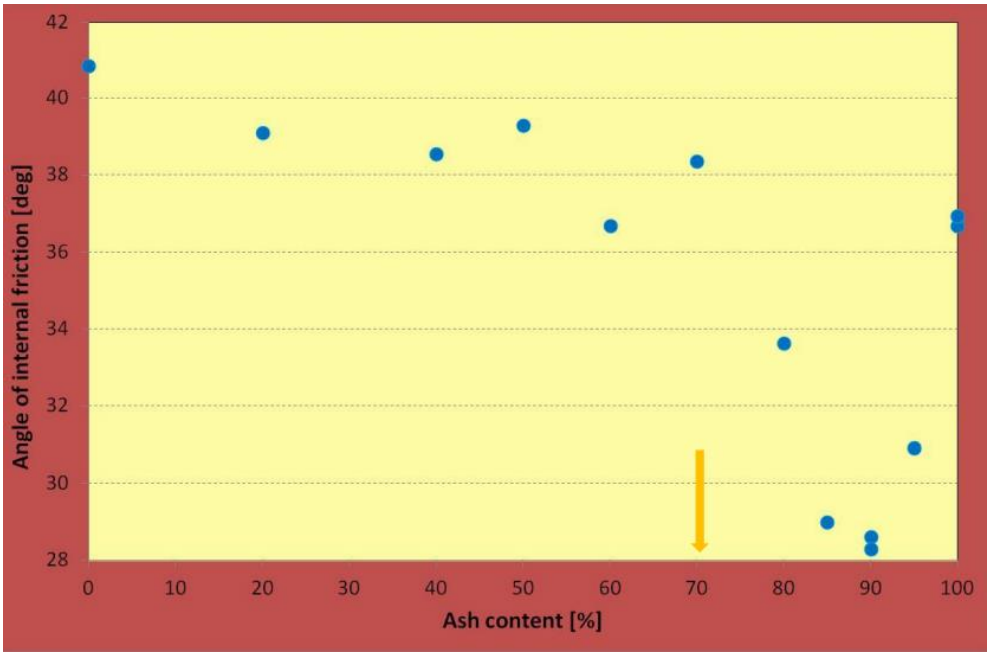

Figure 22: Direct shear test: angle of internal friction

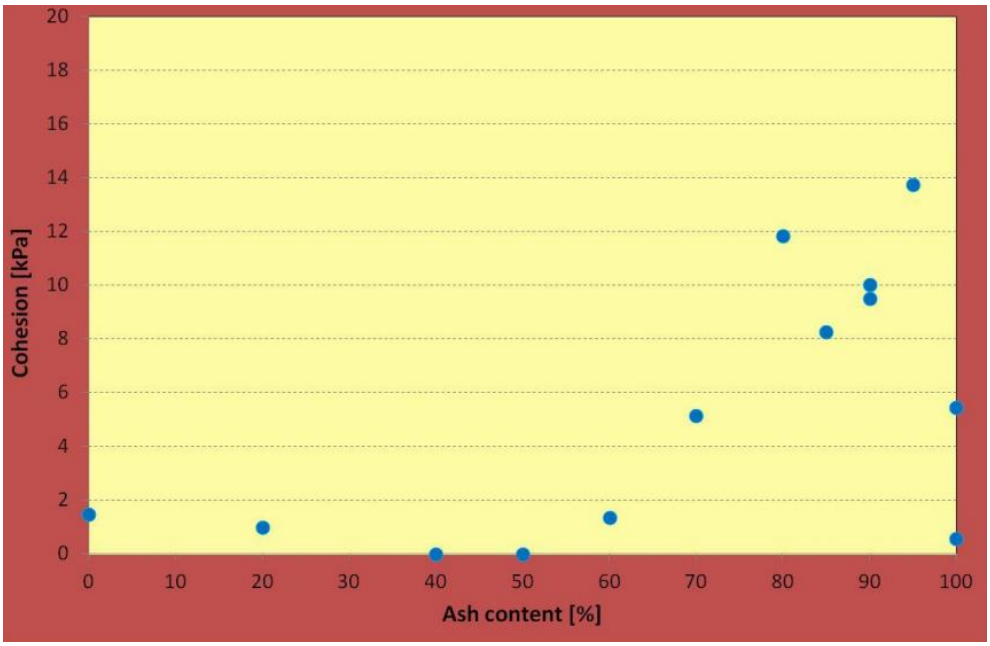

Figure 23: Direct shear test: cohesion

At the end of the tests, an optimum mixture 70/30 (ash/sand) has been chosen for test dike construction. The figures below show the direct shear test and the oedometric test for this mixture.

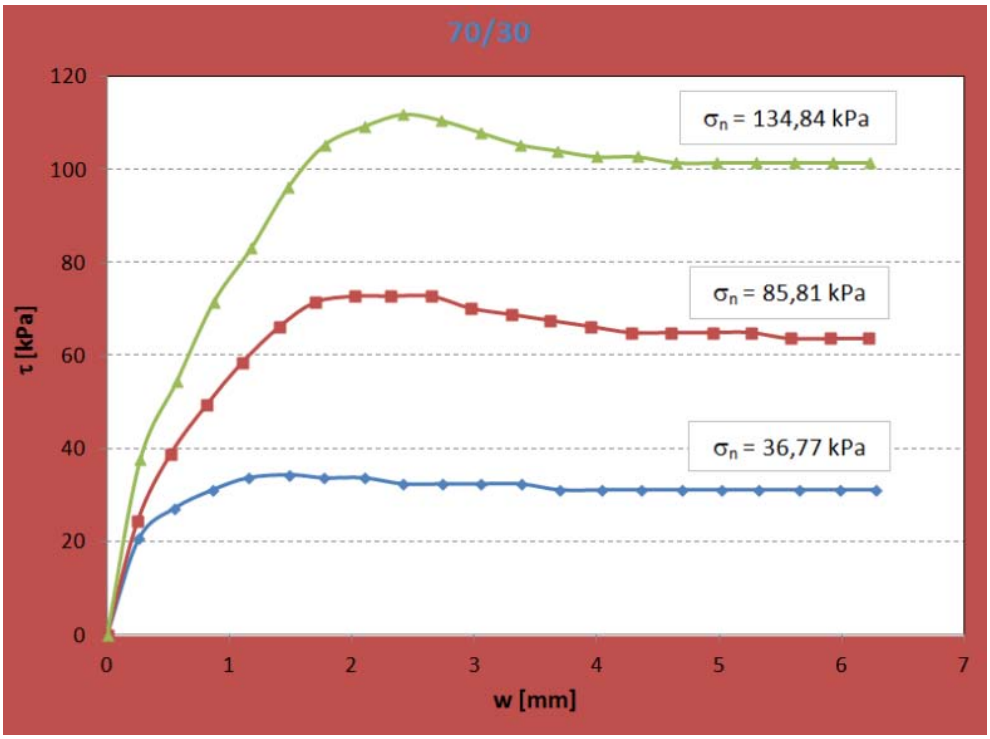

Figure 24: Shear test for 70/30 mixture

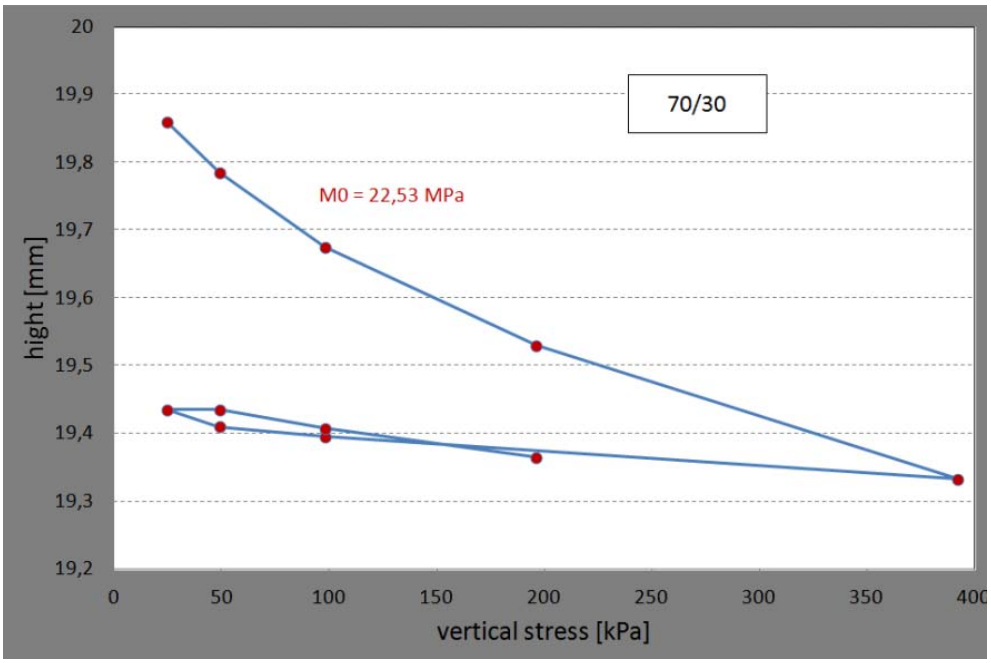

Figure 25: oedometric tests for 70/30 mixture

The mixture has a relatively high permeability coefficient ($k = 1 \times 10^{-6}\, m/s$), but it will probably decrease with time, because of the cementation due to pozzolanic properties of the coal ashes. As the permeability coefficient decreases, the strength of the mixture increases.

The properties of the materials are collected in the Table 5.

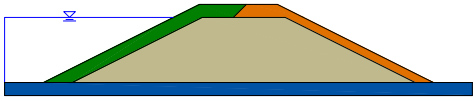

Table 5: Properties of the materials

Material	-	CLAY	TEPHRA - SAND	ASH - SAND	LOAM
Strength Type	-	Mohr-Coulomb	Mohr-Coulomb	Mohr-Coulomb	Mohr-Coulomb
Total Unit Weight	$\gamma \left[{kN}/{m^3}\right]$	19	19	13	19
Satured Unit Weight	$\gamma_{sat} \left[{kN}/{m^3}\right]$	21	20	16,3	20
Hydraulic Conductivity at saturation	$k_s [{m}/{s}]$	1 e -7	1 e -7	1 e -6	1 e -9
Void Ratio	$e[-]$	0,79	0,64	0,69	0,67
Porosity	$n[-]$	0,44	0,39	0,41	0,40
Cohesion	$c \left[{kN}/{m^2}\right]$	30	50	10	20
Phi	φ [°]	25	32	37	27
Phi B	ψ [°]	0	0	0	0
Young's Modulus	$E \left[{kN}/{m^2}\right]$	15 000	30 000	22 500	15 000
Poisson's Ratio	$\nu[-]$	0,35	0,30	0,25	0,35

Mechanical parameters: Mohr-Coulomb soil model

For every soil layers the Mohr-Coulomb failure criterion was assumed. The Mohr-Coulomb criterion is the most common way in modeling the soil shear strength, and can be used to analyze the stability of the dams and slopes. It is also applicable to evaluate if the shallow foundations are resistant or not.

The Mohr-Coulomb soil model describes a linear relationship between normal and shear stresses (or maximum and minimum principal stresses) at failure.

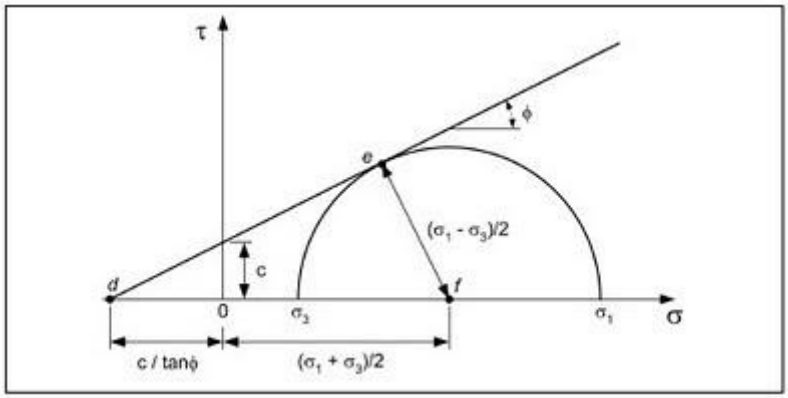

Figure 26: Mohr's circle of stress used to derive equations for Mohr-Coulomb diagram

The direct shear formulation of the criterion is given by the next equation:

$$\tau = c' + (\sigma - u)tan\varphi' = c' + \sigma' tan\varphi'$$

The parameters defining failure criteria are:

- effective frictional angle φ'
- effective cohesion c'

This model can also be used for total stress conditions: in this case water pressure is not considered $(u = 0)$ and the equations is transformed into:

$$\tau = c + \sigma_{tot} tan\varphi$$

Concerning the embankment analyzed, the Mohr-Coulomb strength function for Sand-Ash mix of the dike's core is shown in the figure below.

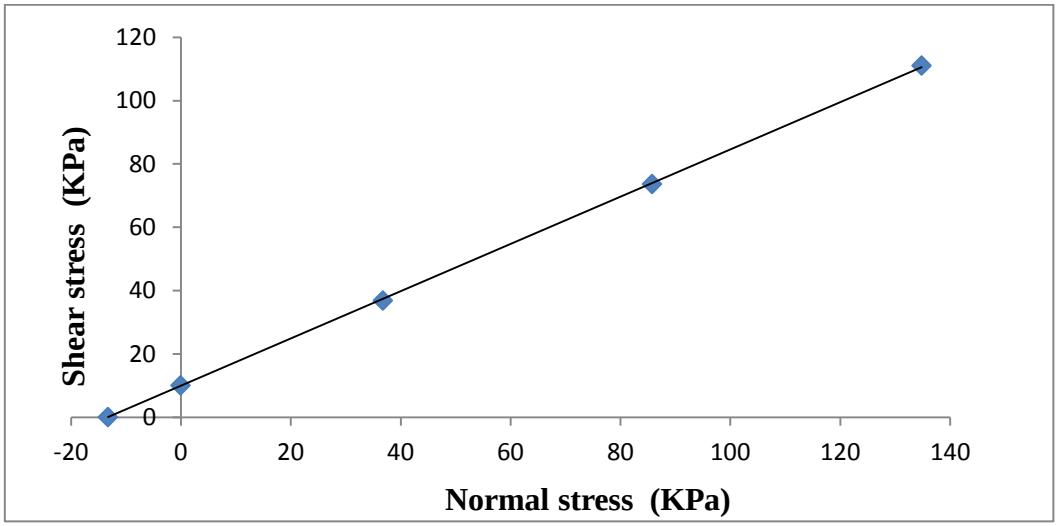

Figure 27: Mohr-Coulomb strength function for Ash -Sand mix

Steady-State Analysis

A system in a steady state has numerous properties that are unchanging in time: the recently observed behavior of the system will continue into the future.

The test dike in this study was modeled in two-dimensional space using *Slide*® software version 5.0. Within this program, *Slide*® has the capability to carry out a finite element based groundwater seepage analysis for saturated/unsaturated, steady-state flow conditions.

Finite element numerical methods are based on the concept of subdividing a continuum into small pieces, describing the behavior or actions of the individual pieces and then reconnecting all the pieces to represent the behavior of the continuum as a whole. This process of subdividing the continuum into smaller pieces is known as discretization or meshing. The pieces are known as finite elements.

Discretization or meshing involves defining geometry, distance, area, and volume. It is one of the three fundamental aspects of finite element modeling: the other two are defining material properties and boundary conditions.

The groundwater analysis in *Slide*® is a finite element analysis, and therefore a finite element mesh is required in order to solve the problem.

A three-noded triangles mesh is used to analyze the flow in the embankment, as shown in Figure 29.

For maximum precision in estimating the water flow, the mesh is dense: the mesh has got 4624 elements connected together by 2424 nodes. The calculations are executed for maximum 500 iterations for each stage or for time needed to reach maximum tolerance equal 10^{-6}.

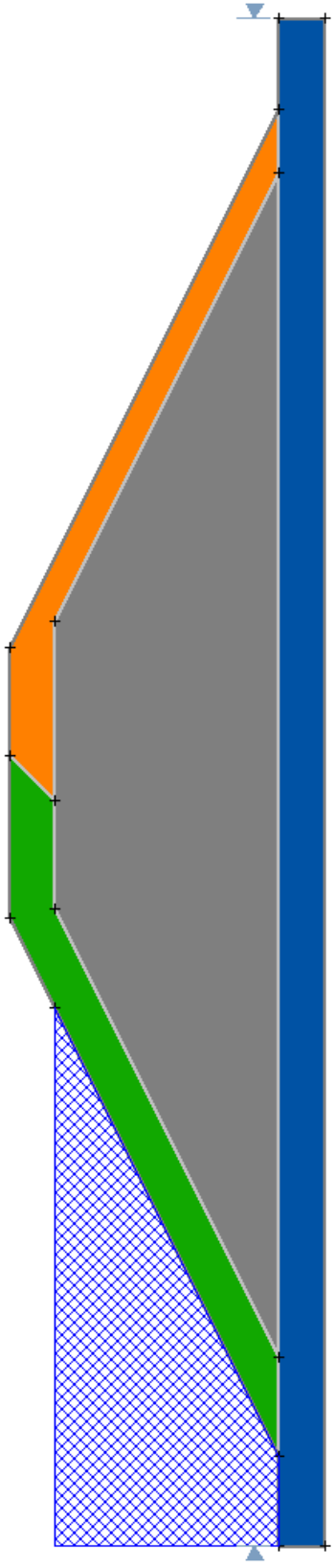

Figure 28: Model for groundwater analysis on Slide 5:0

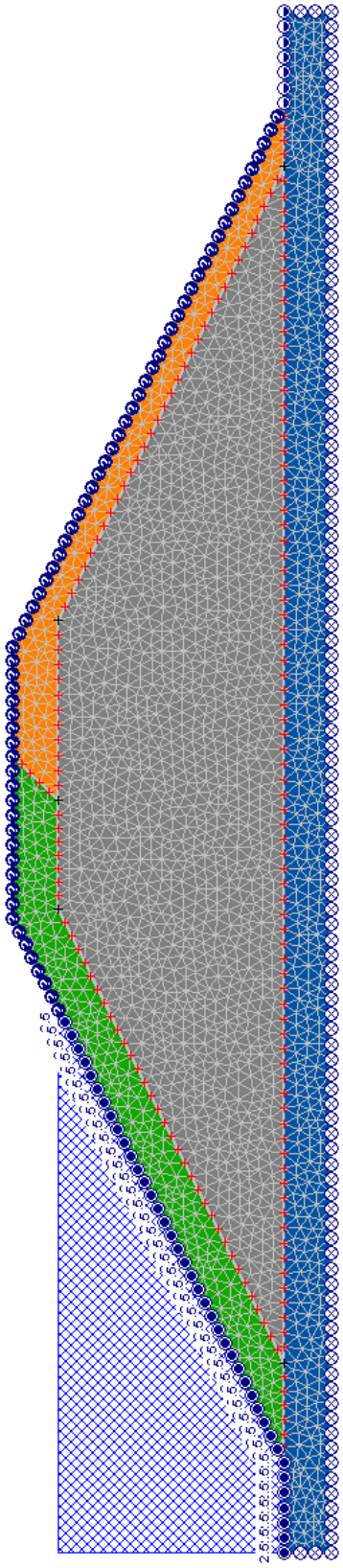

Figure 29: Mesh discretization of the model

After the finite element mesh has been generated, it is necessary to define the boundary conditions which describe the groundwater problem.

The boundary condition used in the model is *Total Head.*

The total hydraulic head is made up of pressure head and elevation. The elevation represents the gravitational component. In equation form the total head is defined as:

$$H = \frac{u}{\gamma_w} + z$$

Where:

$H =$ the total head (m);

$u =$ the pore-water pressure (Pa);

$\gamma_w =$ the unit weight of water (kN/m^3);

$z =$ the elevation (m).

The term $\frac{u}{\gamma_w}$ is referred to as the pressure head, represented in units of length.

The *Total Head* hydraulic boundary condition defines the conditions that exist along the bottom of a reservoir, that is the elevation head at the top of the reservoir (ponded water).

For the test dike the fully supply level of the reservoir is 2,5 m.

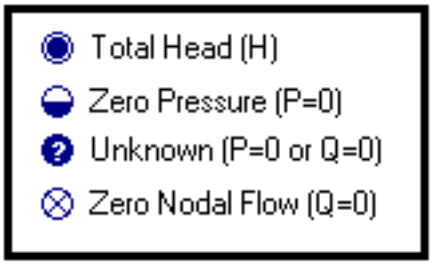

Figure 30: Boundary conditions

The slope surface on the right is given an *Unknown* boundary condition: this type of boundary is suitable for calculations if the groundwater flow is unconfined.

The *Zero Pressure (P=0)* boundary condition is set to model the ground on the opposite side respect the river (ground side). The bottom of the external boundary, is given the *Zero Nodal Flow (Q=0)* boundary conditions, which indicates that no additional flux is going to be added or removed at these nodes. The *nodal flow* equal to zero condition does not allow the water to exit.

The hydraulic properties (permeability characteristics) previously specified for the materials were put in the program, and the groundwater analysis was performed. The Figure 31 show the results.

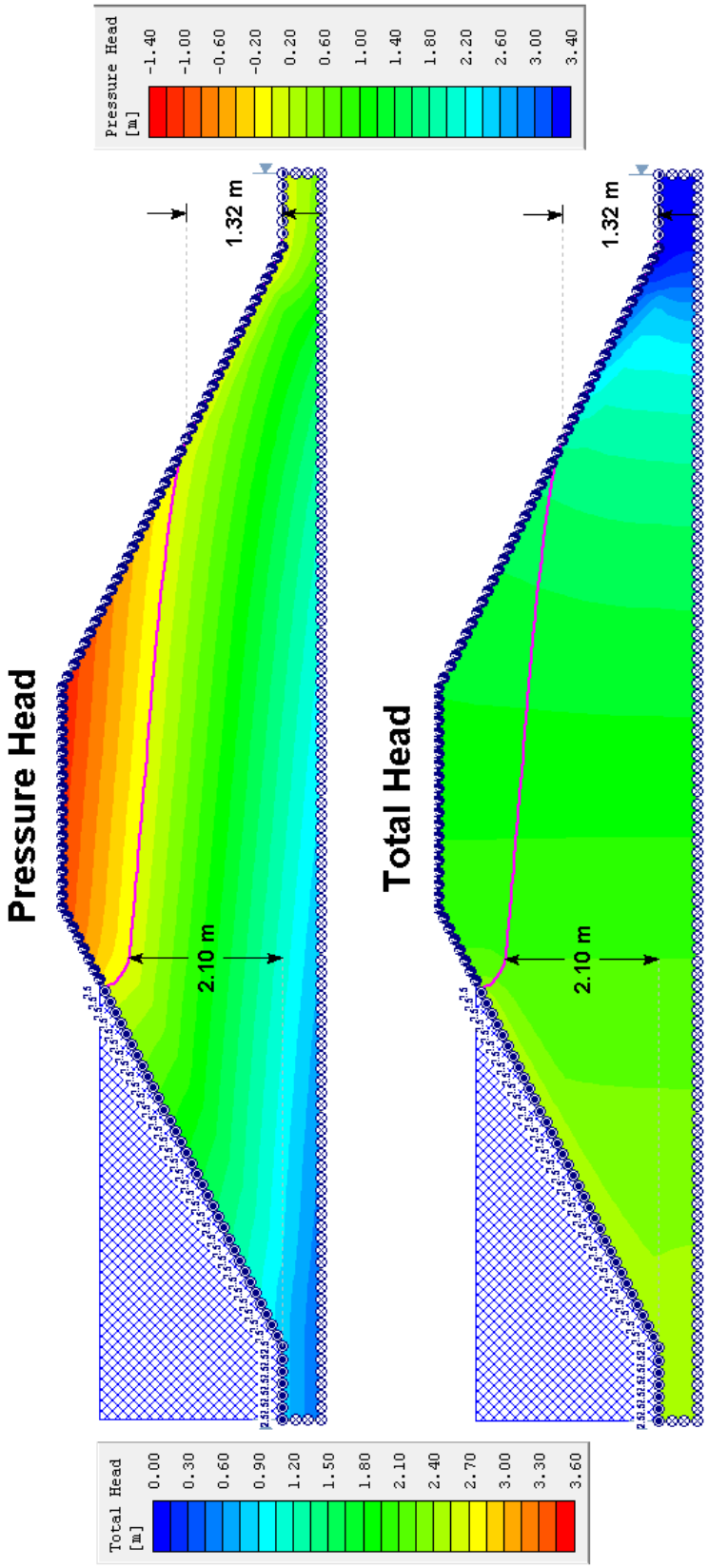

Figure 31: Groundwater analysis: pressure head (a) and total head (b) results. Slope 1:2

A pink line is displayed on the model: this line highlights the location of the *Pressure Head=0* contour boundary. For a slope model, this line represents the position of the Water Table (phreatic surface) determined from the finite element analysis.

The Water Table touches the external facing 1,32 m above the toe of the levee: due to the high permeability of the material in the most central part of the embankment, the hydraulic load is not dissipated.

To verify if the program leads to acceptable results, the Shaffernak schema is utilized:

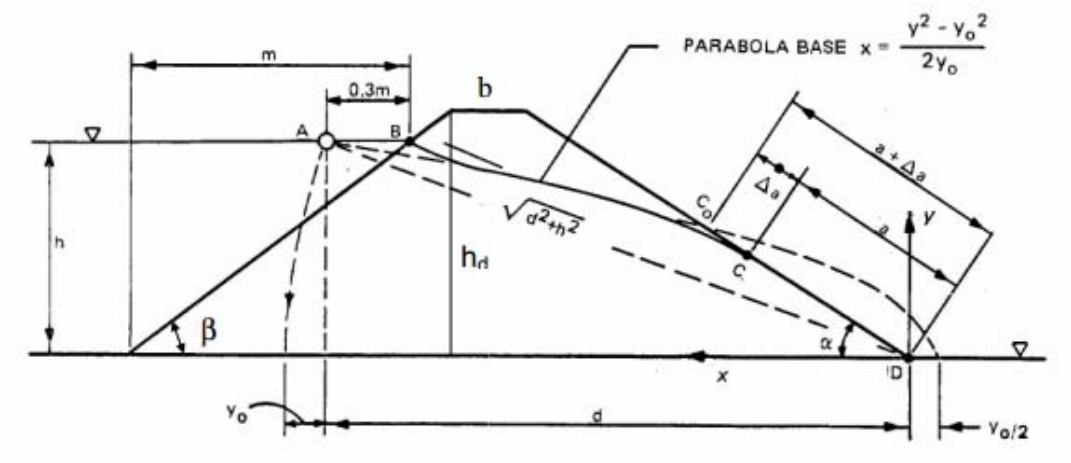

Figure 32: Dike's section, Shaffernak schema

Because the angles at downstream side is ≤ 30° , it is possible to use either the equation proposed by Shaffernak-Van Iterson, or the one proposed by Casagrande (*Casagrande*, 1937)..

The length off the segment between the exit of water and the end of the slope is given by:

$$a = \frac{d}{cos\alpha} - \sqrt{\frac{d^2}{cos^2\alpha} - \frac{h^2}{sin^2\alpha}} \qquad \rightarrow \quad Shaffernak - Van\ Iterson$$

$$a = S_0 - \sqrt{{S_0}^2 - \frac{h^2}{sin^2\alpha}} \qquad \alpha \leq 60° \Longrightarrow S_0 = \sqrt{d^2 - h^2} \qquad \rightarrow \quad Casagrande$$

Using both the previous equations, the following results are obtained. The value of the exit water height from the analysis is similar to the analytic results, so it is acceptable.

GeoStudio™ 2007	1.32
Shaffernak-Van Iterson	1.226
Casagrande	1.359

The toe of the embankment is under a high pressure, and if this one is not dissipated, it will probably cause the removal of the external layer.

Correctly, the flux goes towards the dike external toe. There, the water comes out.

The seepage coming through the levee above the ground surface (through seepage) are very detrimental: when seepage velocity is sufficient to move materials, the resulting internal erosion is called *piping* (movement of soil material).

Three types of piping can occur as a result of seepage through a levee:

- cracks or void in the dike due to hydraulic fracturing, decay of vegetation, animal activity, low density adjacent to conduits, or any similar location where there may be a preferential path of seepage. For piping to occur, the tractive shear stress exerted by the flowing water must exceed the critical shear stress of the soil.
- high exit gradients on the downstream face of the levee may cause piping and possible progressive backward erosion.
- internal erosion or removal of fine grains by excessive seepage forces may occur; this type of piping occurs when the seepage gradient exceeds a critical value.

The dike's core is made of an ash and sand mixture, i.e. fine particles in granular soil. The seepage flow can displace the fine grains, and create preferential pathways, with instability risk for the dam. To evaluate if there is the possibility of particles movement, it is necessary to estimate the hydraulic exit gradient and compare it with the critical one.

The hydraulic gradient is the rate of change of total head along the direction of flow :

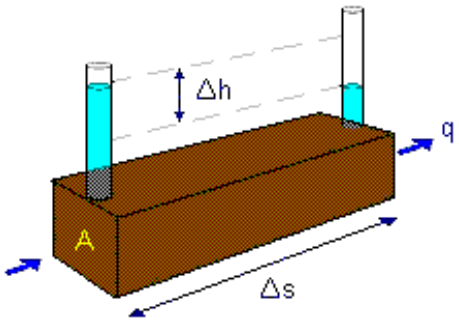

The rate of flow of water q (volume/time) through cross-sectional area A is found to be proportional to hydraulic gradient in according to Darcy's law:

$$v = \frac{Q}{A} = k \cdot i = k \cdot \frac{\Delta h}{\Delta s}$$

where **v** is flow velocity and **k** is coefficient of permeability with dimensions of velocity (length/time).

The hydraulic critical gradient is given by:

$$i_c = \frac{\gamma'}{\gamma_w}$$

To avoid particles displacement, it should be:

$$FS = \frac{i_c}{i} \geq 2{,}5 \div 4$$

In the previous analysis, considering the dike's core, the exit gradient results as $i_e \approx 1$ (Figure 33), the critical gradient is $i_c = 0{,}662$ and the safety factor results as $FS = 0{,}662$, so movement of particles will occur.

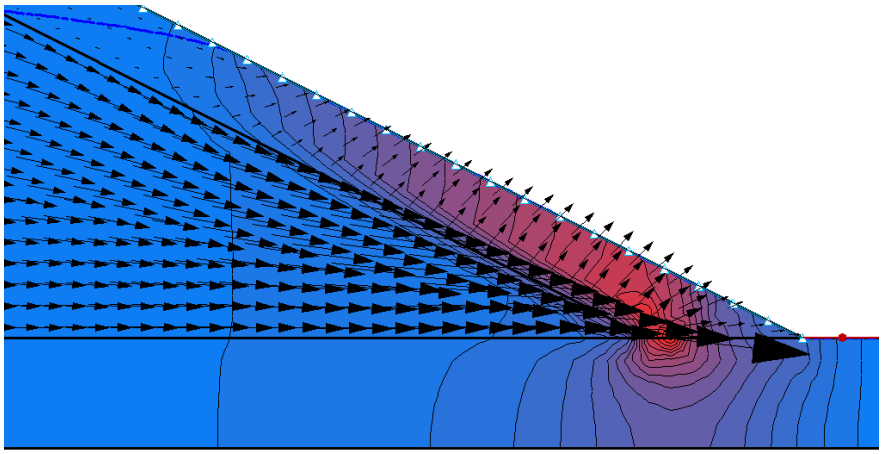

Figure 33: Gradient at downstream side's toe

The external clay layer prevents the spillage of the fine particles from the dike's core, so in this embankment we do not have to fear internal erosion, at least until the clay layer is undamaged and cracks do not occur.

Because of the impervious external layer, at dam's downstream side toe high pore-water pressures occur, and it is necessary to verify that the weight of the clay layer can resist to these pressures, i.e. $S_w < \gamma_{sat} V$. At interface between the core and the top layer the pore-water pressure is $PWP = 5\ kPa$, as indicated in Figure 34, so the upward buoyant force is given by: $S_w = PWP * A = 15\ kN$.

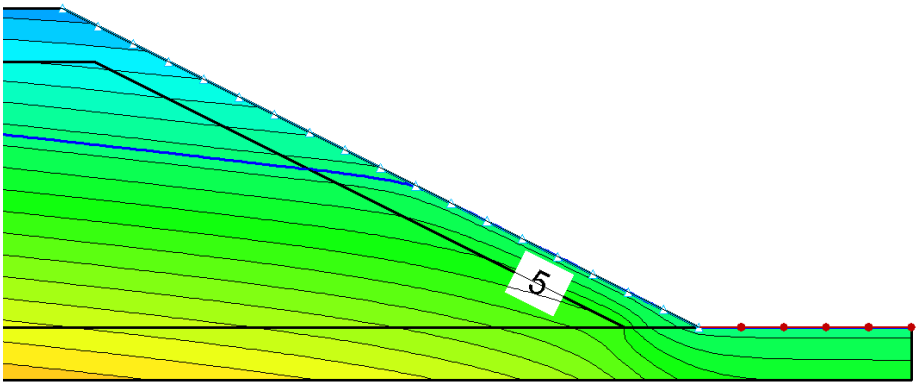

Figure 34: Pore-water pressure at core-external layer interface

The weight of the clay layer is $\gamma_{sat} V = 21 \cdot V = 18{,}9\ kN > S_w = 15\ kN$, so the stability of the clay in external toe is verify.

The analysis was performed again, to evaluate which is the best solution to increase the stability of the levee.

Different slopes

First of all, the ***slope*** of the downstream side was changed: from 1:2, to 1:2,5 and 1:3.

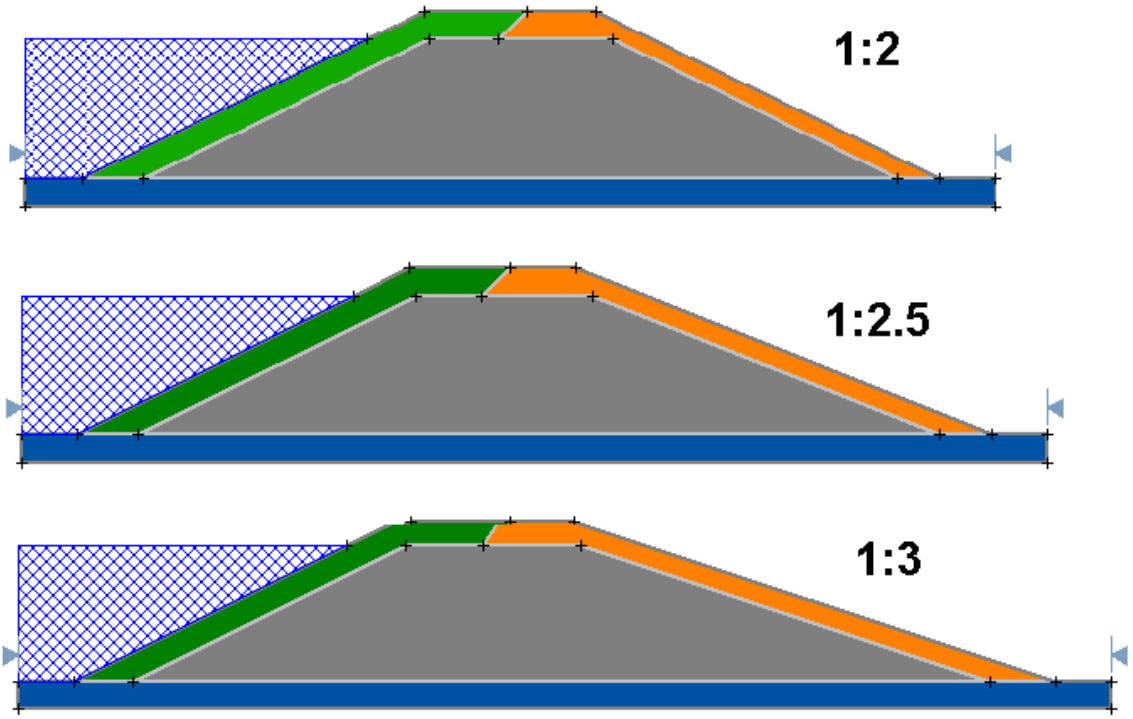

Figure 35: Change of slopes

The different height of water escape are collected in Table 6. As it is shown in the graph below, this modification did not lead to acceptable results. The pore-water pressures are

not so different respect to the case described before, so problems in the dike's toe do not occur.

Table 6: Water exit heights for different slopes

Slope	Water exit height [m]
1:2	1,32
1:2.5	1,35
1:3	1,36

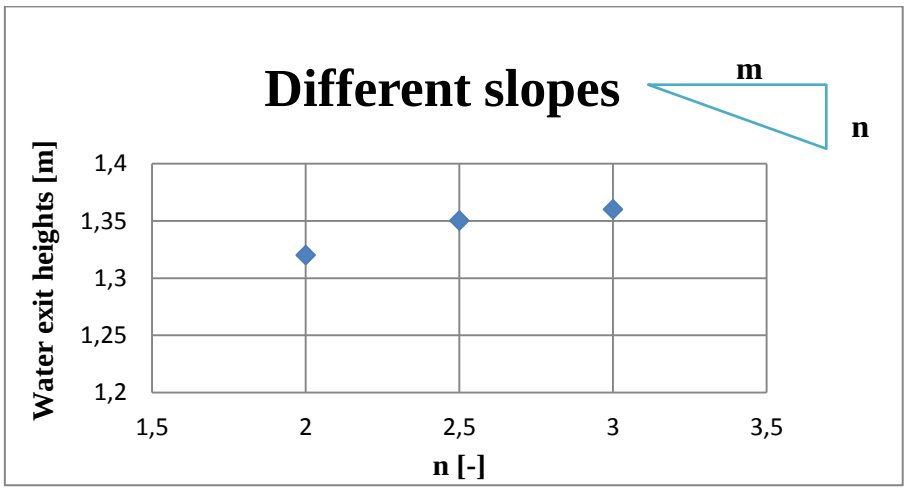

Figure 36: Change of water exit height for different slopes

Different thickness

The second parameter changed was the thickness of the impermeable layer at downstream side (tephra and sand layer).

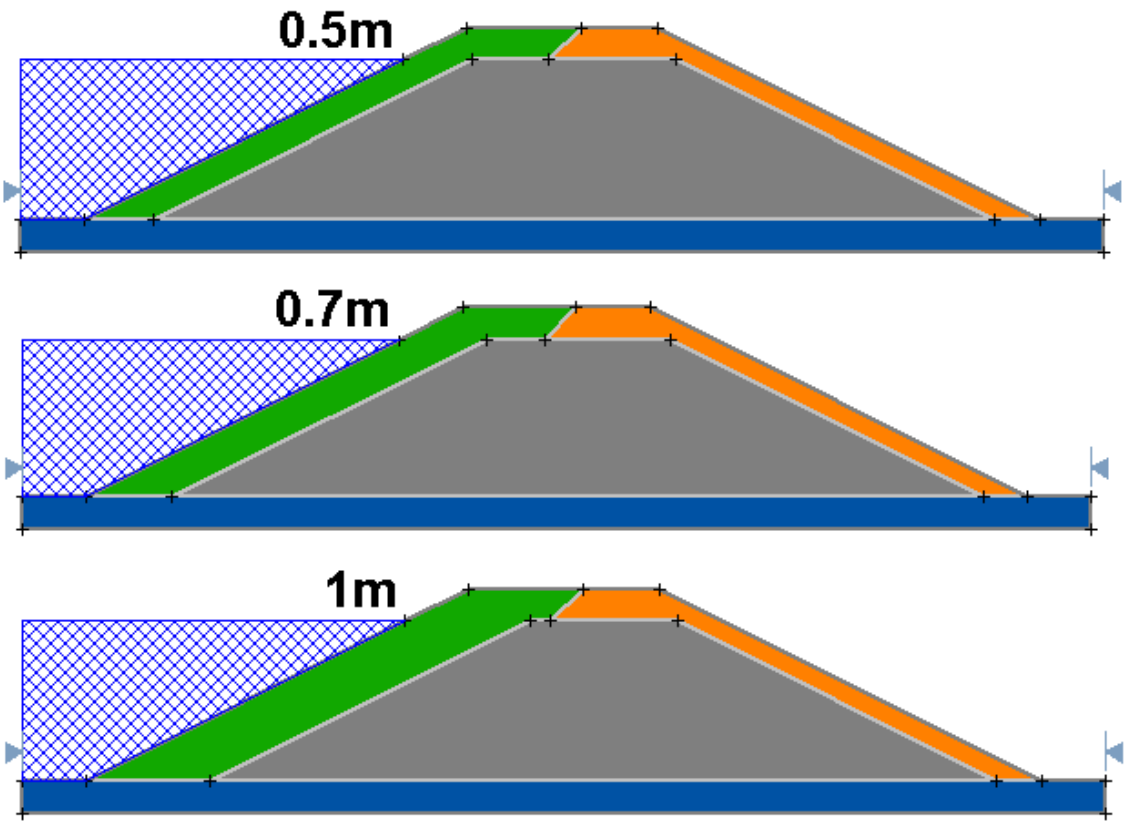

Figure 37: Different thickness

This solution is much better respect the previous one, because a decrease of the water exit height occurs as the thickness of the first layer increase. The Table 7 and graph in Figure 38 show as change the results in this case.

Table 7: Water exit heights for different thicknesses

Thickness [m]	Water exit height [m]
0,5	1,32
0,7	1,29
1,0	1,21

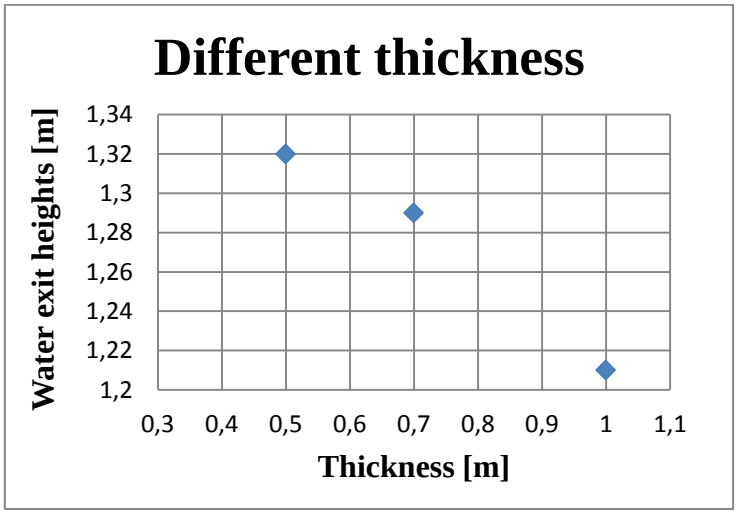

Figure 38: Change of water exit height for different thicknesses

Different conductivity coefficient at saturation

As last step, I supposed to change the mixture of the layer on the river side, using two different materials with lower conductivity coefficient at saturation: 10^{-8} and 10^{-9}, respectively.

This solution leads to values of exit heights of the water that are lower of the previous ones:

Table 8: Water levels for different riverside material

K_s	Interface layer-core [m]	Water exit height [m]
1,00E-07	2,1	1,32
1,00E-08	1,43	0,80
1,00E-09	0,61	0,37

The level of the phreatic surface at the interface between the tephra and sand layer and the core of the dike decreases as the hydraulic conductivity decreases, because the dissipation of the hydraulic load occurred mostly in the first impervious layer.

The graph in Figure 39 shows the different water heights after changing the material of the layer on the riverside.

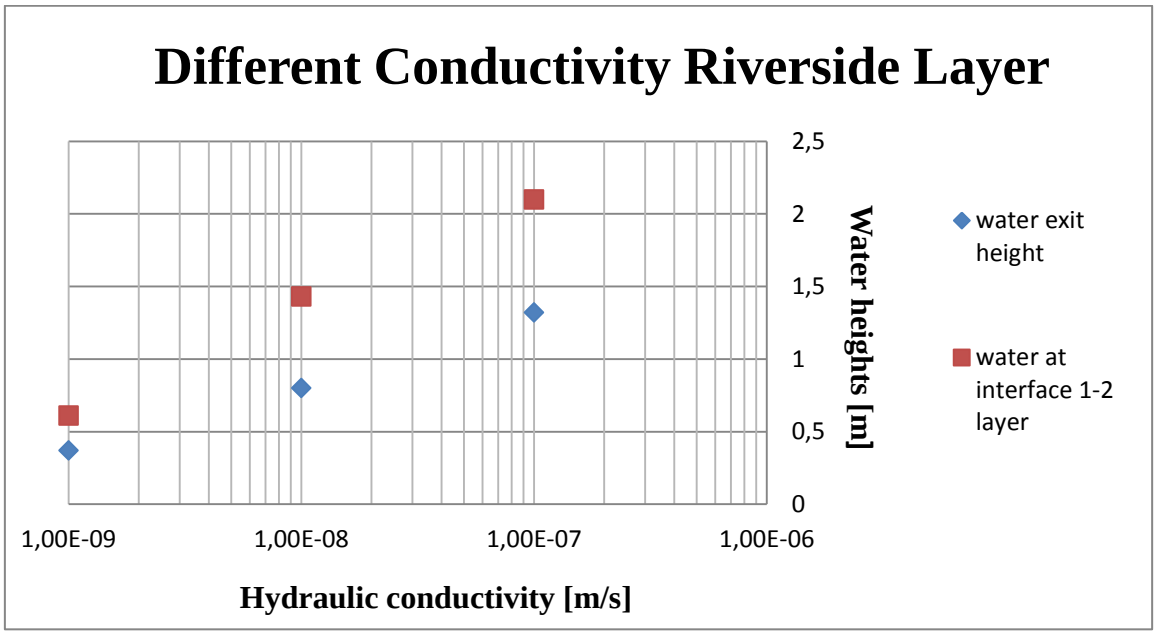

Figure 39: Different water heights for different hydraulic conductivity

The last step of this analysis was the change of the material in dike's core. The conductivity function changed from 10^{-6} to 10^{-7} m/s (as the dike was made of only one material, i.e. clay) and 10^{-8} m/s (as the core was more impervious than the external layers).

Table 9: Water levels for different core's material

K_s	Wter exit height [m]
1,00E-06	1,29
1,00E-07	0,95
1,00E-08	0,29

The condition of dam's core more impermeable of the externals layers is the best solution, because the water exit height of almost 30 cm is the smallest in comparison of all the previous analyses.

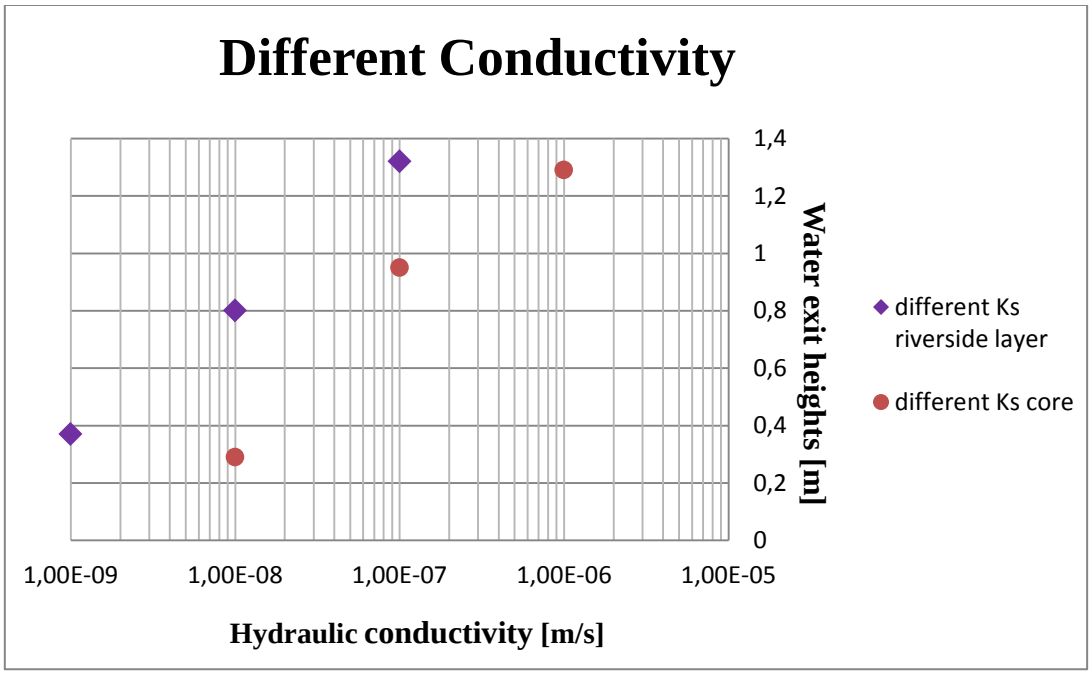

Figure 40: Comparison of different hydraulic conductivity

Toe-drain

A toe drain in the embankment is now introduced Figure 41.

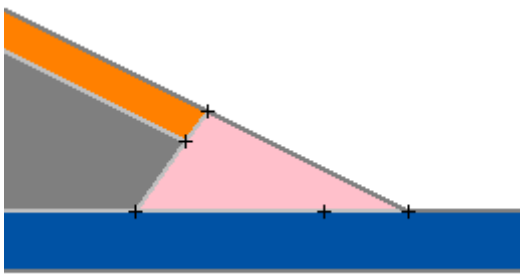

Figure 41: Toe drain in the embankment

The drain is so permeable relative to the other embankment materials that it does not contribute to the dissipation of the head (potential energy) loss through the structure. We assume that the drain will be capable of removing all the seepage that arrives at the drain, this means that the drain will not be under positive pressures at any time (water pressure in the drain will be zero). Physically, the drain needs to exist in the embankment, but it does not need to be present in a numerical model. If the drain becomes clogged with fines so that it begins to impede the seepage flow, just then the drain would need to be included in the numerical model.

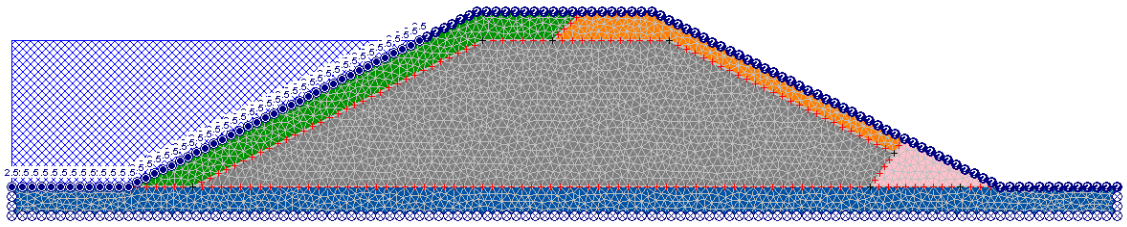

Figure 42: Modeling of the drain. Meshing and boundary conditions

The boundary conditions used in this model are *Total Head* on riverside.

Again, the slope surface on the right and the drain are given an *Unknown* boundary condition; the bottom of the external boundary, is given the *Zero Nodal Flow* boundary conditions.

Using the same permeability characteristics of the materials, the following results as total head pressures are obtained (Figure 43).

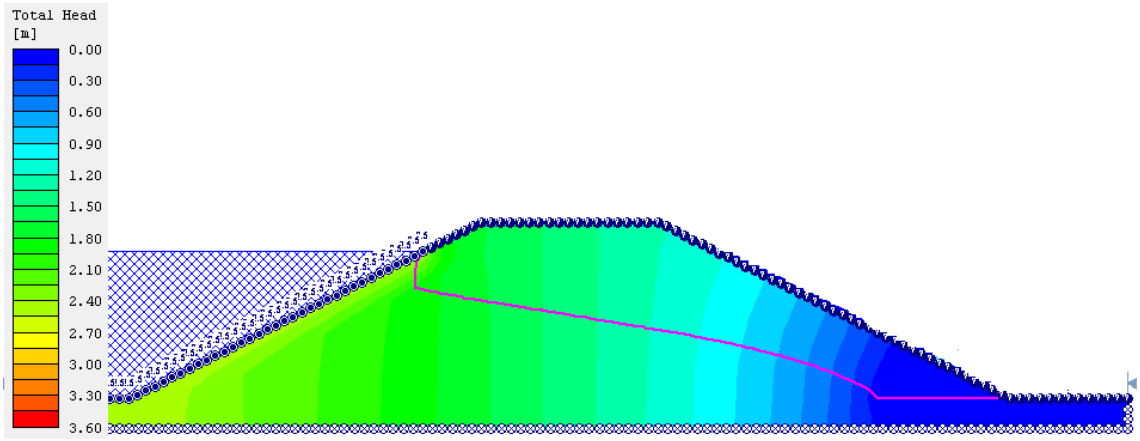

Figure 43: Groundwater analysis with toe-drain

Obviously, this time the water table does not cross the external facing, but there is an important spill of water through the drain.

The maximum period of full supply level of the reservoir, that the dike can withstand without seepage problems, will be analyze later, in the transient analysis.

Slope Stability analysis

The "slope stability" may be defined as the resistance of inclined surface to failure by sliding or collapsing. Slope stability analysis is performed to assess the safe design of a slopes (both natural and human-made) and the equilibrium conditions.

Most of the slope stability analysis computer programs are based on the limit equilibrium concept. The conventional limit equilibrium methods investigate the equilibrium of the soil mass tending to slide down under the influence of gravity with a transitional or rotational movement. This movement describes the "slip surface".

All the different methods to study the slope stability are based on comparison of forces (moments or stresses) resisting instability of the soil mass and those that causing instability.

The most common limit equilibrium techniques are methods of slices where soil mass is discretized into vertical slices, as shown in Figure 44.

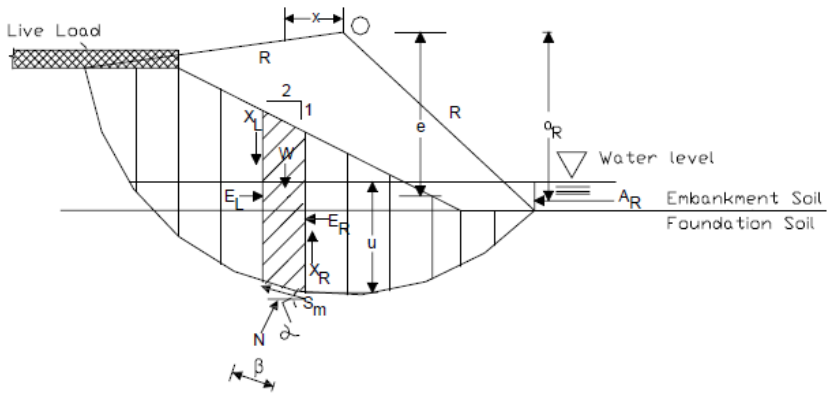

Figure 44: Method of slices

Where:

W = weight of slice,

R = radius of slip circle,

E_L and E_R = left and right side slice normal forces,

X_L & X_R = left side and right side slice shear forces,

N = base normal force ($N = W\,cos\alpha$),

α = slice base inclination,

β = base length,

S_m = mobilized shear strength,

A_R = water pressure,

x = horizontal distance of weight of slice from center of rotation O,

u = pore water pressure above base of slice,

e = vertical distance of center of slice,

a_R = vertical distance of water pressure line from the center of rotation O.

The software *Slide® 5.0* has been used to develop the slope stability analysis. Below, it is possible to find the explanation of all the calculation models used.

Methods of Slices

Ordinary method (1927)

The Ordinary, or Fellenius method (*Fellenius W.*, 1936) was the first method developed. The method ignored all interslice forces and satisfied only moment equilibrium.

The slice weight is resolved into forces parallel and perpendicular to the slice base: the perpendicular one is the base normal force, which is used to compute the available shear strength; the parallel weight component is the gravitational driving force.

To compute the factor of safety, the summation of moments about a point used to describe the trial slip surface is used. The FS is the available shear strength along the slip surface divided by the summation of the gravitational driving forces, that is the mobilized shear. In the absence of any pore-water pressures for a circular slip surface is:

$$FS = \frac{\sum[c\beta + Ntan\varphi]}{\sum Wsin\alpha} = \frac{\sum S_{resistance}}{\sum S_{mobilized}}$$

Figure 45 shows an example of the force polygon for the Ordinary Methods. Due to the poor force polygon closure, the Ordinary method can give unrealistic factors of safety and consequently should not be used in practice.

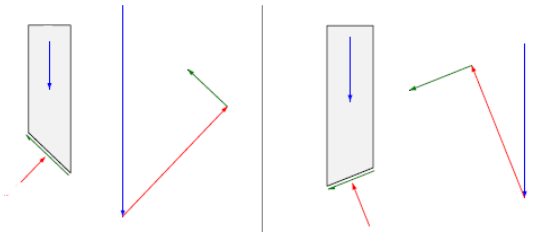

Figure 45: Free body diagram and force polygon for the Ordinary Method

Bishop simplified (1955)

Bishop devised a method which included interslice normal forces, but ignored the interslice shear forces (*Bishop A.W.*, 1955).

Again, this method satisfies only moment equilibrium, not overall horizontal force equilibrium. Bishop developed an equation for the normal at the slice base by summing slice forces in the vertical direction, so the base normal becomes a function of the factor of safety. The FS appears on both sides of the equation, so the factor of safety equation

becomes nonlinear and an iterative procedure is consequently required to compute the factor of safety. Bishop's Simplified factor of safety equation in the absence of any pore-water pressure is:

$$FS = \frac{1}{\sum W sin\alpha} \sum \left[\frac{c\beta + Wtan\varphi - \frac{c\beta}{FS} sin\alpha \cdot tan\varphi}{cos\alpha + \frac{sin\alpha \cdot tan\varphi}{FS}} \right]$$

The Figure 46 shows the slice free body diagrams and forces polygons for the same slices as for the Ordinary method. The force polygon closure is now fairly good with the addition of the interslice normal forces.

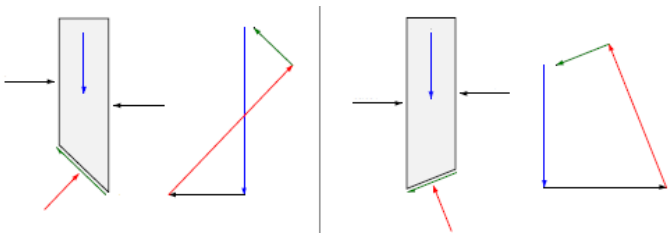

Figure 46: Free body diagram and force polygon for Bishop's Simplified Method

Janbu's simplified method (1954, 1973)

The Janbu's Simplified method (*Janbu N. et al.*, 1956) is similar to the Bishop's Simplified method: it included interslice normal forces, but ignored the interslice shear forces. In contrast, the Janbu's Simplified method satisfies only overall horizontal force equilibrium, not overall moment equilibrium.

Figure 47 shows the free body diagrams and force polygons of the Janbu's Simplified method. The slice force polygon closure is actually better than that for the Bishop's Simplified method. However, the factor of safety calculated for circular slip surfaces, compared to the one of other methods, results too low (underestimation of 20-30%), even though the slices are in force equilibrium.

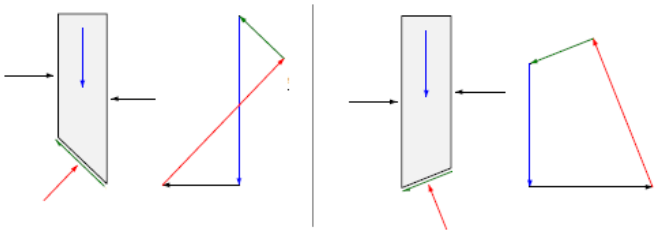

Figure 47: Free body diagram and force polygon for Janbu's Simplified Method

Spencer method (1967,1973)

This method (*Spercer E.*, 1967) considers both shear and normal interslice forces. Spencer developed two factor of safety equations; one with respect to moment equilibrium and another with respect to horizontal force equilibrium. He adopted a constant interslice force function between the interslice shear and normal forces, and through an iterative process altered the interslice shear to normal ratio until the two factors of safety became the same.

Finding the shear-normal ratio that makes the two factors of safety equal, means that both moment and force equilibrium are satisfied.

Figure 48 shows the free body diagram and force polygon for this method: when both interslice shear and normal forces are included, the force polygon closure is very good.

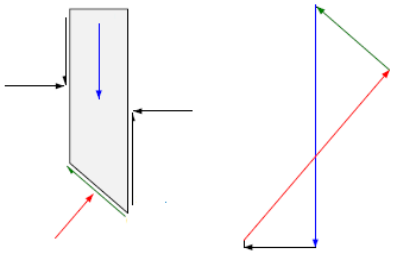

Figure 48: Free body diagram and force polygon for Spencer's Method

Morgenstern-Price method (1965)

Morgenstern and Price developed a method similar to the Spencer method, but they allowed for various user-specified interslice force functions (constant, half-sine, data-point specified,…).

The Morgenstern-Price method (*Morgerstern N.R., Price V.E.*, 1965) considers both shear and normal interslice forces, satisfies both moment and force equilibrium, and allows for a variety of user-selected interslice force function.

The figure below (Figure 49) shows the free body diagram and force polygon for this method, obtained by using a half-sine force function.

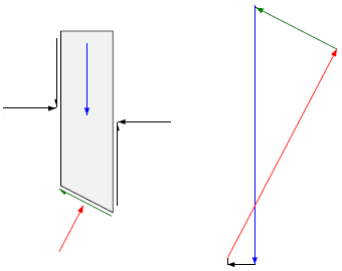

Figure 49: Free body diagram and force polygon for Morgenstern and Price's Method

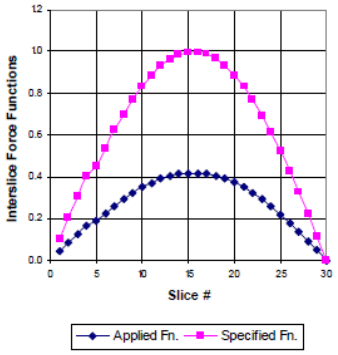

Figure 50: Half-sine function

General limit equilibrium method (GLE) (1981)

This method was developed by Fredlund et al. (1981). Like Spencer's method, the GLE formulation is based on two factor of safety equations: one equation gives the factor of safety with respect to moment equilibrium (F_m), while the other one gives the factor of safety with respect to horizontal force equilibrium (F_f). The interslice shear forces in the GLE method are handled with an equation proposed by Morgenstern and Price:

$$X = E\lambda f(x)$$

where:

f(x) is a function,

λ is the percentage of the function used,

E is the interslice normal force,

X is the interslice shear force.

The GLE factor of safety equation with respect to moment equilibrium is:

$$F_m = \frac{\sum(c'\beta R + (N - u\beta)Rtan\varphi')}{\sum Wx - \sum Nf \pm \sum Dd}$$

The factor of safety equation with respect to horizontal force equilibrium is:

$$F_f = \frac{\sum(c'\beta cos\alpha + (N - u\beta)cos\alpha tan\varphi')}{\sum Nsin\alpha - \sum Dcos\alpha}$$

with:

c' = effective cohesion

ϕ' = effective angle of friction

D = concentrated point load

N = the normal at the base of each slice, its equation is obtained by the summation of vertical forces.

The GLE method satisfies both moment and force equilibrium by finding the cross-over point of the F_m and F_f curves.

It provides a framework for discussing, describing and understanding all the other methods.

The Table 10 indicates what equations of statics are satisfied for each of the methods. The Table 11 gives a summary of the interslice forces included and the assumed relationships between the interslice shear and normal forces.

Table 10: Satisfied equation of static

Method	Moment Equilibrium	Force Equilibrium
Ordinary or Fellenius	Yes	No
Bishop's Simplified	Yes	No
Janbu's Simplified	No	Yes
Spencer	Yes	Yes
Morgenstern-Price	Yes	Yes

Table 11: Interslice force characteristics and relationships

Method	Interslice Normal (E)	Interslice Shear (X)	Inclination of X/E Resultant, and X-E Relationship
Ordinary or Fellenius	No	No	No interslice forces
Bishop's Simplified	Yes	No	Horizontal
Janbu's Simplified	Yes	No	Horizontal
Spencer	Yes	Yes	Constant
Morgenstern-Price	Yes	Yes	Variable; user function

Results

In the slope stability analysis for the test dike in Gdansk, all the methods described above have been used.

The same model used for the seepage analysis has been used, in order to consider also a part of the soil under the dam, because it could be involved in the instability. Again, the model considered the dike itself, and a 0,5 m thick layer of loam under it, as shown in Figure 51:

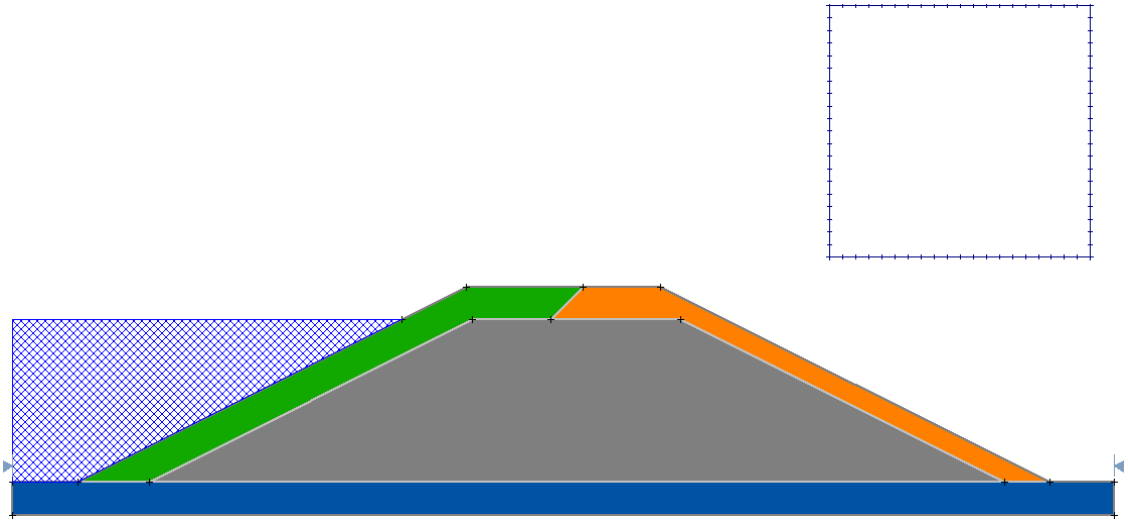

Figure 51: Model for slope-stability analysis (Slide 5.0)

The resulting solutions are summarized for each methods used in the analysis in the following table (Table 12):

Table 12: FS from different methods (Slope 1:2)

Slope	Ordinary	Bishop simplified	Jambu Simplified	Spencer	Morgenstern-Price
1:2	3.346	3.516	3.453	3.515	3.519

The result obtained with Bishop's method is almost equal to the one obtained with Morgenstern and Price method.

This means that a simpler method like Bishop's simplified, that ignores interslice shear forces, does not always err on the save side. This method has been used to discuss the next analysis.

The results obtained by using the Bishop's simplified method are shown in Figure 53.

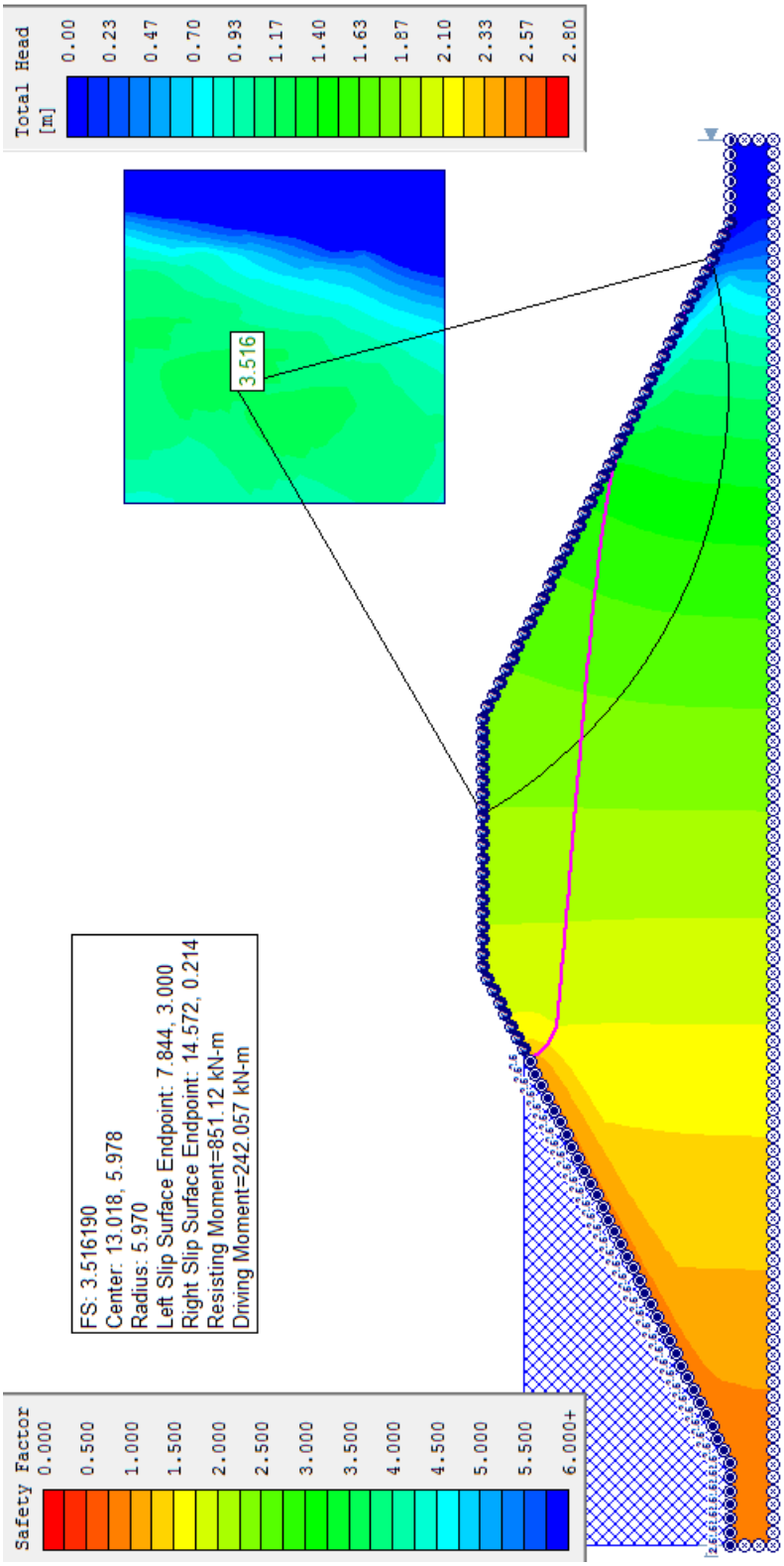

Figure 52: Slope stability analysis (Slope 1:2)

With Slide 5.0 is also possible to focus on each slice, to see the forces considered in the model and all the data about the slice. The next image (Figure 53) shows an example of this.

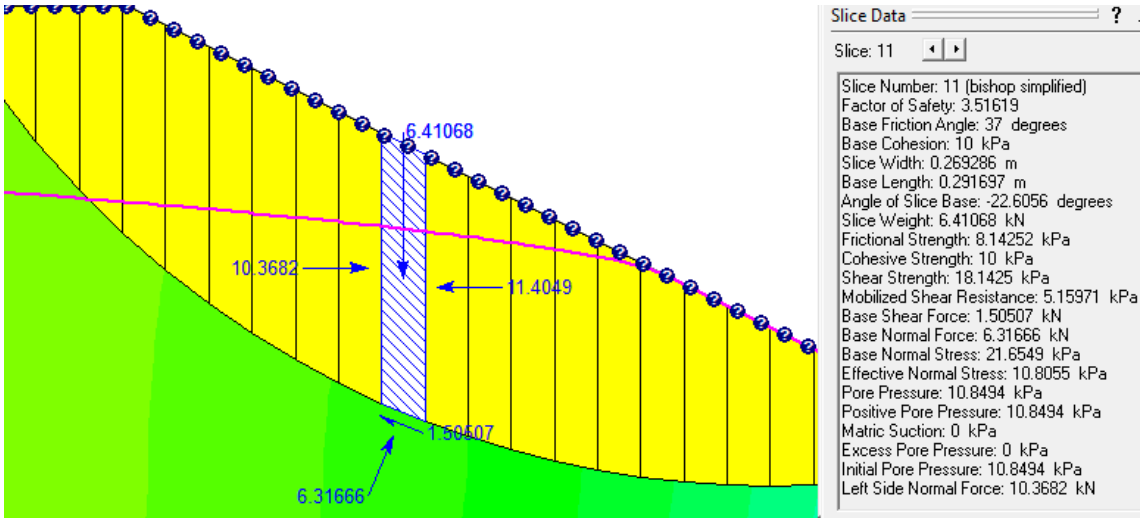

Figure 53: Query slice data

Concerning the slope stability, the Figure 54 shows the minimum surfaces referring to each point of the grid (different centrums and radius).

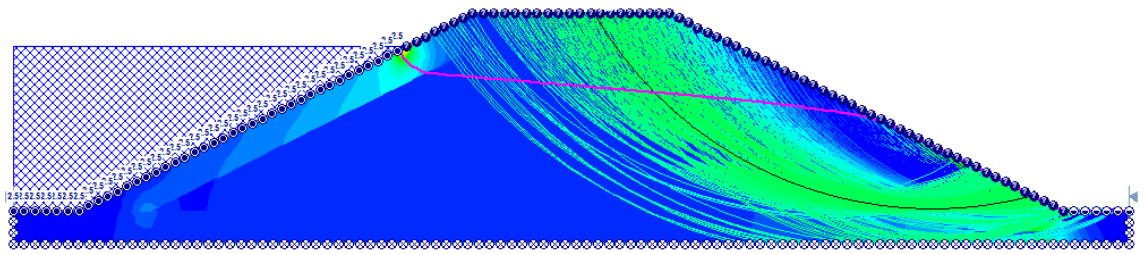

Figure 54: Minimum surfaces (Slope 1:2)

Different slopes

The results obtained changing the slope in downstream side were also examined.

The Table 13 summarizes the FS obtained with the different methods after changing slopes: it is evident as, a decrease of the slope of the downstream side causes the increase of the FS (of 10-15%).

Table 13: FS from different methods and slopes

Slope	Ordinary	Bishop simplified	Jambu Simplified	Spencer	Morgenstern-Price
1:2	3,346	3,516	3,453	3,515	3,519
1:2,5	3,762	3,961	3,836	3,949	3,96
1:3	4,188	4,433	4,258	4,427	4,434

Different materials

Again, was change the material of the riverside layer, and the one of the dike's core. The new materials chosen presented a lower permeability: the tephra-and-sand mixture had a hydraulic conductivity equal to $k_s = 10^{-7}\ m/s$, and now it is assumed $k_s = 10^{-8}\ m/s$ and $k_s = 10^{-9}\ m/s$; the core presented $k_s = 10^{-6}\ m/s$, and now it changes in $k_s = 10^{-7}\ m/s$ and $k_s = 10^{-8}\ m/s$.

The different situation leads to the results below (Table 14):

Table 14: FS for different materials

K_s External layer	FS (Bishop)	K_s Core	FS (Bishop)
1,00E-07	3,516	1,00E-06	3,516
1,00E-08	3,889	1,00E-07	3,627
1,00E-09	4,287	1,00E-08	3,784

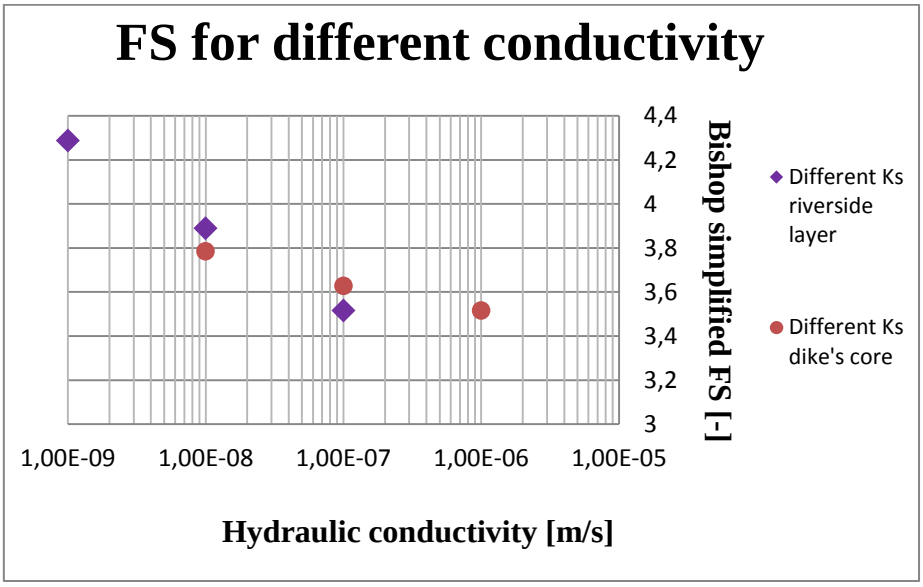

Figure 55: Comparison between FS

With a very impervious external layer, less water arrives to downstream side, so less stability problems occur.

Different cohesion

In this section, Bishop's safety factor is evaluated changing the cohesion of the embankment core.

It is assumed to modify the percentage of ash in the mixture: the cohesion decreases if the percentage of fly ashes in the mixture is reduced; increases in the opposite situation. The initial cohesion was 10 kPa, and for this analysis it is assumed first equal to 5 kPa and then equal to 15 kPa.

The results show that there is a great change in FS, as the cohesion is modified, and that a low cohesion penalizes the stability of the embankment. For this reason, the use in the core of materials with a high percentage of clayey or silty ground increases the internal cohesion.

Table 15: FS for different cohesion

Choesion [kPa]	FS (Bishop)
5	2,679
10	3,516
15	4,15

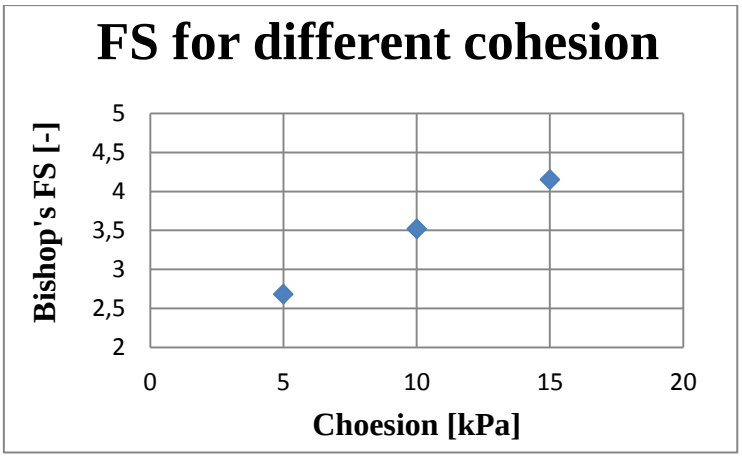

Figure 56: FS for different cohesion values

Different friction angle

The last parameter changed has been the friction angle of the ash-sand mixture. In this situation, the percentage of sand in the mixture is supposed to change; as a consequence the friction angles decreases or increases, respectively with the reduction or the addition of granular material in the mixture.

Table 16: FS for different friction angle

Friction angle [°]	FS (Bishop)
34	3,404
37	3,516
40	3,637

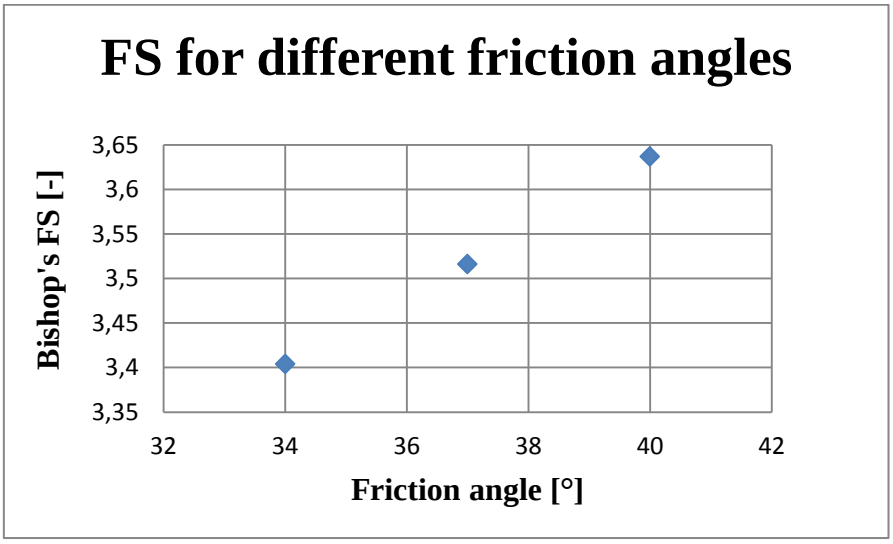

Figure 57: FS for different angles of friction

The FS obtained changes, but in a minor way if compared with the FS determined after changing the cohesion (in previous analysis).

The results point out the correct choice of the ash-sand mixture as dike's core material: this mixture combines the advantages of having a high friction angle (sand), and a high cohesion. The high cohesion derives from the high percentage of fly ashes (70%), that have mechanical characteristics similar to those of silt.

The use of a large amount of tephra is justified since the cohesion of the materials mostly influences the stability of an embankment.

Transient analysis

In a steady-state analysis the pore-water pressures in the ground are at equilibrium with the defined boundary conditions and are not changing with time. On the contrary, in a transient analysis the pore-water pressures in the ground are changing with time.

In general, flow is considered to be transient if changes in water level in wells and piezometers are measurable. Freeze and Cherry (1979) state that transient flow (unsteady flow) occurs when at any point in a flow field the magnitude or direction of flow velocity changes with time. In addition, Lambe and Whitman (1969) define transient flow as the condition during fluid flow where pore-water pressure, and thus total head, changes with time.

Transient seepage analyses are applicable to dams because the boundary conditions acting on them change with time, which induces pore-water pressure changes with time in the embankment and foundation strata. These boundary conditions are rapid such that steady state conditions may not have time to develop.

In a steady-state analysis, the amount of flow into the system is equal to the flow rate out of the system. In contrast, in a transient seepage analysis the amount of flow into the system may differ from the flow out of the system because the system stores or releases water: it therefore becomes necessary to consider how much water is flowing and how fast the water is flowing. As a result, a function of the change in storage and the amount of water in the system and a function of the hydraulic conductivity must be defined.

A transient analysis requires:

- *Initial Conditions:* a point from which to start moving ahead in time. It is possible to establish the initial condition from a certain step in the transient analysis, or by running a steady state analysis.

- *Volumetric Water Content Function (VWC) and Conductivity Function:* the first function describes how water is stored or released in the soil due to changes in pore-water pressure and the second function describes how easily the water will flow through the soil at a given pore-water pressure
- *Time Steps:* an incremental time sequence is required for this kind of analyses. Each time step is equivalent to a mini steady-state analysis.

Both the material property functions will be described in detail below.

Volumetric Water Content (VWC) Function

Soil consists of a collection of solid particles and interstitial voids. The pore voids can be filled either with water or air.

The Volumetric Water Content (VWC) is defined as:

$$\Theta_w = \frac{V_w}{V} = nS$$

where:

Θ_w = volumetric water content,

V_w = volume of water,

V = total volume,

n = porosity of the soil,

S = degree of saturation.

In a saturated soil, all the voids are filled with water, the degree of saturation is 100% and the volumetric water content of the soil is equivalent to soil porosity, which is defined as the volume of voids divided by the total volume.

In an unsaturated soil, the volume of water stored within the voids will vary depending on the matric suction within the pore-water (*GeoStudio*™, 2007), where matric suction is defined as the difference between the air (Ua) and the pressure (Uw) as: $Ua - Uw$.

A function is required to describe how the water contents change with different pressures in the soil, since there is no fixed water content in time and space.

The VWC function describes the capability of the soil to store water under changes in matric pressures, therefore it describes what portion or volume of the voids remains water-filled as the soil drains (negative pore-water pressures).

The three main features that characterize the volumetric water content function are:

- the air-entry value, (AEV), which corresponds to the value of negative pore-water pressure that can be applied to the pore-water before the largest pores begin to drain freely;
- the slope of the soil-water characteristic curve for both the positive and negative pore-water pressure ranges (m_w), which represents the rate of change in the amount of water retained by the soil in response to a change in pore-water pressure;
- the residual water content, (Θ_r), which represents the volumetric water content of a soil where a further increase in negative pore-water pressure does not produce significant changes in water content.

The three main features of the volumetric water content function as described above are most strongly influenced by the size of the individual soil particles and the distribution of particle sizes in the soil.

Water can be released from the soil in two ways: by draining the water-filled voids, thus desaturating the soil profile by gravitation forces (negative pore-water pressure); or by compressing the soil skeleton and reducing the size of the voids, effectively squeezing water out of a saturated system (positive pore-water pressure).

Consider a completely saturated soil where the pore-water pressure is near zero, and the total external load of the soil remains constant. As the pore-water pressure becomes more positive, the effective stress will decrease. This cause the soil to swell and results in an increase in its water content. As the pore-water pressure becomes negative, the soil begins to desaturate and the water content decreases. When the soil becomes completely desaturated, the water content is no longer changes with a further decrease in pore-water pressure.

In the positive pore-water pressure region, m_w becomes equivalent to m_v, the coefficient of compressibility for one-dimensional consolidation; in the negative pore-water pressure region the volume of water stored within the soil changes over a range of values from the AEV (a function of the maximum pore size), to the pressure at the residual water content (a function of the smallest pore size) (Figure 58).

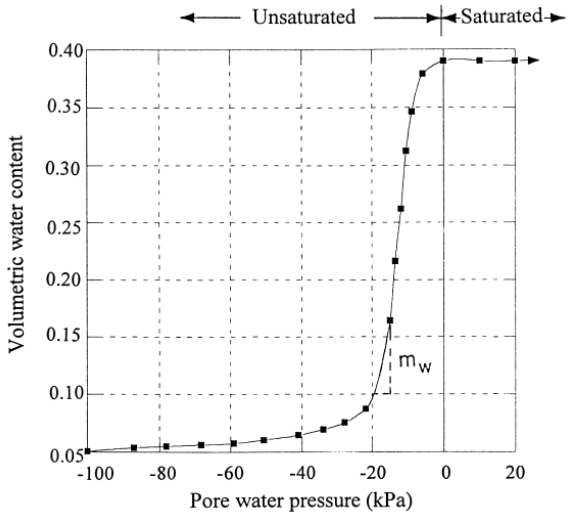

Figure 58: Volumetric Water Content function

Material property function: VWC function

The first material studied was the sand-ash mixture, thus the dike's core.

Six independents samples, taken from the test dike in Trzcinsko, were examined in an external laboratory in Germany. The measured values of volumetric water content at different suction heads are collected in the Table 17and Figure 59, as shown below:

Table 17: Volumetric water content for different water pressure

Pore-Water Pressure	$u\ [kPa]$	0,3	2	6	13	30	60
Pressure Head	$h = -\frac{u}{\gamma_w}\ [m]$	0,03	0,2	0,61	1,33	3,06	6,12
Volumetric water content	$\Theta[-]$	0,4120	0,4014	0,3502	0,2697	0,2298	0,2182

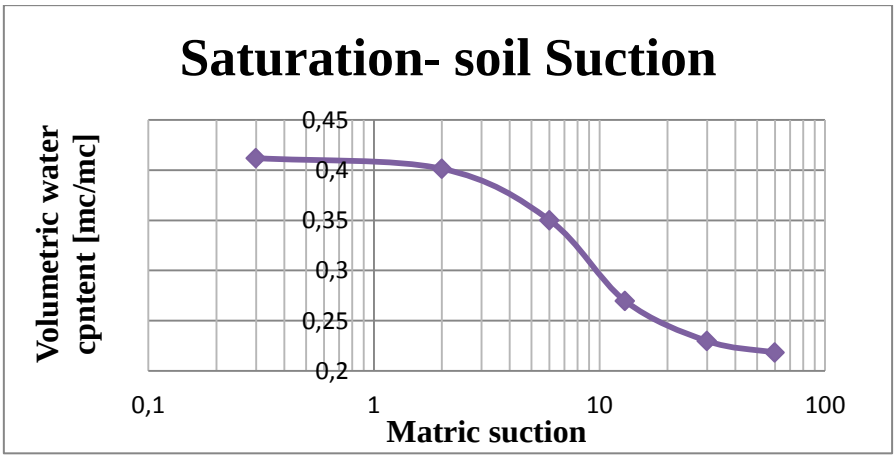

Figure 59: VWC function

By insert these data in *GeoStudio™ 2007* software, the following functions (Figure 60) were obtained.

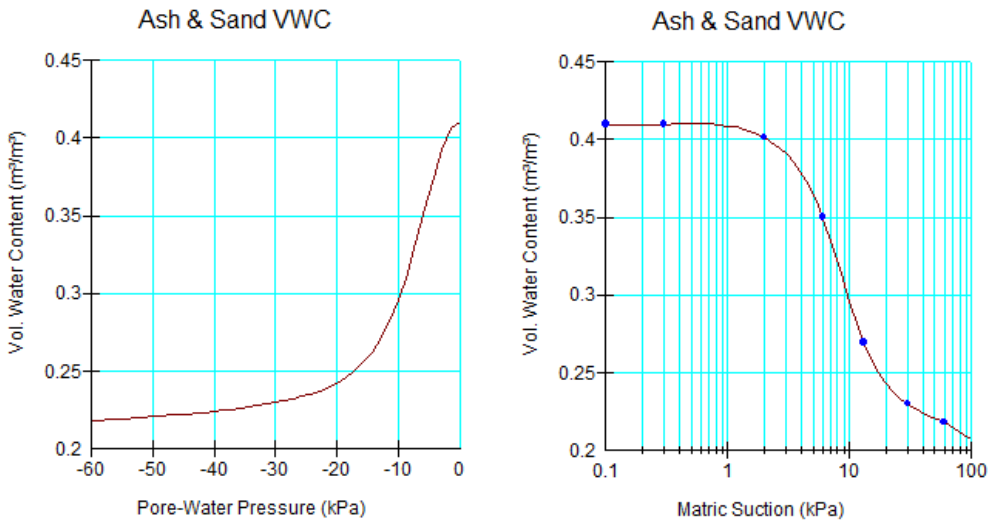

Figure 60: VWC for sand-ash mixture

The image shows the same VWC function, but the function on the right is represented in the more common way, thus with Ylog axe.

The slope of the VWC function is very steep, it means that the change in volumetric water content for increasingly negative pore-water pressures would be more than for a soil with a flatter function.

There were no sample available for the others material used to construct the dike, so the values of storage were find out in literature. The water content at saturation (equal to the porosity) became the input to estimate the VWC function.

The parameters referring to the *clay* layer were inserted in the *GeoStudio*™ software and, after specifying the kind of material, it provided the following function (Figure 61):

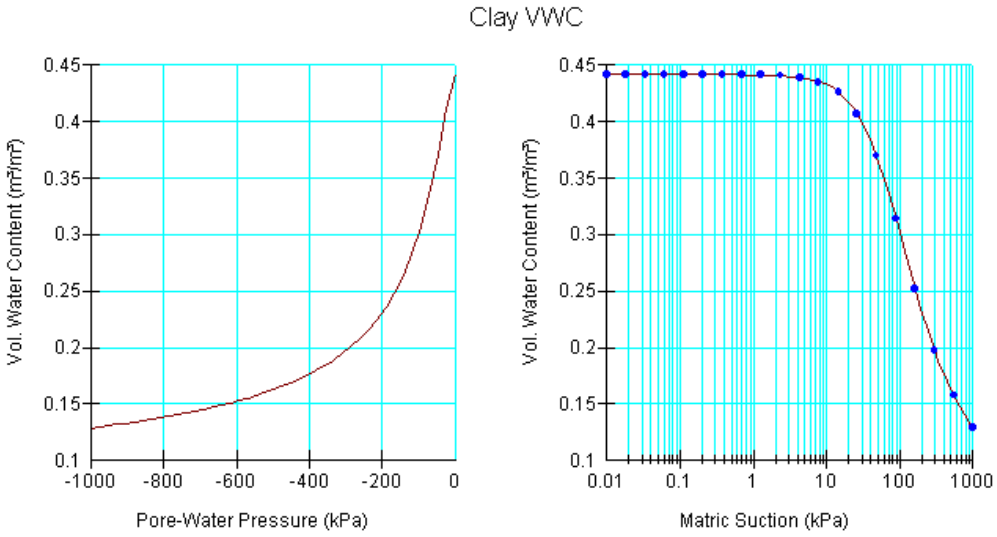

Figure 61: VWC for clay

There are not many studies concerning the properties of a Tephra-Sand material, so it was necessary make a reasonable hypothesis about the characteristics of this mixture. A study on coal ashes showed that the behavior and the dimensions of the fly ashes (used in this layer in the test dike), are similar of the ones of silt (*Prakash K. PhD and Sridharan A. PhD*, 2006), so the tephra-sand mixture was assumed to have the same characteristics of a silty-sand material. The VWC function for this layer is showed in the following image (Figure 62).

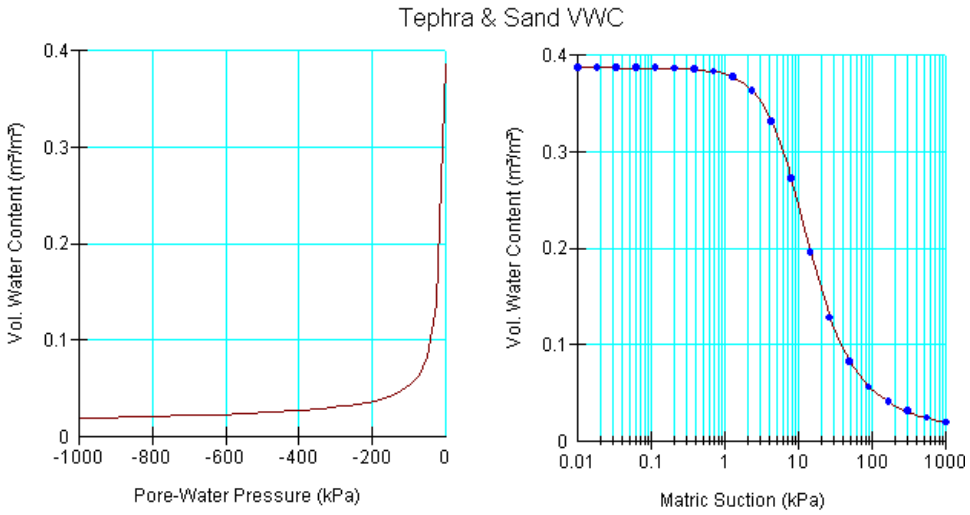

Figure 62: VWC for sand-tephra mixture

To run, the analysis needed also the definition of the hydraulic functions of the foundations ground (loam). Figure 63 shows the obtained function.

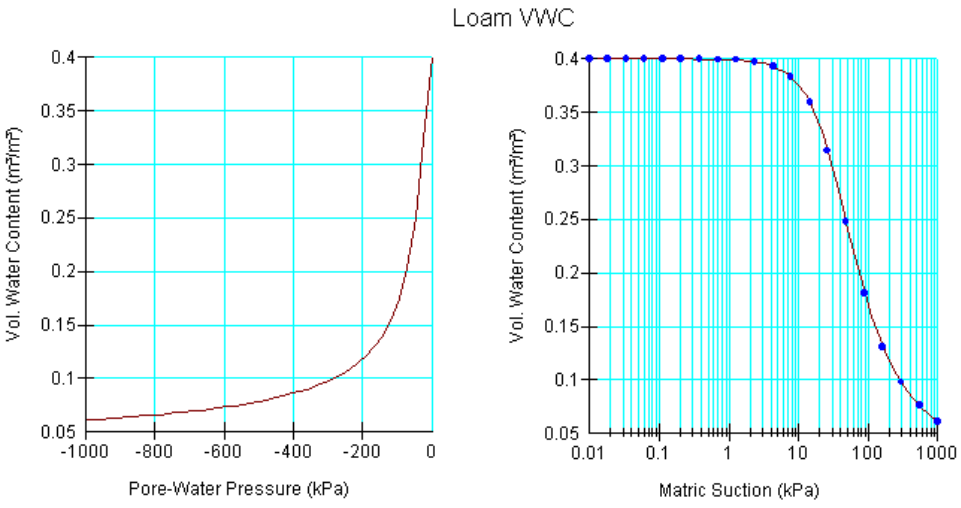

Figure 63: VWC for loam

Hydraulic conductivity

The ability of a soil to transport or conduct water under both saturated and unsaturated conditions is reflected by the hydraulic conductivity function (*GeoStudio™ Manual*, 2007).

Water can be considered to flow along a web of interconnected and continuous conduits: when the soil is saturated, all of the available conduits are utilized, and the water hydraulic conductivity capacity is at the maximum; when the water content decreases, at a certain point the air enters the largest pores (i.e. the AEV is exceeded) and the air-filled pores become non-conductive conduits to flow and increase the tortuosity of the flow path. As a result, the capacity to conduct water through the soil (the hydraulic conductivity) decreases. Ultimately, when the soil is dry, the capacity to conduce water along continuous water-filled conduits disappears.

This means, that the ability of water to flow through a soil profile depends on how much water is present in the soil, which is represented by the volumetric water content function. Since the VWC is a function of pore-water pressure and the hydraulic conductivity is a function of water content, it follows that hydraulic conductivity is also a function of pore-water pressure.

The following figure (Figure 64) presents a curve showing a typical hydraulic conductivity function and the relationship between hydraulic conductivity and pore-water pressure. Defining the hydraulic conductivity for negative pore-water pressure regions makes it possible to analyze problems involving unsaturated flow as well as saturated flow.

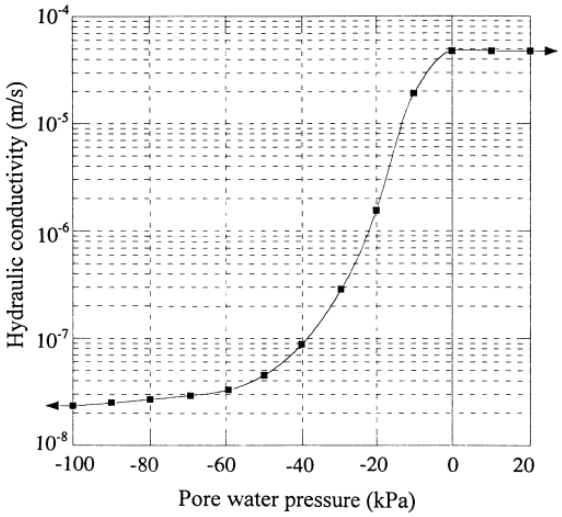

Figure 64: Hydraulic Conductivity function

Material property function: Hydraulic Conductivity function

A hydraulic conductivity function shall be specified for all materials in a problem that has an unsaturated zone. Adopting a perfectly flat hydraulic conductivity function for an unsaturated soil, as assumed in steady state analysis, can lead to unrealistic results: this occurs because with a horizontal conductivity function, water can flow through the unsaturated zone with the same ease as through the saturated zone.

For the test dike in Trzcinisko, there were no measure of the hydraulic conductivity function, so it was necessary develop the function using a predictive method that utilized the parameters of the measured volumetric water content function and the saturated hydraulic conductivity.

To performed the transient analysis, the Van Genuchten's closed-form solution (*Van Genuchten,* 1980) for predicting the volumetric water content function. The governing equation is as follows:

$$\Theta = \frac{\theta - \theta_r}{\theta_s - \theta_r} = \left[\frac{1}{1 + (\alpha|h|)^n}\right]^m$$

where:

$\Theta =$ the effective degree of saturation, i.e. the volumetric water content,

$\theta_s =$ the saturated volumetric water content,

$\theta_r =$ the residual volumetric water content

$|h| = \left|-\frac{u}{\gamma_w}\right|$ = pressure head,

α, n, m = curve fitting parameters.

The fitting parameters for the VWC curve would become the input data to calculate the hydraulic conductivity function.

An appropriate software was used to predict the unknown parameters and coefficients.

The code uses the parametric models of Brooks-Corey and Van Genuchten (Brooks R.H. and Corey A.T., 1964).to represent the soil water retention curve, and the theoretical pore-size distribution models of Mualem and Burdine (Burdine N.T., 1953; Mualem Y., 1976) to predict the unsaturated hydraulic conductivity function from observed soil water retention data (*Van Genuchten M.Th., Leij F.J., Yates S.R.*, 1991).

For the sand-ash mixture, the Van Genuchten's and the Mualem's models were used: it means that the parameter $m = 1 - \frac{1}{n}$.

The program may be used to predict the hydraulic conductivity from observed soil water retention data assuming that one observed conductivity value (not necessarily at saturation) is available.

The unknown coefficients are estimated using non-linear least squares models. Least square methods consist of finding parameters or given function to best fit data set. The fitted parameters are optimal when the squared difference between two following iterations reaches the minimum.

The number of iterations and the final results are shown in Table 18.

Table 18: Fitted parameters

NIT	SSQ	ThetaS	Alpha	n
0	.39646	.4300	14.5000	2.6800
1	.12217	.4373	3.0838	1.0050
2	.01866	.4300	110.2047	1.1111
3	.00659	.4509	58.0327	1.1052
4	.00600	.4561	50.9594	1.1083
5	.00563	.4593	46.8345	1.1121
6	.00533	.4618	43.5778	1.1158
7	.00508	.4637	40.7549	1.1192
8	.00487	.4652	38.2278	1.1224
9	.00470	.4664	35.9296	1.1254
10	.00455	.4671	33.8171	1.1281
11	.00441	.4676	31.8597	1.1307
12	.00380	.4583	17.2643	1.1418
13	.00343	.4560	17.0392	1.1467
14	.00329	.4552	16.2457	1.1499
15	.00271	.4462	9.3735	1.1637
16	.00239	.4442	9.3251	1.1693
17	.00228	.4435	8.9901	1.1729
18	.00186	.4377	6.2192	1.1876
19	.00161	.4299	3.6557	1.2173
20	.00127	.4226	2.5600	1.2559
21	.00112	.4249	2.9967	1.2512
22	.00111	.4237	2.8403	1.2574
23	.00111	.4241	2.8929	1.2560
24	.00111	.4239	2.8751	1.2566
25	.00111	.4240	2.8810	1.2564
26	.00111	.4240	2.8790	1.2565
27	.00111	.4240	2.8797	1.2565
28	.00111	.4240	2.8795	1.2565

The permeability $k(\Theta)$ is related to the saturation ($k_s = 10^{-6}\ m/s$) via effective water content Θ (*Van Genuchten*, 1980):

$$k(\Theta) = k_s\left[\sqrt{\Theta}\left(1-\left(1-\Theta^{\frac{1}{m}}\right)^{m}\right)^{2}\right]$$

The results and the relationship between the permeability and the pore-water pressure for the sand-ash mixture and the curve inserted in *GeoStudio™ 2007* software for the FEM analysis are shown below (Table 19, Figure 65 and Figure 66).

Table 19: Calculated relative permeability of the soil

Pore-Water Pressure	$u\ [kPa]$	0,3	2	6	13	30	60
Pressure Head	$h = -\frac{u}{\gamma w}[m]$	0,03	0,2	0,61	1,33	3,06	6,12
Volumetric water content	$\Theta[-]$	0,4120	0,4014	0,3502	0,2697	0,2298	0,2182
Hydraulic Conductivity	k [m/s]	2,22 E-07	3,90 E-08	5,56 E-09	9,72 E-10	1,25 E-10	2,10 E-11
Hydraulic Conductivity	k [m/day]	1,92 E-02	3,37 E-03	4,80 E-04	8,40 E-05	1,08 E-05	1,81 E-06

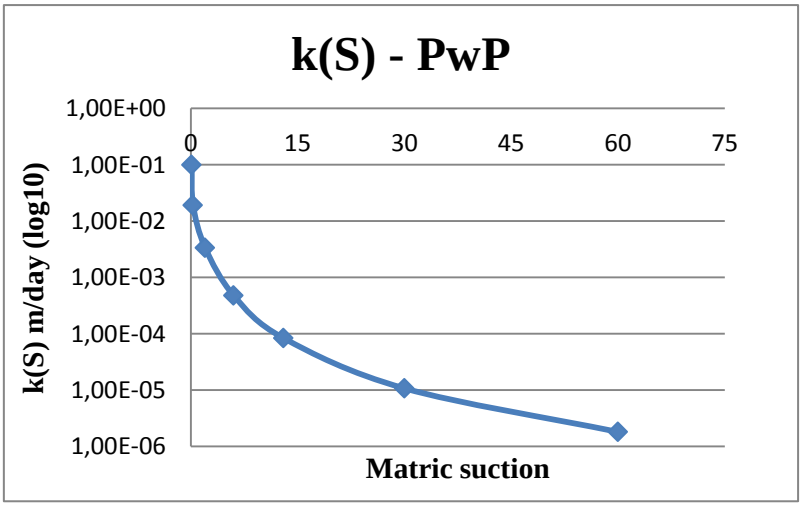

Figure 65: Conductivity function for ash-sand mixture

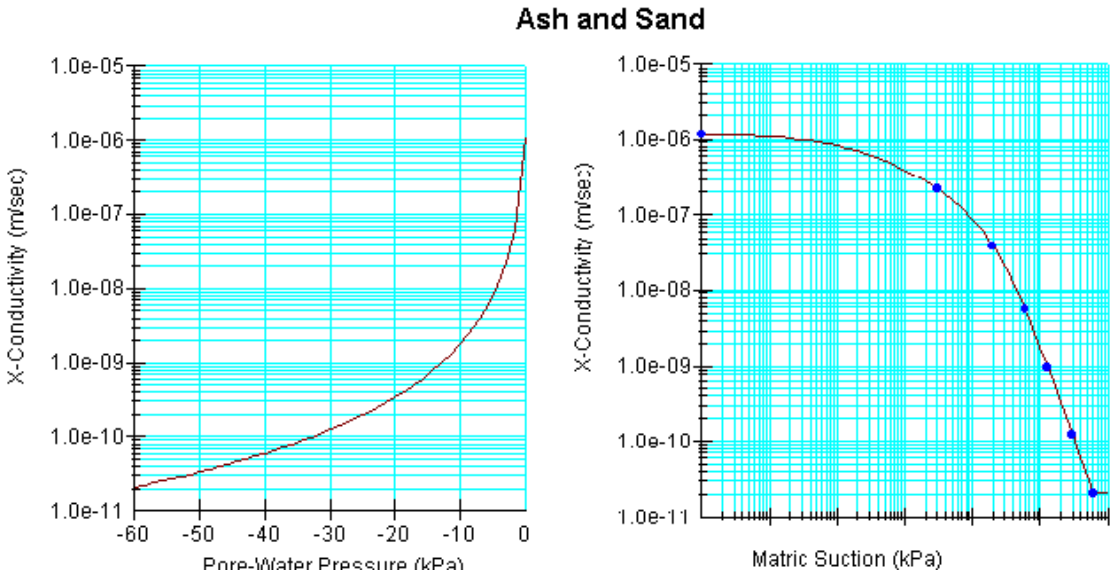

Figure 66: Hydraulic Conductivity curve for sand-ash mixture

Again, to estimate the function for the other materials, Van Genuchten equation was used. The water content at saturation (equal to porosity) and the residual water content were used as data input in *GeoStudio*™ software. The Hydraulic Conductivity functions related to the VWC curves for clay (Figure 67), tephra-sand mixture (Figure 68) and loam (Figure 69) have the following trend:

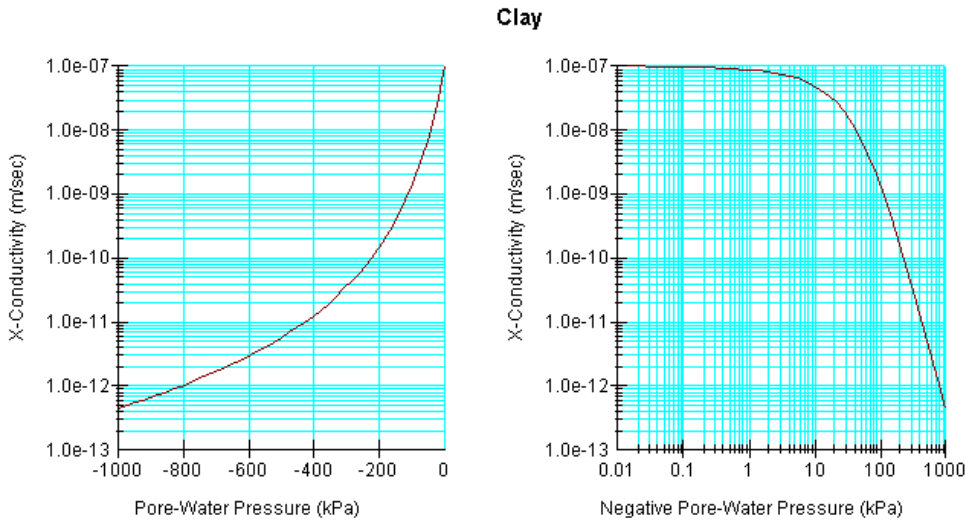

Figure 67: Hydraulic conductivity curve for clay

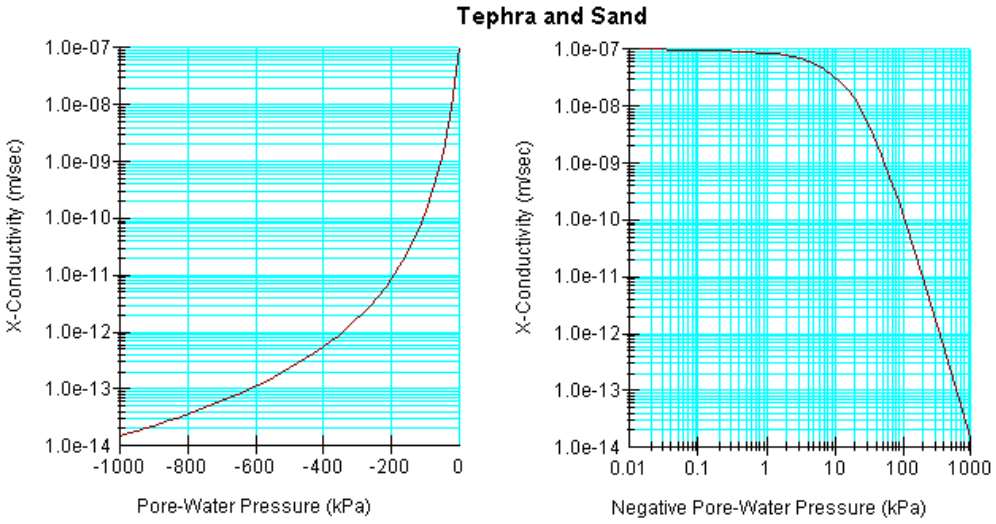

Figure 68: Hydraulic conductivity curve for tephra-sand mixture

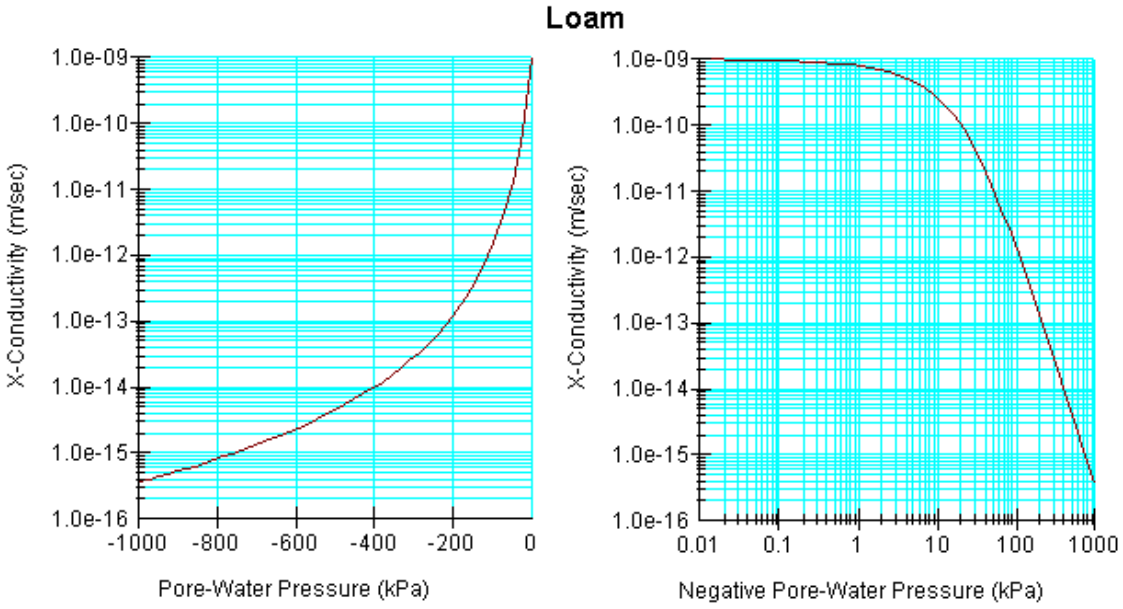

Figure 69: Hydraulic conductivity curve for loam

Figure 70 compares the conductivity functions for all the materials involved in the analysis: the material on riverside is the most impervious, while the core is the most

permeable. The clay present a low conductivity at saturation, but it does not decrease very much as the suction decreases.

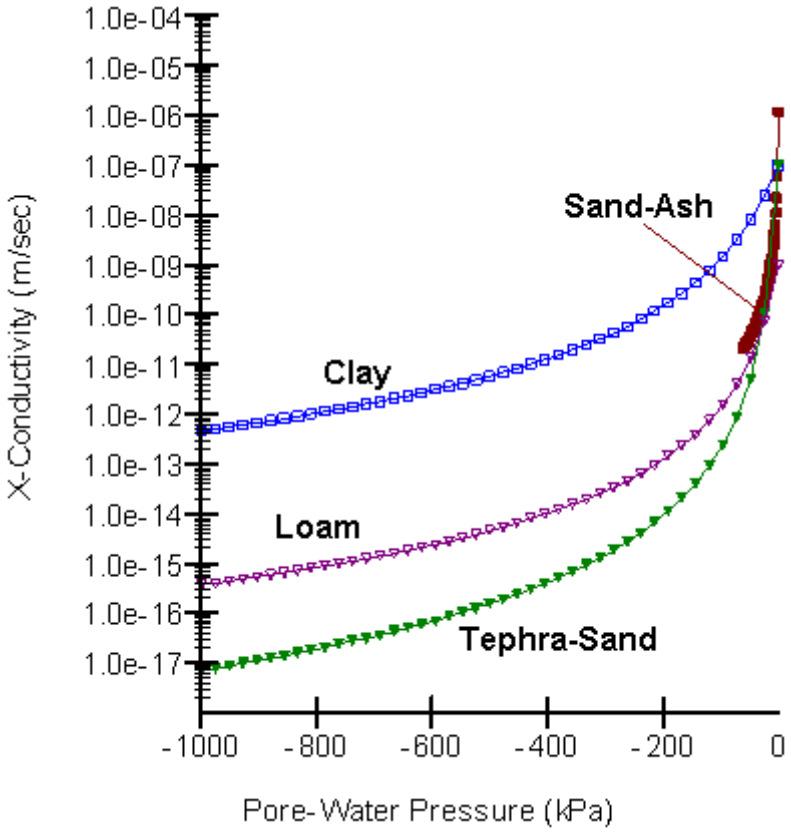

Figure 70: Comparison between hydraulic conductivity of different materials

Transient seepage problem. Fill of the reservoir

The first transient analysis performed, was the one concerning the flow thorough the dike during the filling stage of the reservoir.

For this kind of analysis, the software *GeoStudio™ 2007 (SEEP/W DEFINE)* has been used.

Initial conditions

For a transient analysis, it is essential to define the initial soil pressure conditions (*Total Head*) at all node. In this case the initial conditions are established by running a steady-state analysis, as in the reservoir the height of ponded water was 0,1 m.

Obviously, the same geometry and the materials of the steady-state analysis performed before have been used, and also the same type of boundary conditions: *Total Head* in the upstream side equal to 0,1 m, and *Total Flux (Q=0)* on the downstream side. In simple soil groundwater analysis, soil's permeability function may be treated constant.

The initial condition that has been assumed was the level in the reservoir equal to 10 cm. The following figure (Figure 71) shows the results of the steady-state.

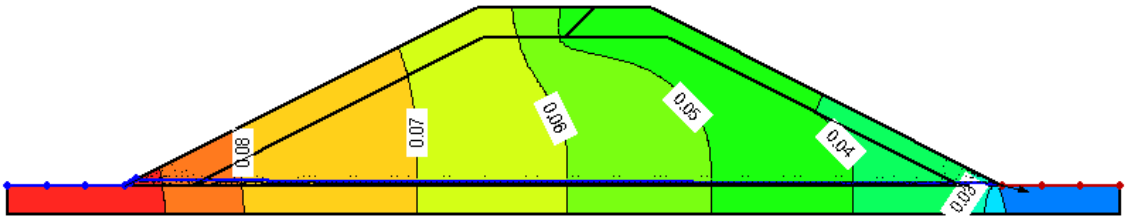

Figure 71: Results of steady-state analysis (10 cm)

Boundary conditions

In a steady state analysis, all of the boundary conditions are fixed values. In a transient analysis, the conditions on the boundaries may change with time, thus, boundary conditions can be functions.

The level in the reservoir takes a finite time period to change, therefore, to simulate the fill of the reservoir, the following Head-versus-Time boundary function has been applied to the upstream face (Figure 72):

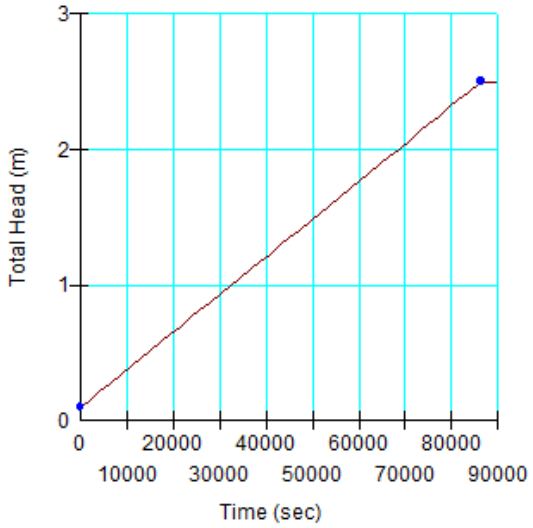

Figure 72: Hydraulic boundary function. Fill of the reservoir

It means that, starting from the steady-state analysis described before, every hour there is a 0,1 m water level rise, so 24 hours (i.e. 86.400 sec) are necessary to completely fill the reservoir.

Time steps

The time steps are the last things that need to be specified before running the transient analysis.

To run the groundwater transient analysis for the dike in Trzcinisko, a 50 days-long period was analyzed. It was divided in 20 steps, and it was chosen an exponential time increase sequence, with initial increment size equal to an hour.

Results

The figures in this sections (from Figure 73, to Figure 76) shows the results of the transient analysis, under the non-reasonable hypothesis that the level in the reservoir, after 24 hours rising, remains the same until the system reach the steady-state condition.

The time period of 50 days chosen results adequate to describe the several steps of the groundwater analysis.

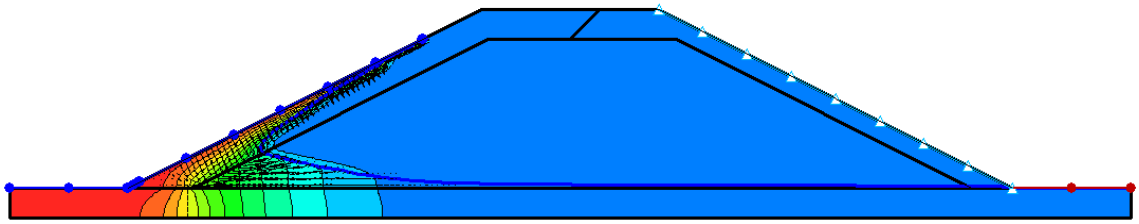

Figure 73: Water table after 24 hours (filled reservoir)

When the reservoir reaches the maximum height of water (equal to 2.5 m), the impermeable layer at riverside dissipates a big part of the hydraulic load: in fact, the level of the phreatic surface at the boundary between tephra and sand and the core of the dike is 0,58 m (Figure 73).

The phreatic surface arrives at the downstream side after 14 days (Figure 74). The levee must preserve the water filtration for the time of flood, that is typically considered 14 days long. That means that the test dike constructed fulfills its function and the materials can be used in building embankments.

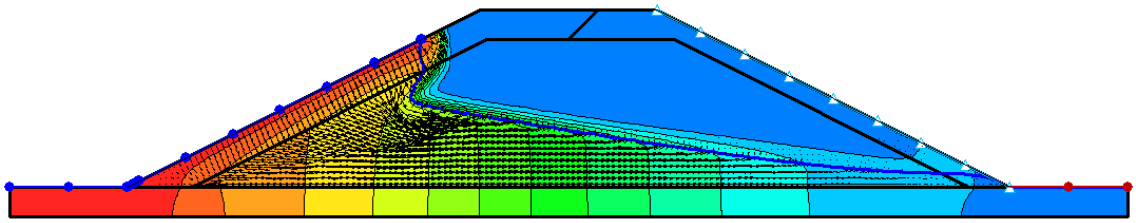

Figure 74: Water table after 14 days (filled reservoir)

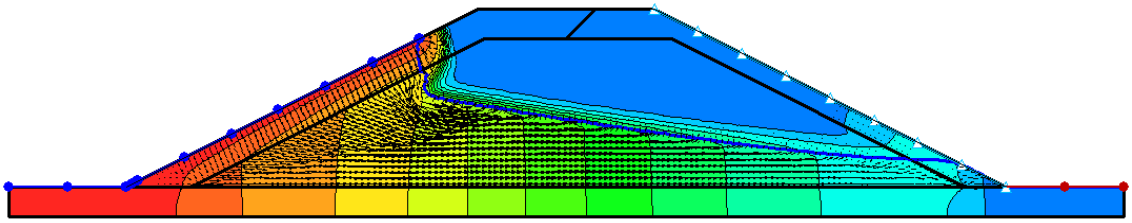

Figure 75: Water table after 20 days: phreatic surface at downstream side

After 20 days (Figure 75) the seepage through the levee flows out at the downstream face of the dike at 36 cm height. The toe of the dike begins to be under pressure, also in this case, an evaluation of the pore-water pressure is required. It is necessary to verify that the weight of the clay layer can resist to th pressures, i.e. $S_w < \gamma_{sat}.V$, at the interface between the core and the top layer. Here, the pore-water pressure is $PWP = 2\,kPa$, so the upward buoyant force is given by: $S_w = PWP * A = 0{,}3\,kN < 2{,}85\,kN = \gamma' V$. The stability of the toe in the external layer is ensured.

Finally, after 50 days (Figure 76) the water exit height is 1 m, this means that the dike need more than 50 days to arrive at steady state conditions.

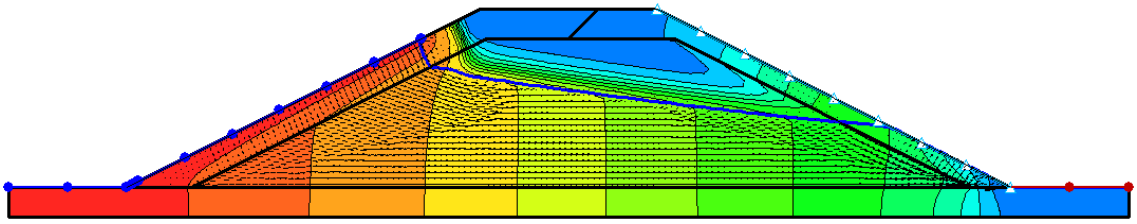

Figure 76: Water height after 50 days

Different speed of the reservoir filling

A similar analysis was conducted, to evaluate which differences occur if the reservoir fills with a double speed (0,2 m/hour) or half speed (0,05 m/hour) respect the previous study. In both this case the level in the reservoir remains the maximum after filling.

The phreatic surface arrives at downstream side after 11 days, thus faster as the previous situation. If rapid filling (0,20 m/hour) occurs, after 20 days the water exit level is 0,41 m, and it is possible to have problems of particles displacement.

If the reservoir fills with a rapidity of 0,05 m/hour, the water line reaches the slope of the levee after 14 days, but is a little minor than the other situation, because after 20 days the water exit height is 0,32 m.

The different speed in filling the reservoir does not lead to very different result, so to extend the moment in which the water arrive at downstream side, a change in other parameters is necessary.

Different thickness of the tephra and sand layer

The analysis has been run again after changing the thickness of the riverside layer: from 0,5 m to 0,7 m and 1 m. The level in the reservoir is assumed constant, after 24 hours of filling, and equal to 2,5 m.

For 0,7 m thick layer, the water needs one more day to reach the downstream side, and after 20 days the level of the phreatic surface is 0,22 m high, so there is no problem of particle's displacement in 20 days of maximum level in the reservoir. Problems occur after 22 days, as the height of the water line is 0,30 m.

With a 1 m thick riverside layer, the water needs 17 days to arrive at downstream side, and the problems of breaking in the toe of the dam start to happen after 25 days, with the water exit height equal to 0,29 m.

Changing the thickness of the tephra-sand mixture layer, allows to increase the number of days necessary to the water to arrive to downstream side, and so the period of flood without problems in the toe of the levee is extended.

Different riverside layer

In this section, the different results obtained changing the material of the more impervious layer are evaluated.

First, it was assumed to build the external layer only with clay (Figure 77).

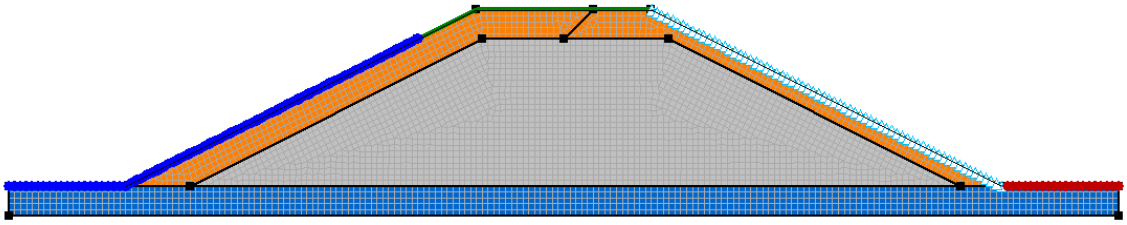

Figure 77: External layer made up with clay

The water in the reservoir increases its level 0,1 m/hour speedy, and the water exits from the dike after 10 days, so the dike's toe starts to be under pressure before respect the previous analysis.

Then, it was assumed to use a material with very low permeability at saturation: $k_s = 10^{-8}\, m/s$. The material has been considered as a silty sand and the new conductivity function is the following (Figure 78).

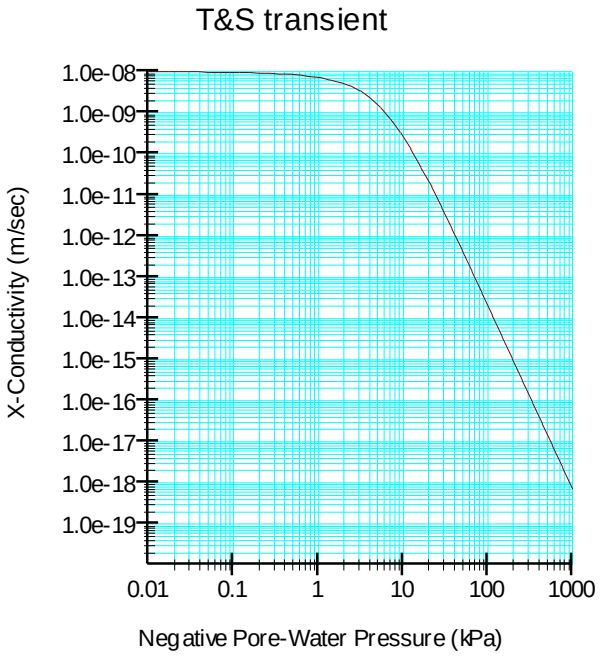

Figure 78: Different impervious material's conductivity function

In this condition, the phreatic surface arrives at downstream side after 38 days. Changing the riverside layer confirms to be the best way to prevent the flow through the embankment.

Insertion of a drain

The transient analysis was performed also for a dike after the introduction of a 2,5 m long drain in the downstream toe.

The material property functions remains the same, as the time steps and the initial conditions. To model the drain in *GeoStudio™ 2007* it was decided to use the *Pressure Head* boundary condition: the pressure is assumed equal to 0, such as the pressure in the drain is the atmospheric one.

After 24 hours the level in the reservoir stops to rise and remain constant in time. By inserting a horizontal toe-drain in the downstream of the dike, the system takes only 27 days to arrive at steady-state condition.

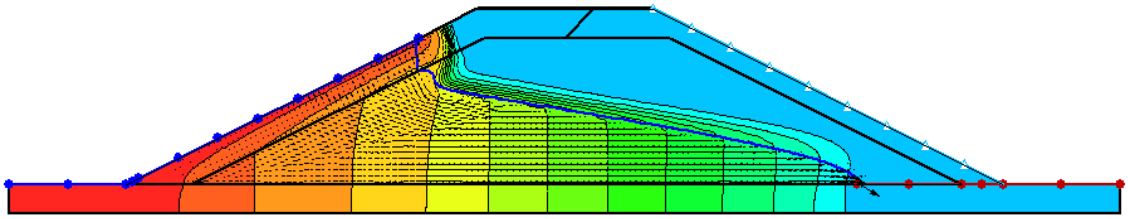

Figure 79: Transient analysis with a drain

The insertion of a drain in the dike's basement is a good way to prevent damage in the toe of the levee, because the water will not arrive at downstream side.

Monitoring

A different way to prevent the exit of the water at downstream side is to provide the monitoring of the level in the reservoir: after filling, the level in the reservoir was assumed constant as maximum for 7 days (a reasonable time for flood condition). After this period it was considered decreasing in a linear way: 0,05 m/ hour, so it needed 48 hours to go back to initial conditions, as shown in Figure 80. The empting must be slow, in order to avoid instability for excessive pressure that cannot be dissipated on upstream side (as analyzed in next transient seepage problem) (Figure 80).

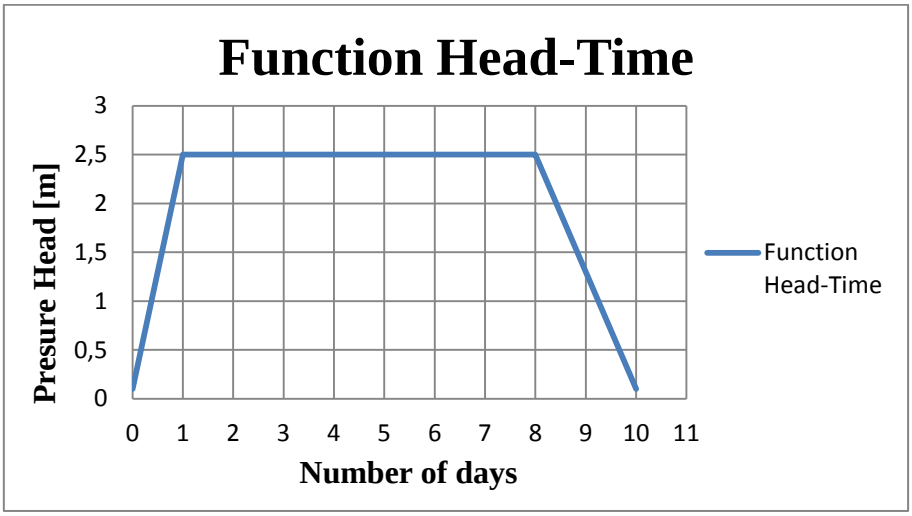

Figure 80: Hydraulic boundary function. Drawdown after 7 days

After 10 days the level in the reservoir remains the minimum (0,1 m) until the end of the analysis. The period of time chosen for this analysis was a 60-days long period.

After 7 days, the phreatic surface does not arrive to downstream side; the level in the reservoir start to decrease and it takes 48 hours to completely empty. The water flows now through upstream side, and it is necessary to check that instability will not occur (as examined in the next chapter). The water line start to decrease on riverside, while it increases on the opposite site because of the seepage through the embankment.

On the 14th day from the beginning of the analysis, the water arrives to downstream side. From this moment there is flow through both side of the embankment and it is necessary to verify that problems for particles displacement do not happen.

After 60 days of observation, the water table on upstream side is still 0,5 m high, and the water exit happens mostly from this side.

On downstream side, the level of phreatic surface remains low (around 0,1 m): due to the impervious core of the dike, the hydraulic load is dissipated in the dam, so only a little part of the water exits from this side of the dike and the toe is not under a high pressure.

Summarizing, the seepage through the dike does not leads to damage in downstream side toe using this kind of monitoring plan of the level in the reservoir.

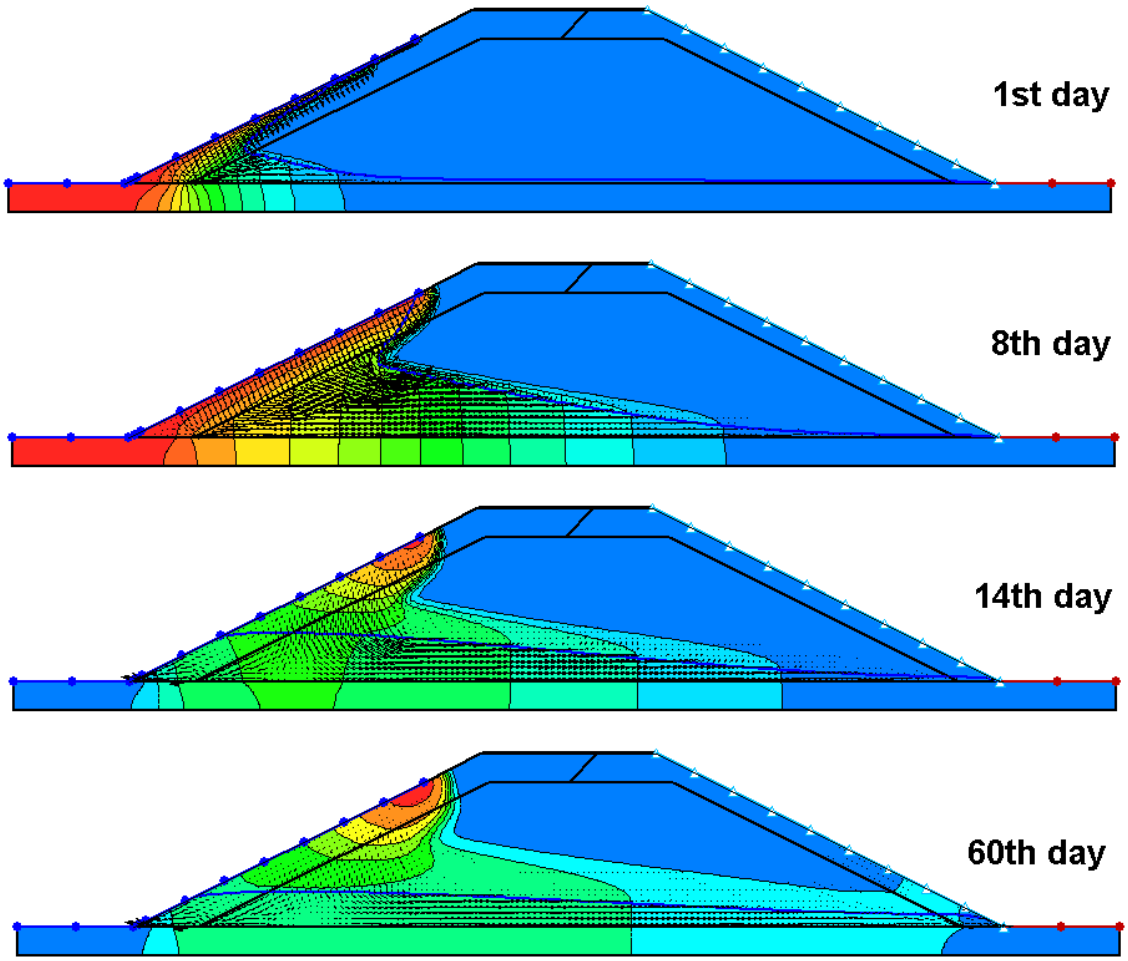

Figure 81: Wetting up and down. First monitoring plan

The analysis is repeated, imaging an exceptional flood: the level of the water in the reservoir rises in 24 hours, it remains constant for 12 days and finally it decreases in 2 days. In next pictures the blue line correspond to the function of first monitoring plan; the red one concerns the current analysis.

Again, after emptying, the level in the reservoir remains constant and equal to 0,1 m.

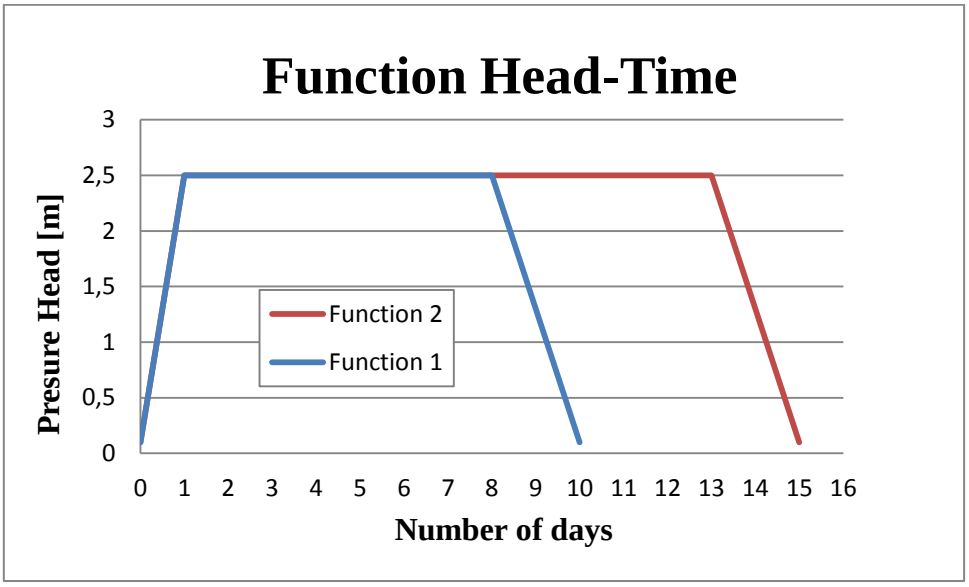

Figure 82: Comparison between function of first and second monitoring plan

After 13 days from the beginning of the filling of the reservoir, the phreatic surface arrives to downstream side, so it is necessary to verify that problems of filtration and excessive pressure will not occur in the toe of the dike also before emptying the reservoir. As it is shown in the figure below (Figure 83), after 60 days the piezometric line's height in downstream side is 0,22 m. Because of the long period of evaluation, we can assume that this will be the maximum water exit height from this side of the dam, so we can say that the toe at downstream side will not present any damage during a flood, not even for outstanding events.

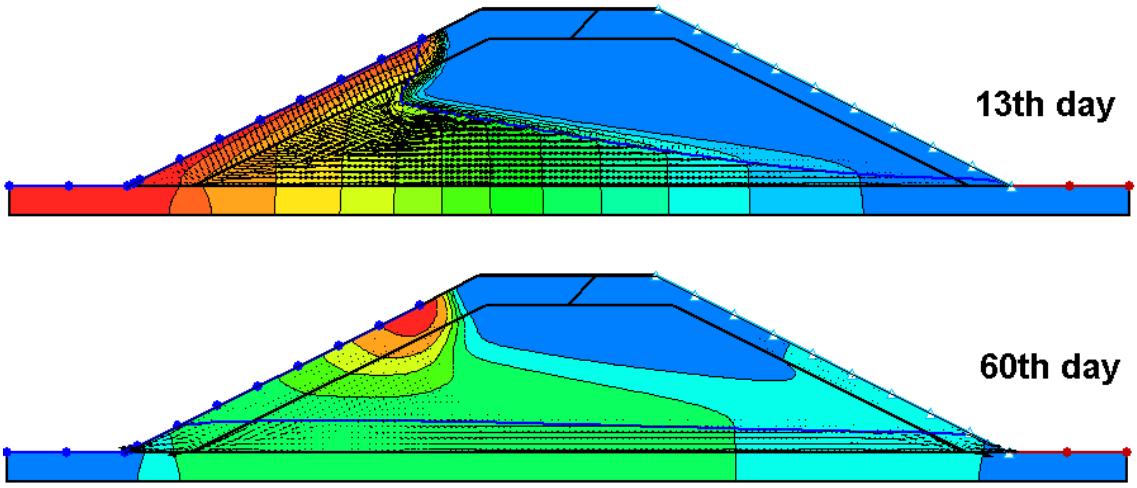

Figure 83: Wetting up and down. Second monitoring plan

Transient seepage problem. Rainfall

In this chapter a transient FEM analysis during rainfall is performed.

The same model described in previous analyses is use, but this time is also necessary to consider the amount of rainwater infiltrated.

Referring on the graph in Figure 84, the average rainfall is determined, considering the rainfall and the wet days in June: the amount of rain per hour is estimate equal to $q = 6{,}5\, e^{-008}\, m/s$.

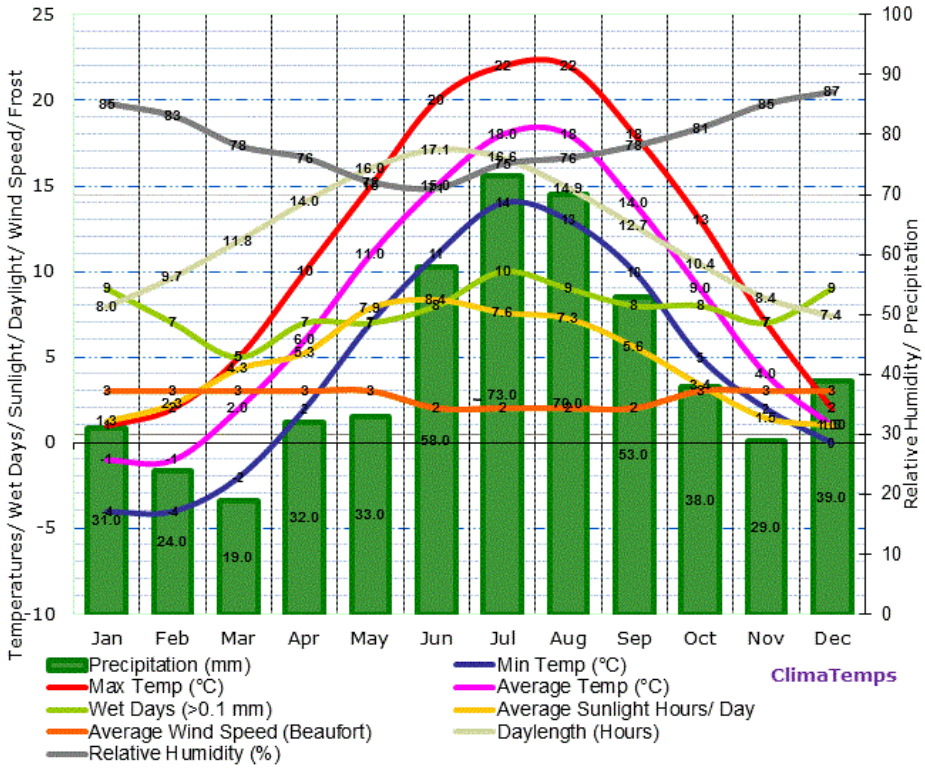

Figure 84: Gdansk, Poland climate graph (altitude 12m)

This datum is inserted as a *Unit Flux (q)* boundary condition, to simulate the rain entering the soil.

The transient analysis is subdivide in 2 steps: firstly I considered 24 hours of rainfall with the water level in the reservoir remaining equal to 0,0 m, after this time the reservoir starts to fill, and it takes 24 hours to arrive at maximum level. This is the same boundary condition assumed in the first transient analysis performed during the filling of the reservoir: the aim of the analysis in this chapter is making a comparison between the behavior of the soil with or without initial saturation of a part of the embankment.

Figure 85 shows the boundary conditions assumed and the results obtained from the analysis after 24 hour of rainfall. The rainfall infiltrates mostly in downstream side, since the clay's permeability is higher than the one of upstream side layer. The soil within the embankment starts to saturate close to both the upstream and downstream side toe.

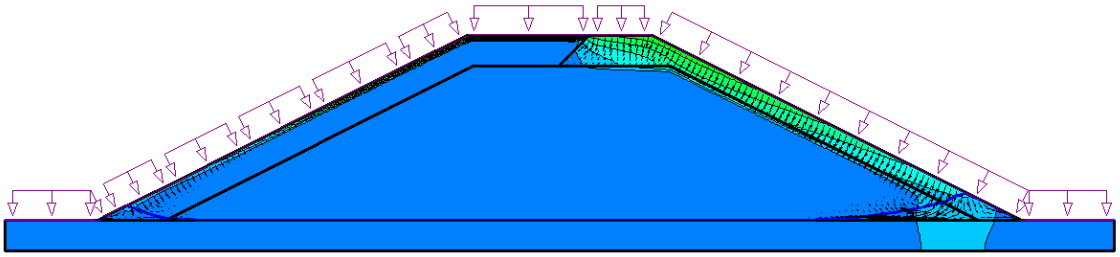

Figure 85: Water level in the embankment after 24 hours of rainfall

The second stage of the analysis begins when the rainfall stops: the water level in the reservoir starts to raise up 0,1 m every hour, so the reservoir takes 24 hours to fills. Afterwards the water level in the reservoir remains constant and the behavior of the piezometric line within the dike is evaluated during the next days.

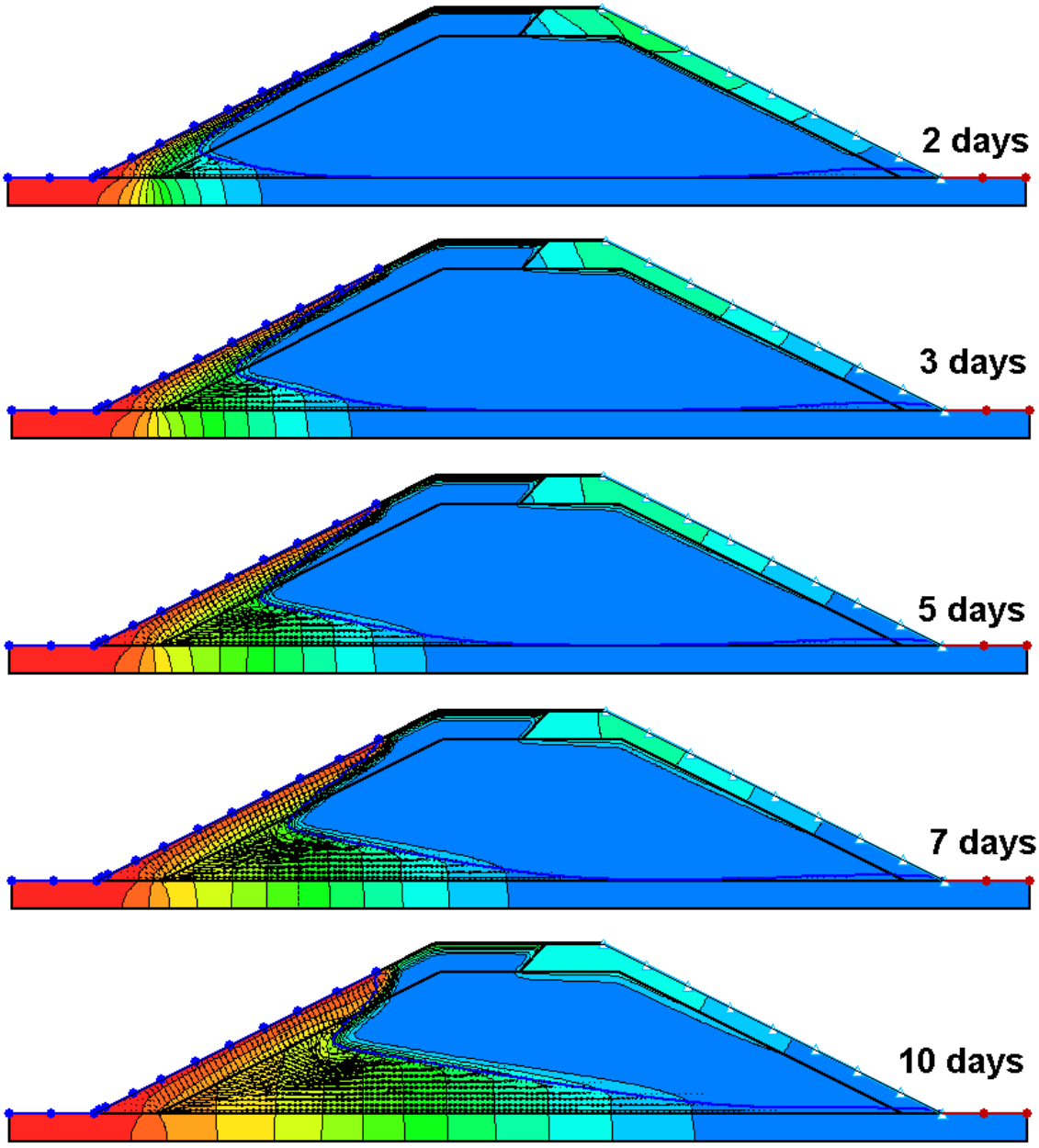

Figure 86: Piezometric level after filling the reservoir

After one day of rainfall, the phreatic line takes 10 days to reach the downstream side slope, while it took 14 days considering the soil within the embankment not saturated.

This means that an increasing in the permeability of the materials occurs, comparing to previous situation, due to the presence of saturated soil in the embankment: the permeability function is derived from the suction curve, which depends on the initial

water content, as a consequence, the water flow is strongly dependent on the initial soil water content. If the soil is saturated, the water flows more easily, and the permeability increases.

The first rainfall analysis has been performed again considering 48 hours of rainfall; the water level in the reservoir remains equal to 0,0 m for 24 hours, after this time the reservoir starts to fill, and it takes 24 hours to arrive at maximum level.

Figure 87 shows the boundary conditions assumed and the results obtained from the analysis after 24 hour of rainfall.

Since it is not possible to assign two different boundary conditions to the same node, this stage of the analysis was subdivide in four steps, making the water level in the reservoir increasing for 0,6 m each step, and considering water infiltration on the remaining boundaries. The reservoir takes 24 hours to fill, and in Figure 87 the increasing height of phreatic surface is shown.

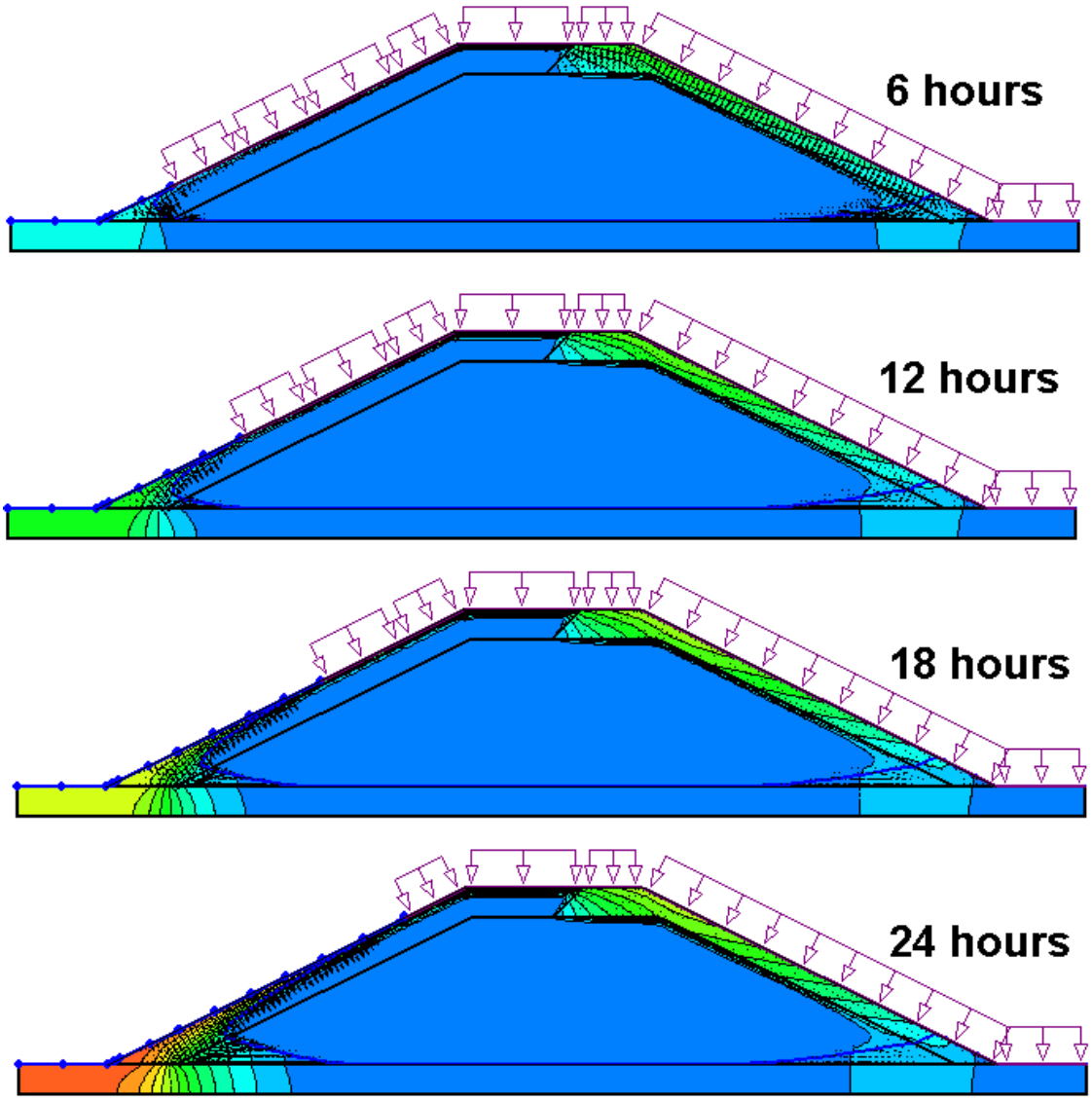

Figure 87: Piezometric level during both rainfall and filling of the reservoir

The maximum water level in the reservoir is assumed to remain constant for 10 days, in order to evaluate the time required for the piezometric line reaches the downstream side slope, that is only 7 days.

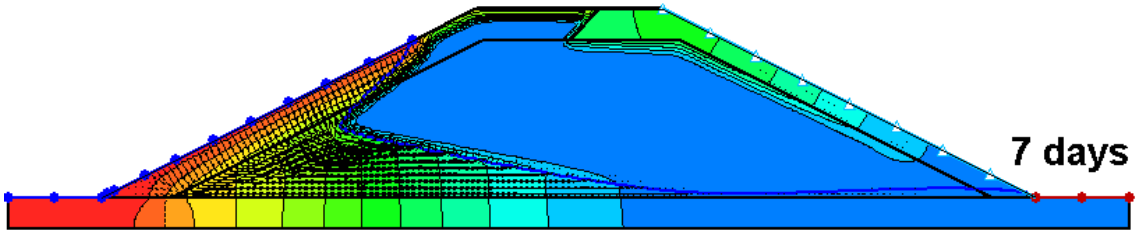

Figure 88: Water level after 7 days

This analysis shows the importance in considering the infiltration of rainwater to evaluate correctly the groundwater seepage.

In reality, the water content in the structure is unknown. The permeability and consequently the water flow are strongly dependent on the initial soil water content, therefore, it is necessary to consider in the analyses different soil humidity conditions.

Drawdown

Failure of an embankment dam can result from instability of either the upstream or downstream slopes. The critical stages for the downstream slope are at the end of construction and during steady seepage when the reservoir is full (as seen before). The critical stages in an upstream slope are at the end of construction and during rapid drawdown.

Embankments may become saturated by seepage flow during a long term high reservoir stage. If the reservoir is drawn down quickly, can happen that the pore-water cannot spillage, so high level of pore-water pressures and consequently reduced stability will result. This is called drawdown.

The case in which the water has to be quickly lowered in presence of impermeable material in the dam slope, so that the phreatic line falls very slowly, is a common problem (*Tho X. Tran*, 2004).

The stability of slopes under drawdown conditions are usually analyzed considering two limiting conditions, namely slow and rapid drawdown. In the slow drawdown situation the water level within the slope is assumed to equalize the reservoir level at any time. In case of rapid drawdown, it is assumed that the pore-water pressure within the embankment continues to reflect the original water level. The lag of the phreatic line depends on factors such as: permeability of soils, drawdown rate, drawdown ratio and slope gradient.

The drawdown is known as one of the most dangerous conditions for the upstream slope. When the water level adjacent to a slope drops rapidly, the total stresses in the slope are reduced, and the soil is in a state of undrained unloading. At the same time, the stabilizing effect of the water at the slope surface is removed, and shear stresses increase.

The rapid drawdown problem is shown schematically in Figure 89. Soils inside the dam body remain saturated and seepage commences from it towards the upstream slope. Unloading from drawdown will cause a decrease in pore pressures within the embankment. At the same time, the increase in shear stress may either raise or lower pore pressures. These pore pressure responses are stress dependent and are difficult to accurately predict. Since the soil shear strength is directly related to the pore pressure, the appropriate strengths for rapid drawdown are hard to evaluate.

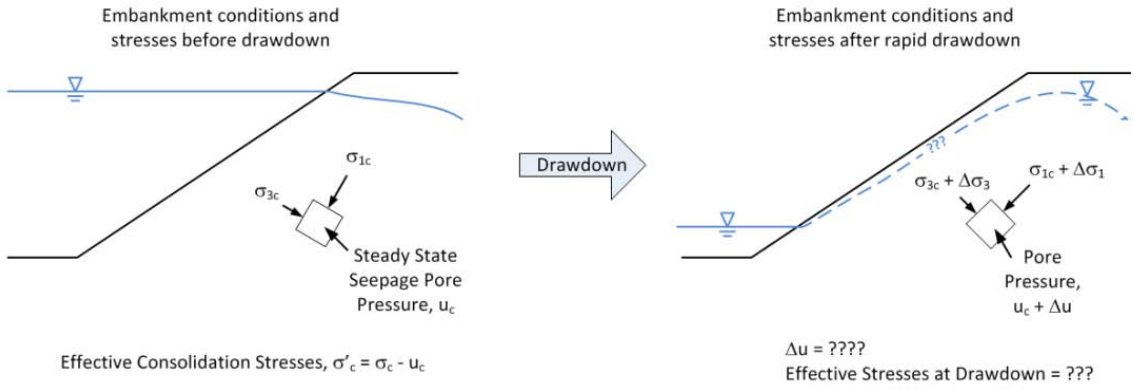

Figure 89: Stress conditions resulting from rapid drawdown

Many different total stress and effective stress stability methods have been developed to analyze the rapid drawdown condition (*VandenBerge*, 2012). The total stress methods follow the traditional geotechnical approach to rapid loading problems by including the effects of pore pressure change (Δu) implicitly in the strength model; effective stress solutions attempt to predict Δu explicitly and calculate strength using drained shear strength parameters. Any case, rapid drawdown analysis remains one of the most misunderstood cases in slope stability, but the need to study the slope stability of earth fill dams during drawdown is necessary.

Slow drawdown

In this situation the water level within the slope is assumed to equalize the reservoir level at any time. The reservoir is drawn down as fast as the pore water can escape, so no excess pore water pressures results.

To model this kind of drawdown a *GeoStudio*™ analysis was performed, using the same model described before.

As in the previous analysis, also in this case the initial conditions are established by running a steady-state analysis. The initial boundary conditions for this analysis are the last ones respect the case of the filling reservoir: *Total Head* equal to the maximum level in the reservoir (2,5 m). The Figure 90 shows the results of the steady-state analysis.

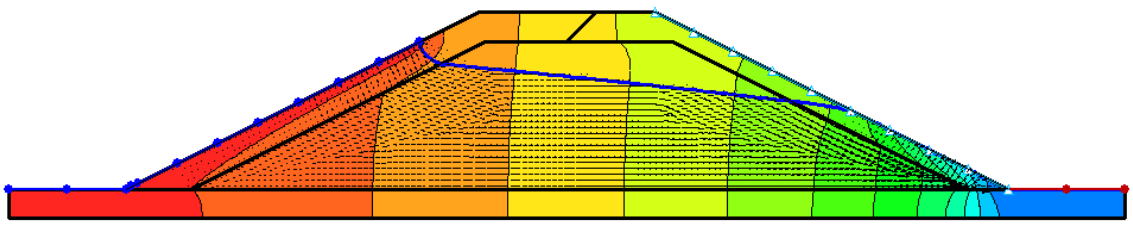

Figure 90: Initial conditions derived from steady state analysis

The water level is considered decreasing in a linear way: it decreases 0,25 m each day (about 0,01 m/hour), so the reservoir takes 10 days to completely empty. This assumption is unlikely, because it is a long period to emptying the reservoir, but in this way the dissipation of excess of pore water pressure is ensured.

A Head versus Time function with the Q=0 if H < 0 elevation option has been specified on the upstream of the dam. The new function used is shown in Figure 91:

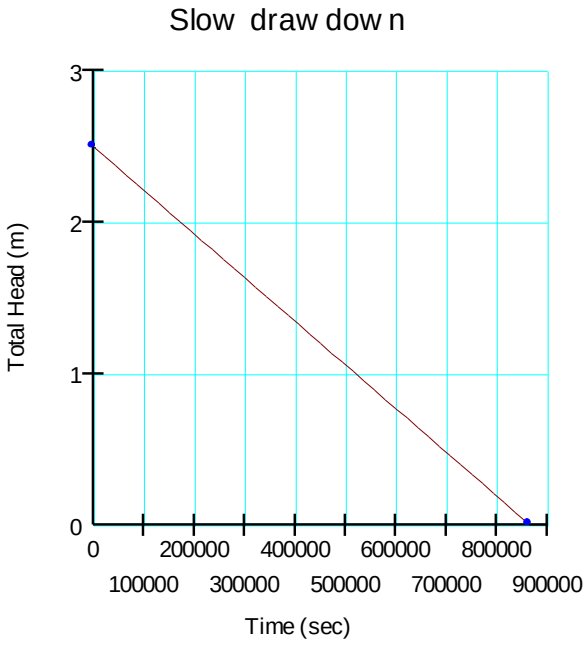

Figure 91: Hydraulic boundary function for slow drawdown

To run this analysis, a 40 days-long period was analyzed, divided in 10 steps: after 10 days of drawdown, the level in the reservoir was assumed to remain constant and equal to 0,0 m for the following month. The behavior of the seepage through the embankment was then examined.

To define the time steps it was chosen an exponential time increase sequence.

Figure 92 shows the result of the seepage analysis.

Initially, the phreatic surface level in the reservoir decreases as the water level in the reservoir, and there is seepage flow only toward the downstream side's toe. When the water passes the level of $H/2$ (H=2,5 m), as happens the fifth day, the water starts to flow toward the upstream side. After this moment, the water will flow toward both dam's toe until empty the embankment.

In Figure 93, it is evident how, also after 40 days (i.e. 30 days with water level equal to 0,0 in the reservoir), a big portion of the dam is still saturated: the water drains slowly because of the high impermeability of the external and inferior layers.

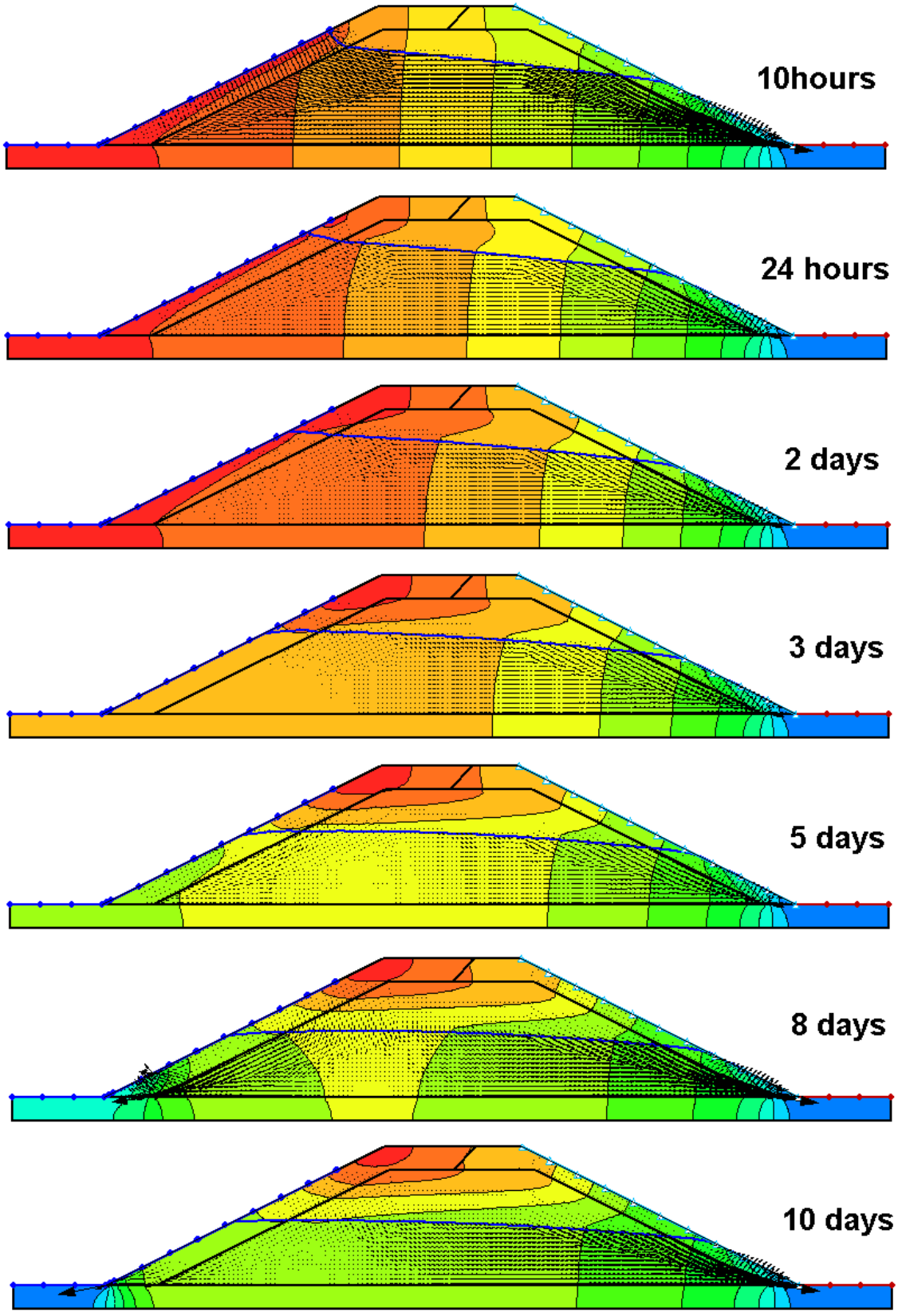

Figure 92: Slow drawdown during emptying of the reservoir

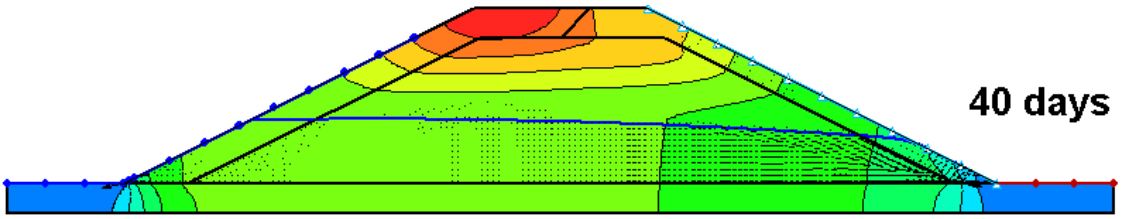

Figure 93: Phreatic surface after 40 days (30 days of empty reservoir)

The slope stability during the slow drawdown has been evaluated. To run the FEM analysis, the previous seepage results have been used as input data.

The limit equilibrium method according to Morgerstern and Price (*Morgerstern N.R., and Price V. E.*, 1965) is applied to define the potential slip surface and calculate the factor of safety of the dam slopes. The failure area is assumed and divided into a number of sections.

The equilibrium of each section is considered and finally a factor of safety for the assumed slip surface is determined, considering the equilibrium of the whole mass. The potential slip surface and factor of safety are iteratively determined until a critical slip surface and minimum factor of safety have been found.

In this analysis, each type of failure surface would be taken into account, and not only the circular ones, as happened with Bishop's simplified method (*Bishop A.W.*, 1955).

First of all the slope stability of steady state analysis has been studied. As shown in Figure 95 the safety factor obtained is equal to 7,264, so the stability is largely verified. This is due to the stabilizing effect of the water pressure on the upstream side slope. When the water in the reservoir is at the maximum level, the potential failure surface dominantly takes place in the downstream slope: the more probable failure mechanism is the breaking of the downstream side toe due to high pore-water pressures developed and to the internal erosion, and the fact that soils in the dam tend to displace to the downstream slope.

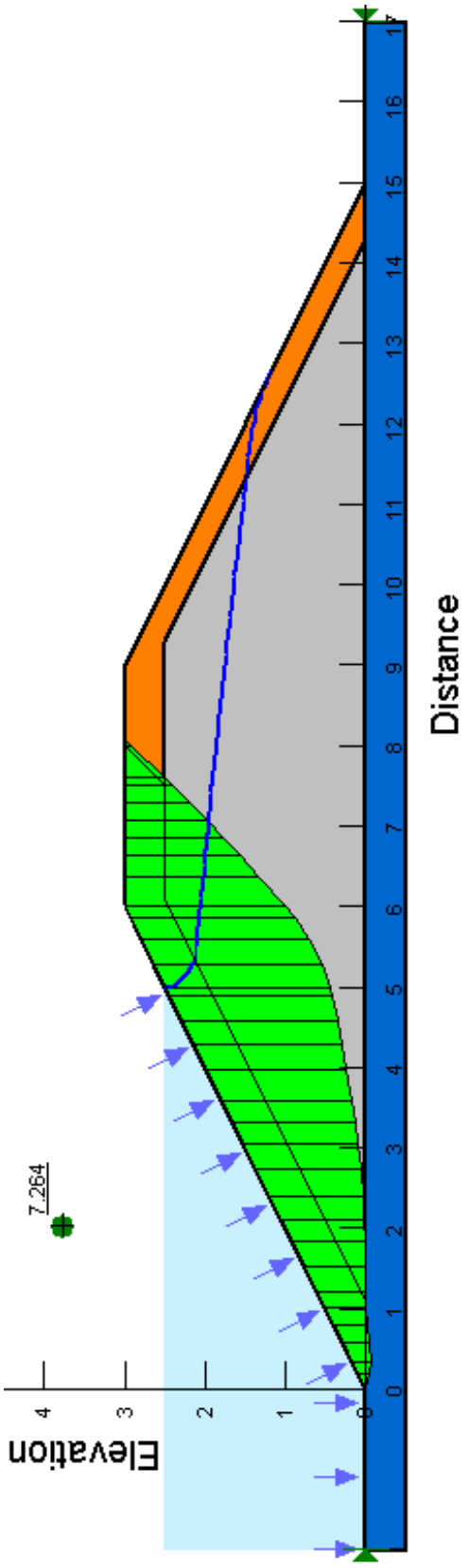

Figure 94: FS=7,264 at steady state conditions

Since the water level commences to lower, soils change to move from the upstream to the upstream slope. The potential slip surface or failure mechanism changes to occur in the upstream slope. When the water just passes the level of $H/2$, the upstream slope is dominant to be destabilized to the downstream one. The potential mechanism of collapse occurs in the upstream and moves from the dam crest to ground level.

From Figure 95 to Figure 104, the factors of safety obtained from the FEM slope stability analysis are shown.

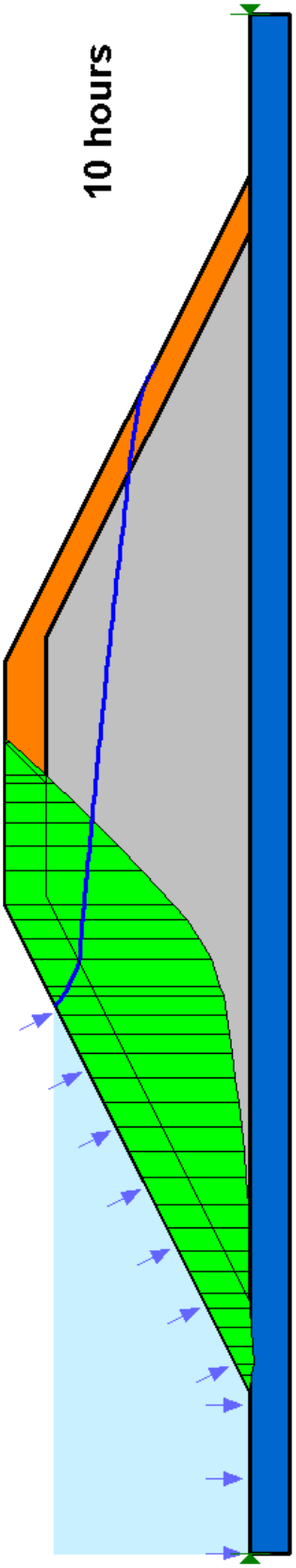

Figure 95: FS= 6,781after 10 hours

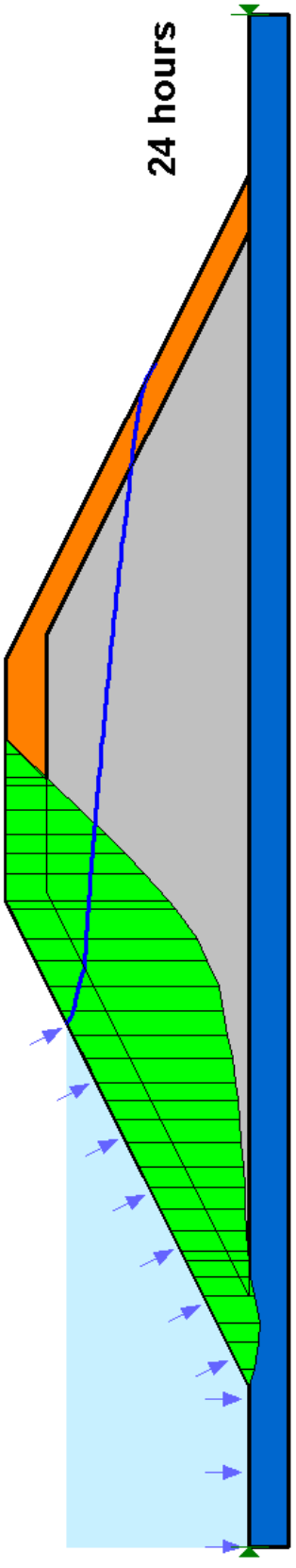

Figure 96: FS=6,341 after 24 hours

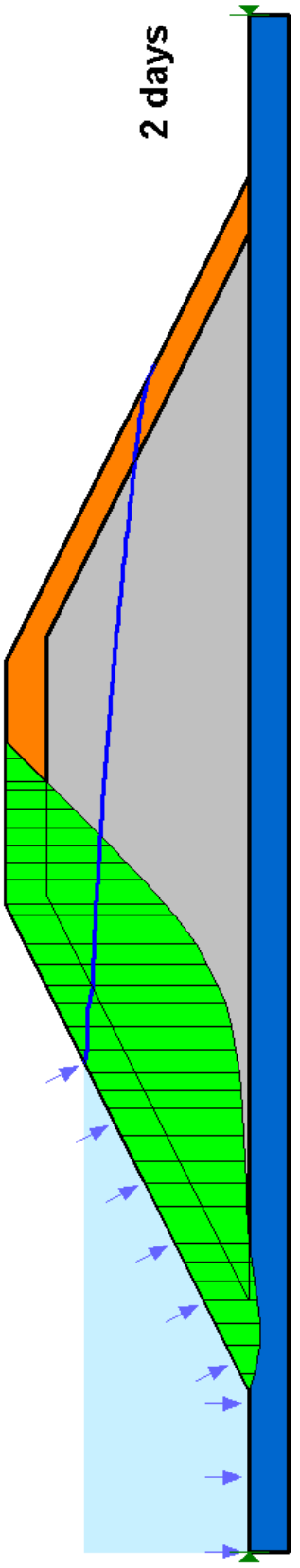

Figure 97: FS= 5,735 after 2 days

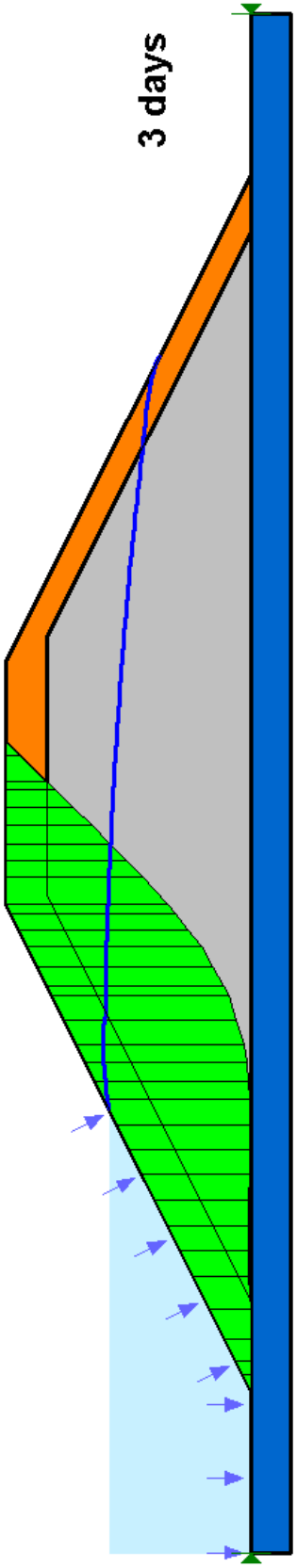

Figure 98: FS=4,862 after 3 days

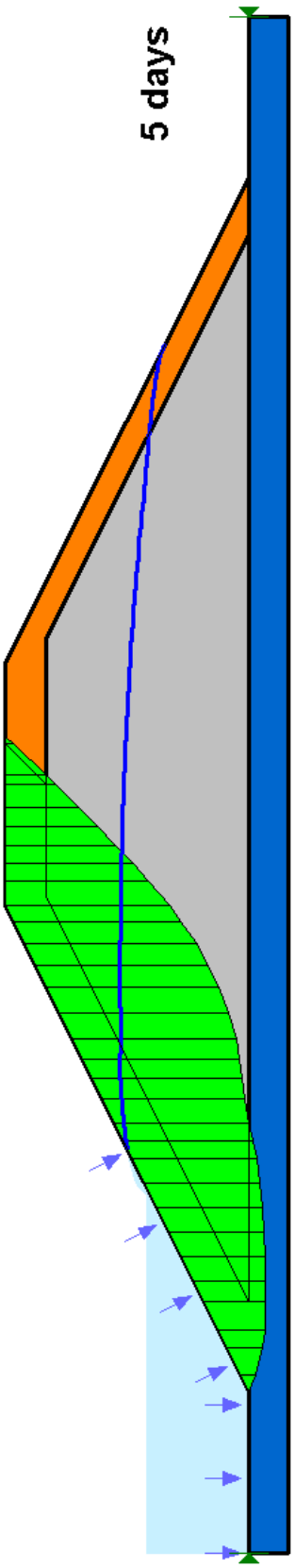

Figure 99: FS= 4,676after 5 days

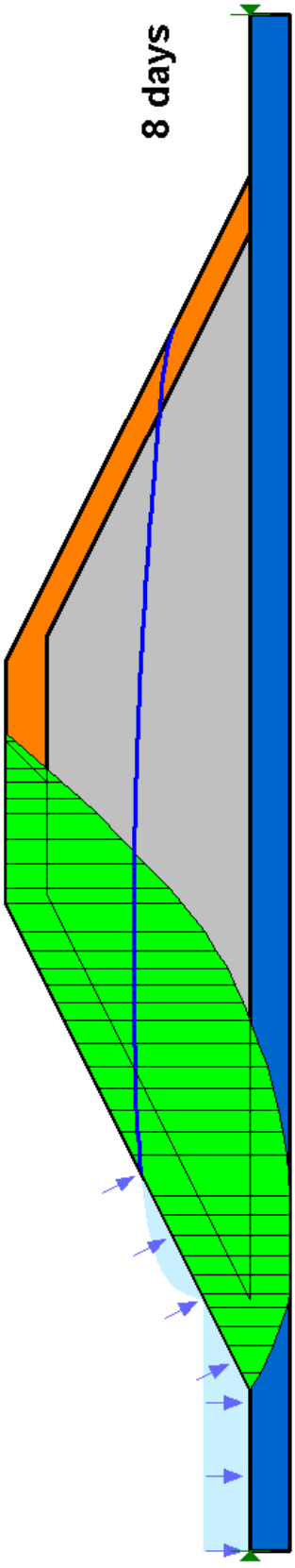

Figure 100: FS=4,194 after 8 days

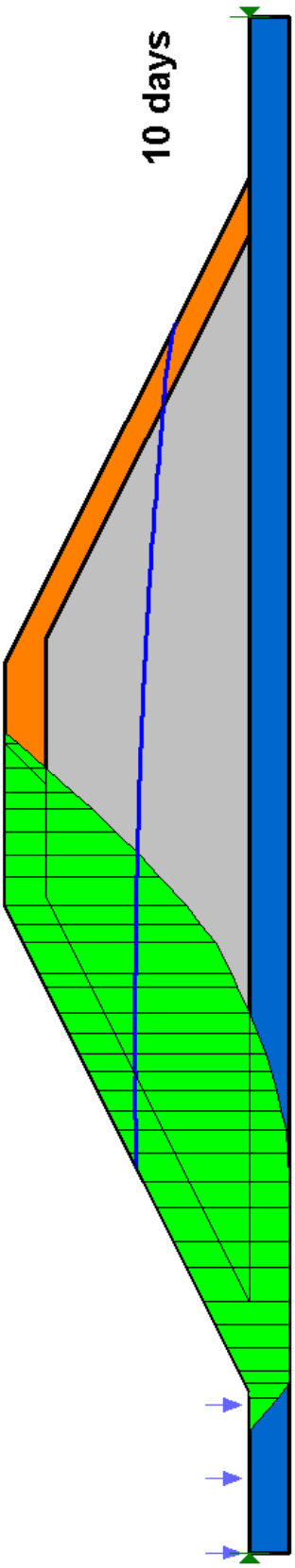

Figure 101: FS= 4,267 after 10 days

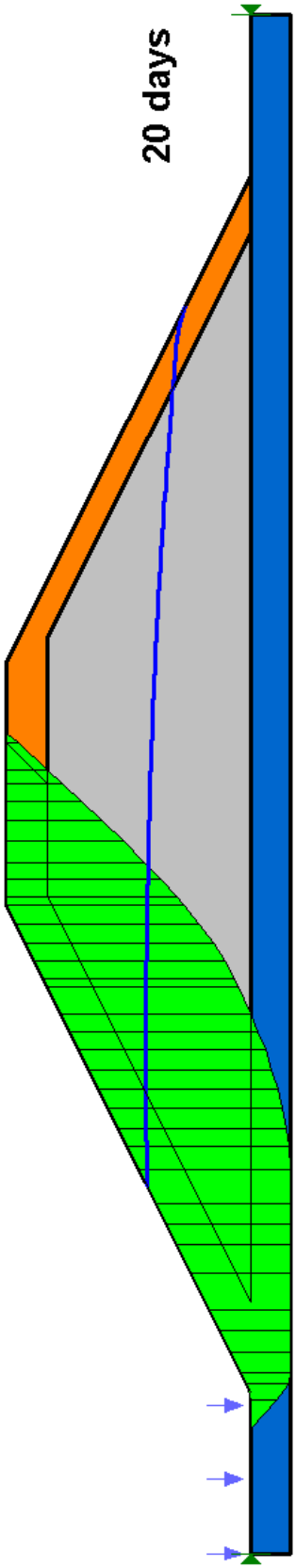

Figure 102: FS=4,441 after 20 days

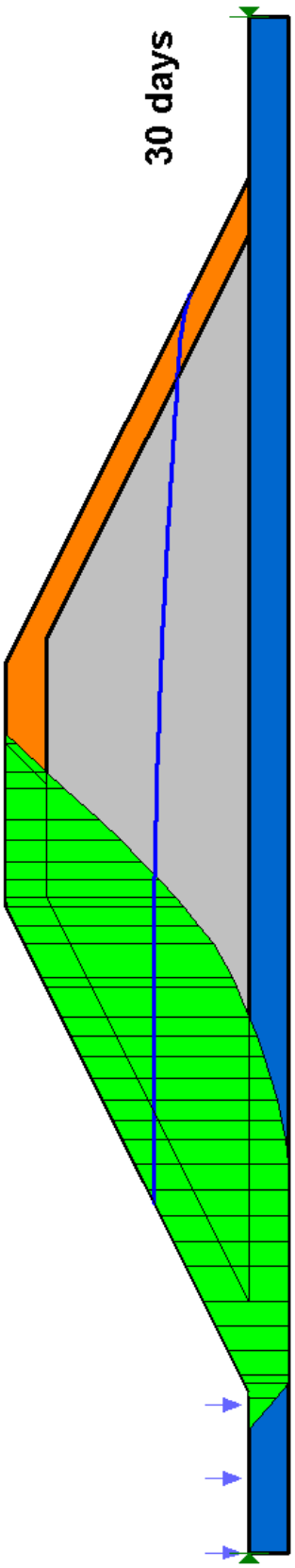

Figure 103: FS= 4,441after 30 days

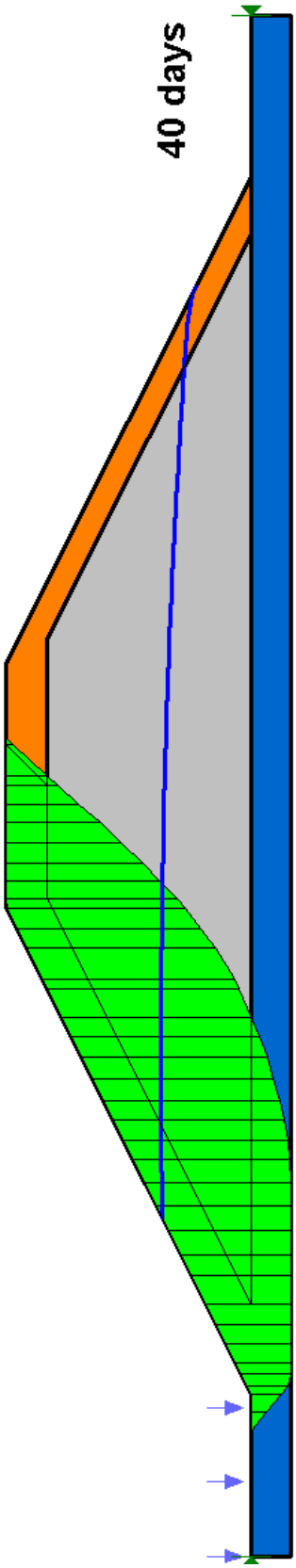

Figure 104: FS=4,446 after 40 days

In Table 20 are collected the safety factor obtained at each step of the analysis. Is it possible to see how, during the emptying of the reservoir, the safety factor decreases with the water level in the reservoir. It reaches the minimum value after 8 hours from the beginning of the analysis: at this time the countervailing effect of the water on upstream slope has disappeared, the phreatic surface in the embankment is still high, so big water pressures occur and the water level in the reservoir already passed the level of $H/2$, so there is filtration also toward the upstream toe. This is the most critical stage in the analysis.

After this time, the water in the dam, had time to spillage, so the water pressure at the upstream toe decreases also if the reservoir is empty, with consequent increase of the factor of safety, which settles around a value $FS = 4{,}45$.

Table 20: Trend of FS in slow drawdown analysis

Time	Water height in the reservoir	FS (Morgerstern-Price)
[days]	[m]	[-]
0	2,5	7,264
0,4	2,38	6,781
1	2,25	6,341
2	1,75	5,735
3	1,5	4,862
5	1	4,676
8	0,5	4,194
10	0	4,267
20	0	4,441
30	0	4,441
40	0	4,448

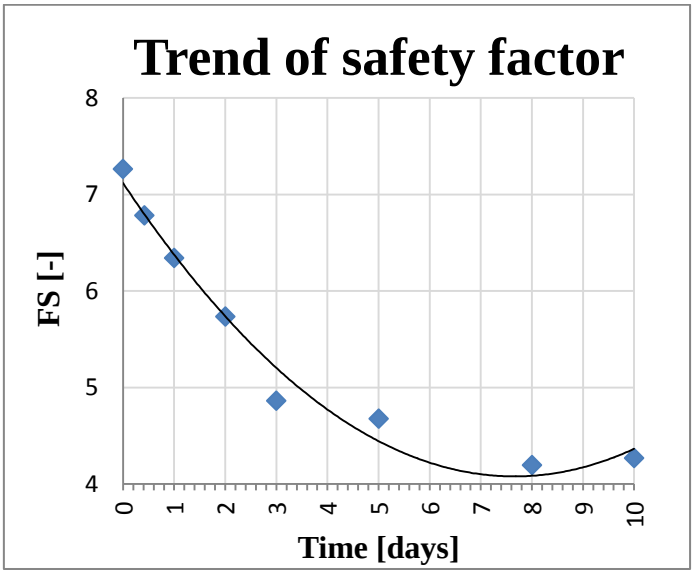

Figure 105: Trend of FS during the emptying of the reservoir in slow drawdown

Rapid drawdown

In case of rapid drawdown, it is assumed that the pore water pressure within the embankment continues to reflect the original water level. There are different kind of analysis to conduced to evaluate the safety factor during rapid drawdown. The first method is to pretend that the water in the reservoir draws down instantaneously; the second one is to use the seepage results from SEEP/W analysis. This more accurate and advanced approach uses the exact pore-water pressures that were in the soil during the drawdown process.

A SEEP/W analysis with *GeoStudio™ 2007* software has been run assuming the reservoir emptying in 4 hours, i.e. about 0,62 m/hour. This period of time is too short to allow the water within the embankment to escape, so the pore water pressure within the embankment remains high.

The model described in the previous analysis has been used, the only difference is in the boundary function, shown in Figure 106:

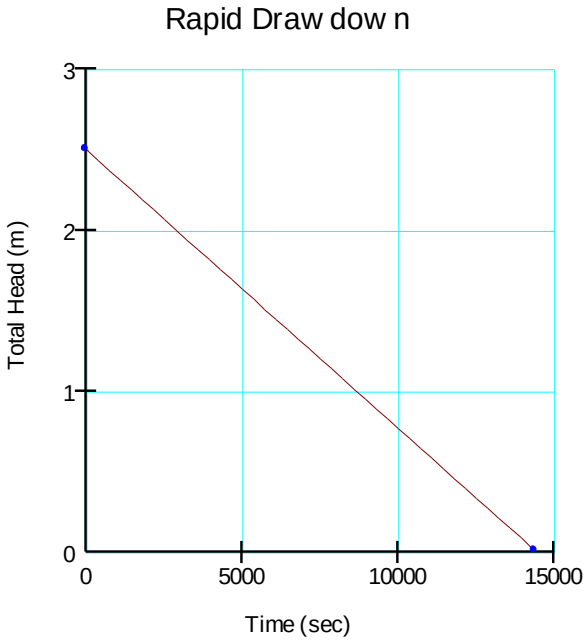

Figure 106: Hydraulic boundary function for rapid drawdown

The same initial conditions are assumed, and also the same 40 days-long period of examination was analyzed, divided in 14 steps: one to each hour of emptying of the reservoir, and one for each time step evaluated in the previous analysis.

After 4 hours of drawdown, the level in the reservoir was assumed to remain constant and equal to 0,0 m for the following days. The behavior of the seepage through the embankment was then examined.

The Figure 107 shows the groundwater seepage during the emptying of the reservoir. It is evident, how the water has no time to exit to the dam. The pore water pressures are high enough to force the water to escape not only from the upstream toe, but also from the slope itself.

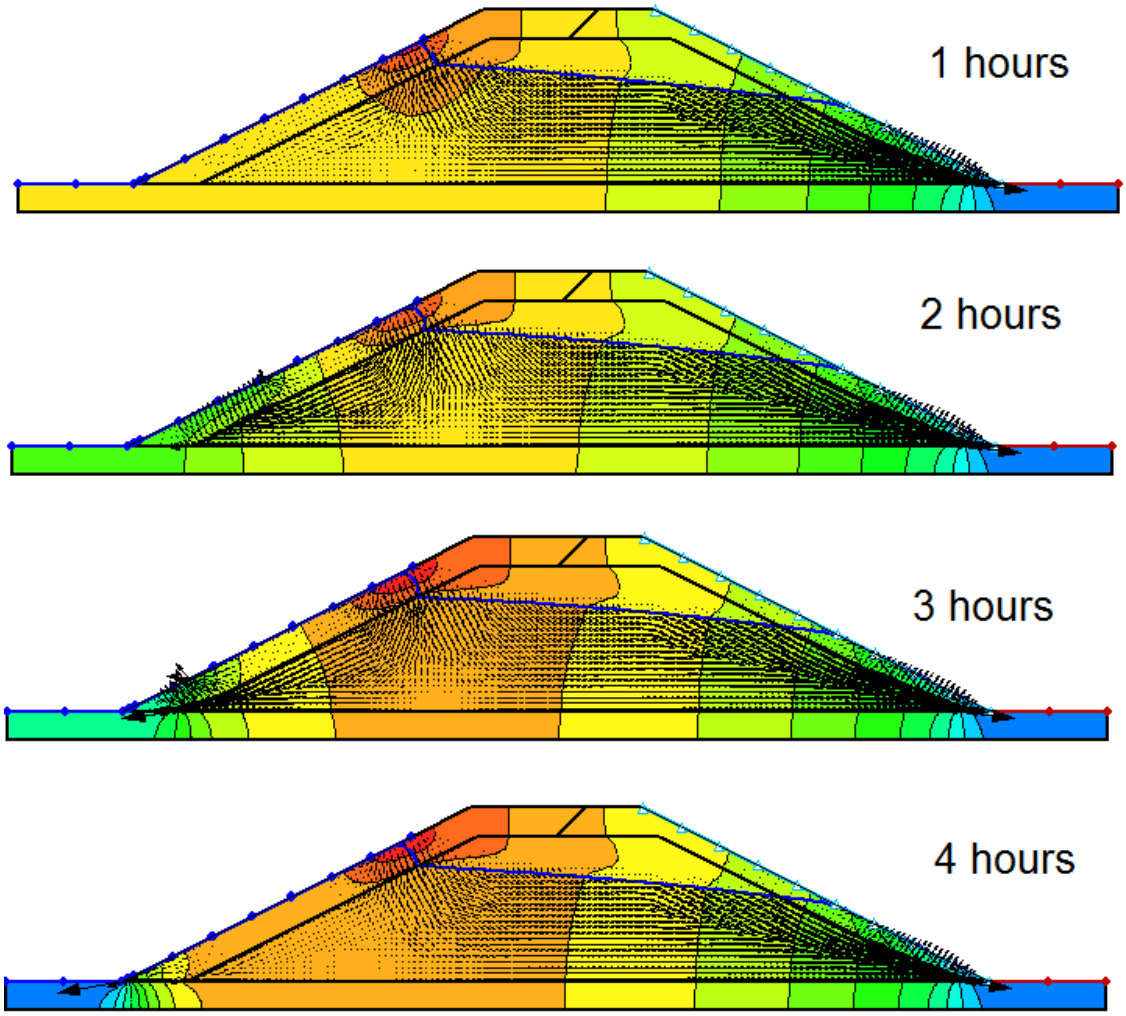

Figure 107: Rapid drawdown during emptying of the reservoir

After 4 hours, the level in the reservoir is equal to 0,0 m, the phreatic surface in the dam starts to decrease gradually in height, as in the previous analysis.

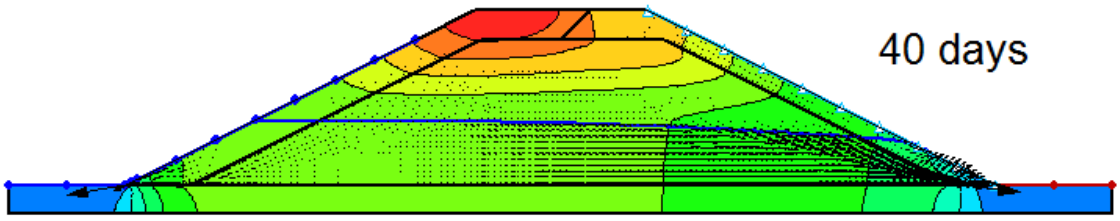

Figure 108: Piezometric line after 40 days

The slope stability during the rapid drawdown has then been evaluated using the previous seepage results as input data. Again, the factor of safety has been determined using the Morgerstern and Price's method, and considering also the composite slip surface.

The Figure 109-Figure 112 show the slope stability during the emptying of the reservoir.

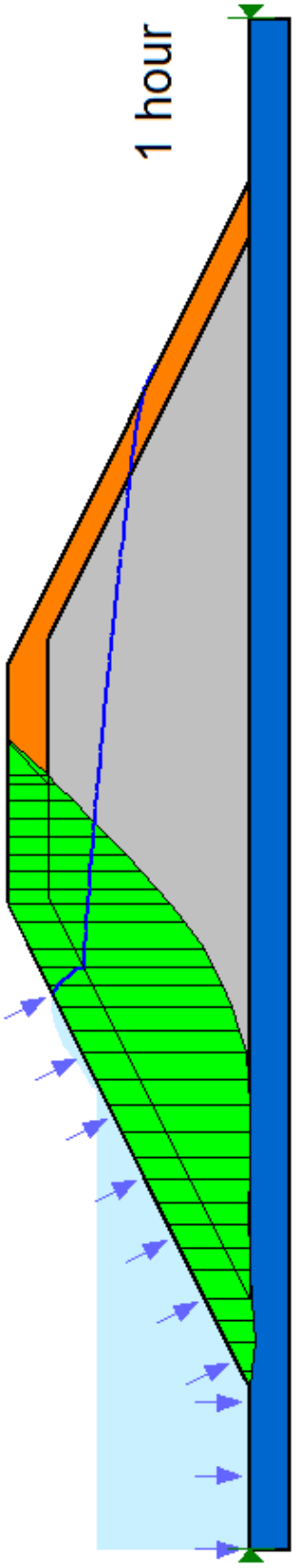

Figure 109: FS=5.051 after 1 hour

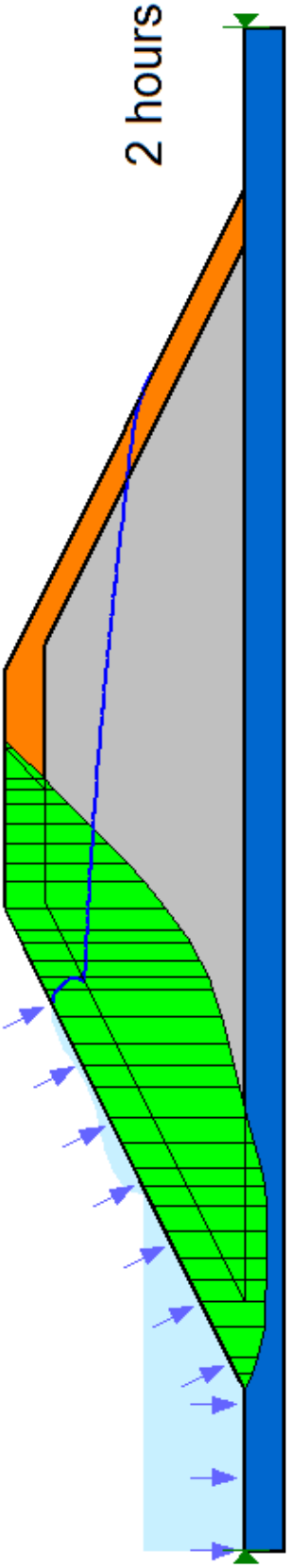

Figure 110: FS= 4.511 after 2 hours

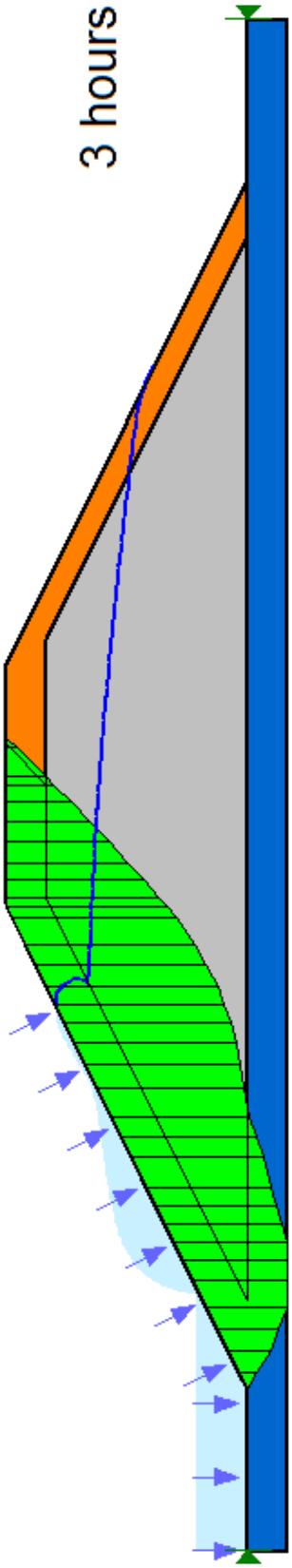

Figure 111: FS= 4.050 after 3 hours

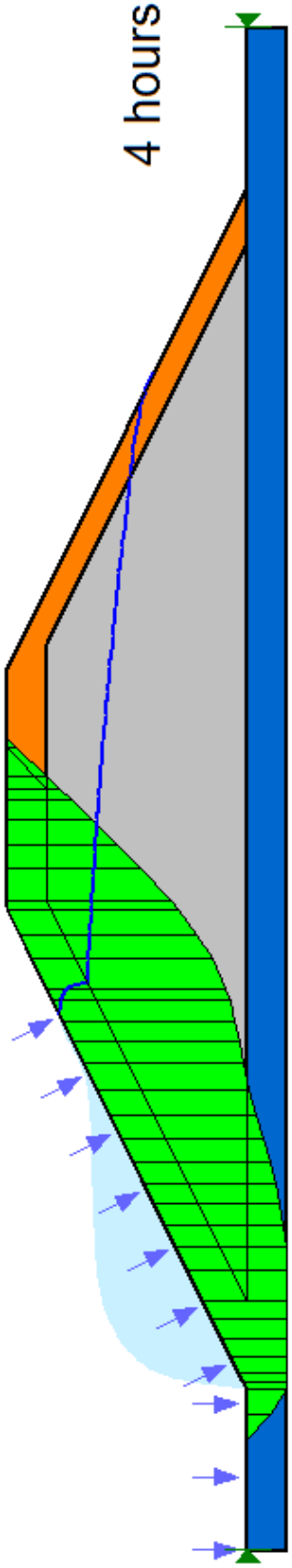

Figure 112: FS= 4.685 after 4 hours

In Table 21 are collected the factors of safety corresponding at each step of the analysis. As the water level draws down quickly, the safety factor lower, because the stabilizing effect of the water on upstream side disappeared, the phreatic line in the embankment continues to reflect the original water level, and the pore water pressure in the dike are high, so the instability risk occurs.

After 4 hours the water level in the dam starts to decrease slowly, the pore water pressure starts to dissipate and the stability of the slope increase. The safety factor finally settles on a value similar to the previous analysis.

Table 21: Trend of FS in rapid drawdown analysis

Time	Water height in the reservoir	FS (Morgerstern-Price)
[days]	[m]	[-]
0	2,5	5,051
0,04	1,9	4,511
0,08	1,2	4,050
0,125	0,6	4,630
0,167	0	4,555
0,4	0	4,564
1	0	4,543
2	0	4,560
3	0	4,511
5	0	4,505
8	0	4,477
10	0	4,455
20	0	4,443
30	0	4,450
40	0	4,451

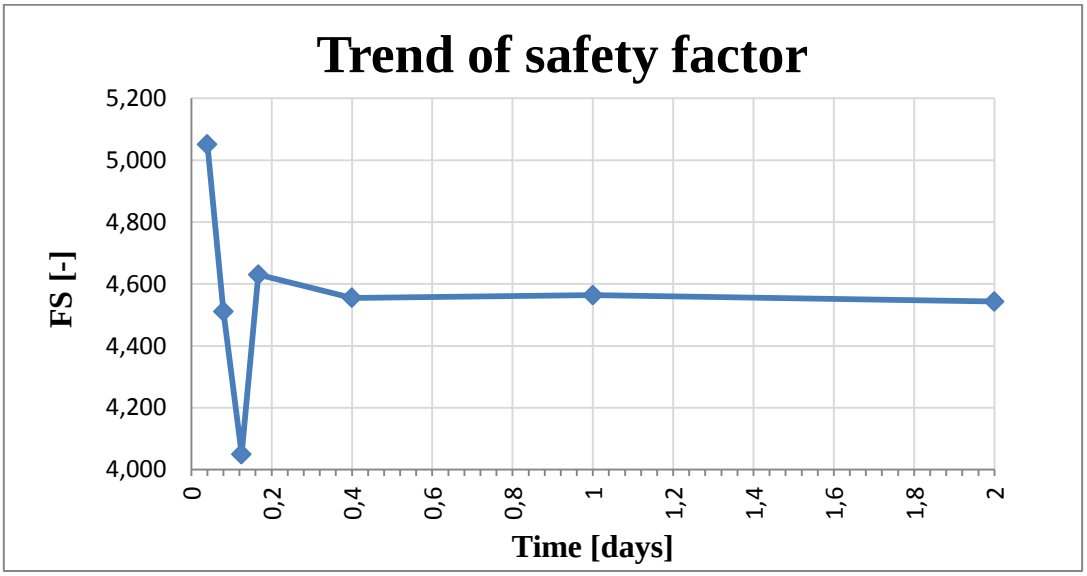

Figure 113: Trend of FS during rapid drawdown

Instantaneous drawdown analysis

A different kind of analysis can be conducted pretending the instantaneous draw down of the water in the reservoir. This situation can be modelled in two different kind: it is possible to draw the piezometric line before and after the drawdown, or it is possible to run a transient analysis with immediate drop down of the water changing the boundary conditions.

Using the first method it is possible to define the initial and the final condition by drawing the piezometric surfaces of the embankment, without conducing a seepage analysis, but only using SLOPE/W. The initial condition is determined by running a steady state analysis when the reservoir is at fully supply level. To model the rapid drawdown conditions in SLOPE/W, we need to remove the ponded water and place the piezometric line along the ground surface. The piezometric line is assumed to follow the upstream ground surface, but remains unchanged inside the embankment (Figure 114).

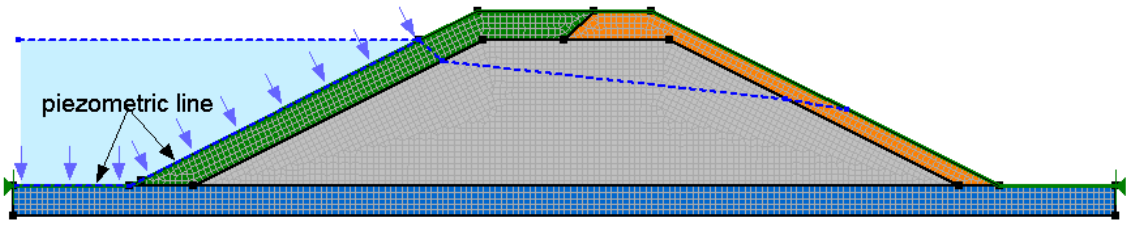

Figure 114: Profile used and assumed piezometric line after instantaneous drawdown

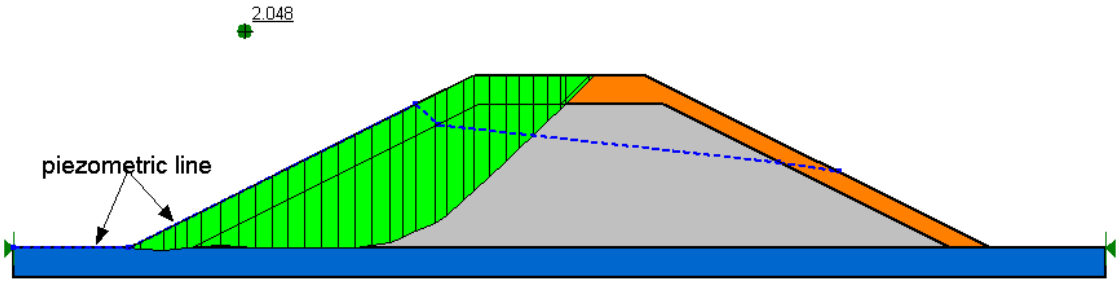

Figure 115: Critical slip surface and FS=2,048 after instantaneous drawdown

The factor of safety obtained is very small in comparison with the ones obtained before, so this approach should be considered conservative, because it bases on the unreasonable hypothesis that the draw down is instantaneous and the decreasing of the water in the reservoir does not lead to change in the phreatic line within the embankment. Besides, the process is treated as an instant of time, so it does not let to obtain acceptable results.

Using the second method, the safety factor for each step of the analysis is determined using the SEEP/W analysis as input data. The model utilized is the same of the rapid drawdown condition, but here the *Total Head* boundary conditions pass instantaneously from 2,5 m to 0,0.

The results of seepage flow are collected in the figures below (Figure 116-Figure 118).

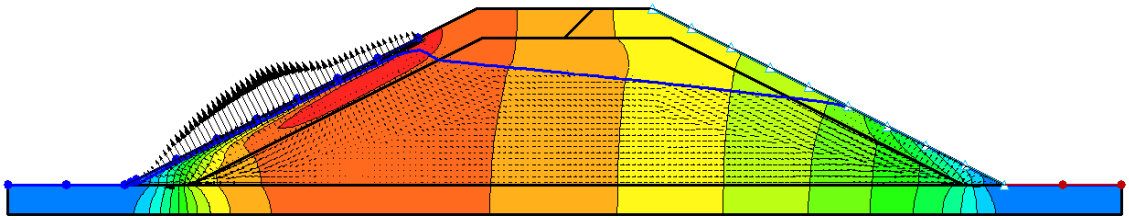

Figure 116: Seepage flow 1 hour after rapid drawdown

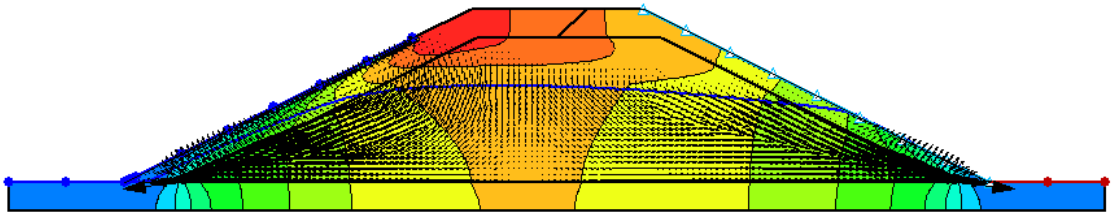

Figure 117: Seepage flow after one day

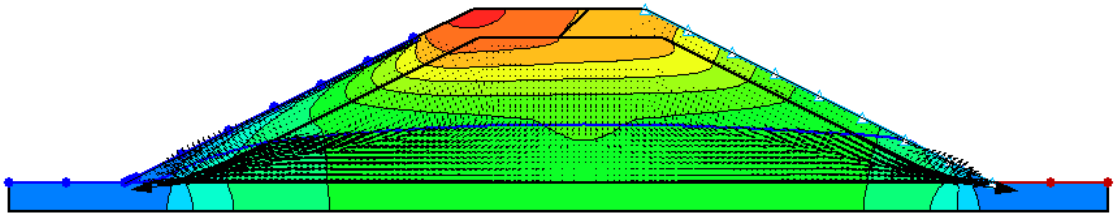

Figure 118: Seepage flow after 20 days

The pore-water pressure within the dam are so high that the water flows toward the upstream slope at the beginning of the analysis, in this condition there is flow toward both the dike's slope.

The slope stability analysis has been conducted, and the results are collected in Table 22:

Table 22: Trend of FS in instantaneous drawdown analysis

Time	Water height in the reservoir	FS (Morgerstern-Price)
[days]	[m]	[-]
0	2,5	5,051
0,04	0	2,987
1	0	3,858
2	0	3,938
3	0	4,017
5	0	4,087
8	0	4,15
10		4,206
20		4,258
30		4,311
40		4,363

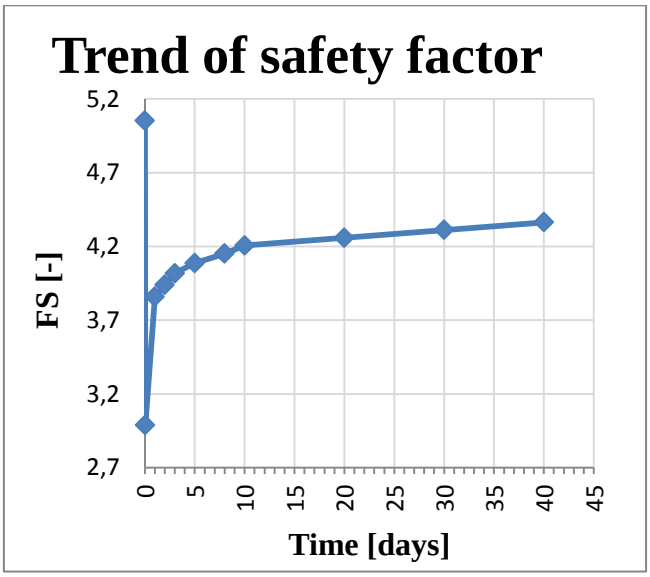

Figure 119: Trend of FS during instantaneous drawdown

The trend of the safety factor in Figure 119 shows as the safety factor drops to low values in the early stage of the drawdown process. After the initial abrupt decrease, it increases above 4.3 when the pore-water pressure in the embankment dissipate with time. This proves that the rapid drawdown is a very critical condition for the upstream slope stability.

In this case the safety factors result smaller than in the rapid drawdown analysis, because of the different modelling of the situation. To work on safe side, is better to use the last analysis described.

The advantage of the approach using the SEEP/W is that the hydraulic properties of the material can be considered and time can be included in the analysis: with this approach rapid drawdown is not just an instance in time, but is a process.

In this analyses, the stability of the dike's toe have not been considered, because it concerned only the slope instability due drawdown conditions. Any case, it would be necessary to conduce this kind of study, as high pore-water pressures occur during the seepage flow. The critical and the exit gradient should be calculated, and the stability must be verified.

Transient flow through the dike: comparison between FEM software

In this paragraph I would like to make a comparison between the results that I obtained by conducing the analysis with *GeoStudio™ 2007* software, the results obtained by Mr. Tomczak using *Slide*® software, and the results obtained by Ph.D. Marcin Cudny using *Plaxis*® software.

This last model was presented during *"DredgDikes Workshop and Steering Group Meeting"* in Gdańsk on 27th November 2012.

In this analysis, the level in the reservoir reaches its maximum in 5 days. The development of phreatic line is evaluated after keeping the water at 2,5 m for a 7-days long period. After this time, the reservoir is empty and the water level drops from 2,5 m to 0,0 m in 1 day.

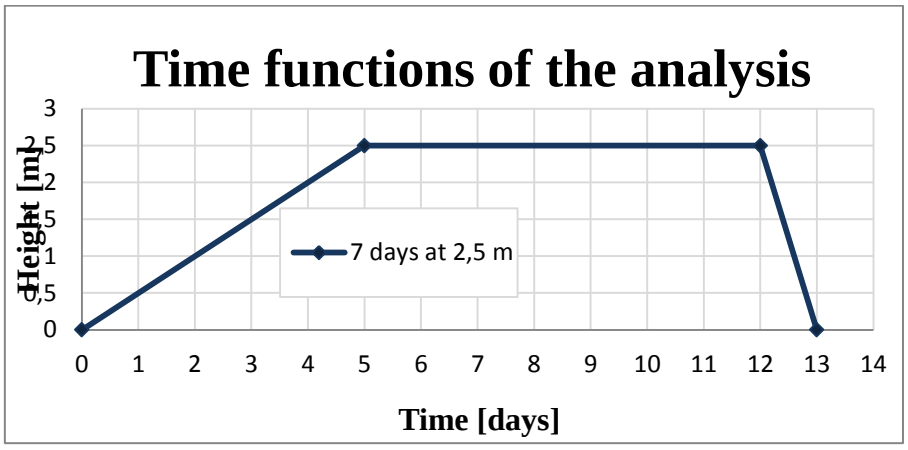

Figure 120: Height in the reservoir for both the simulations

The geometry of the model is similar in each analysis, the differences lie in the external layer. In *Slide*® model, the top layer is made of the same materials as in my analysis, but the tephra and sand layer continues over the top of the dike and ends up in the middle of the slope; *Plaxis*® model presents also two top layers (tephra and clay) but both of this layer have equal hydraulic conductivity, so they are modelled in the same way.

Figure 121 shows a similar development of the piezometric line in all the cases, during the rising up of the level in the reservoir.

After 7 days of keeping the water in the reservoir equal to its maximum value, the results obtained from *Plaxis*® and *GeoStudio*™ are very similar, while the phreatic surface at the interface between the external layer and the dike's core are lower in Slide®, respect to the height in the other software (Figure 122).

After drawdown the piezometric line in *GeoStudio*™ arrives to overlap the upstream side slope, while the piezometric line in the other analysis are far from it.

From this comparison, we can conclude that *GeoStudio*™ can be used to run groundwater seepage analysis, because it leads any case to acceptable results.

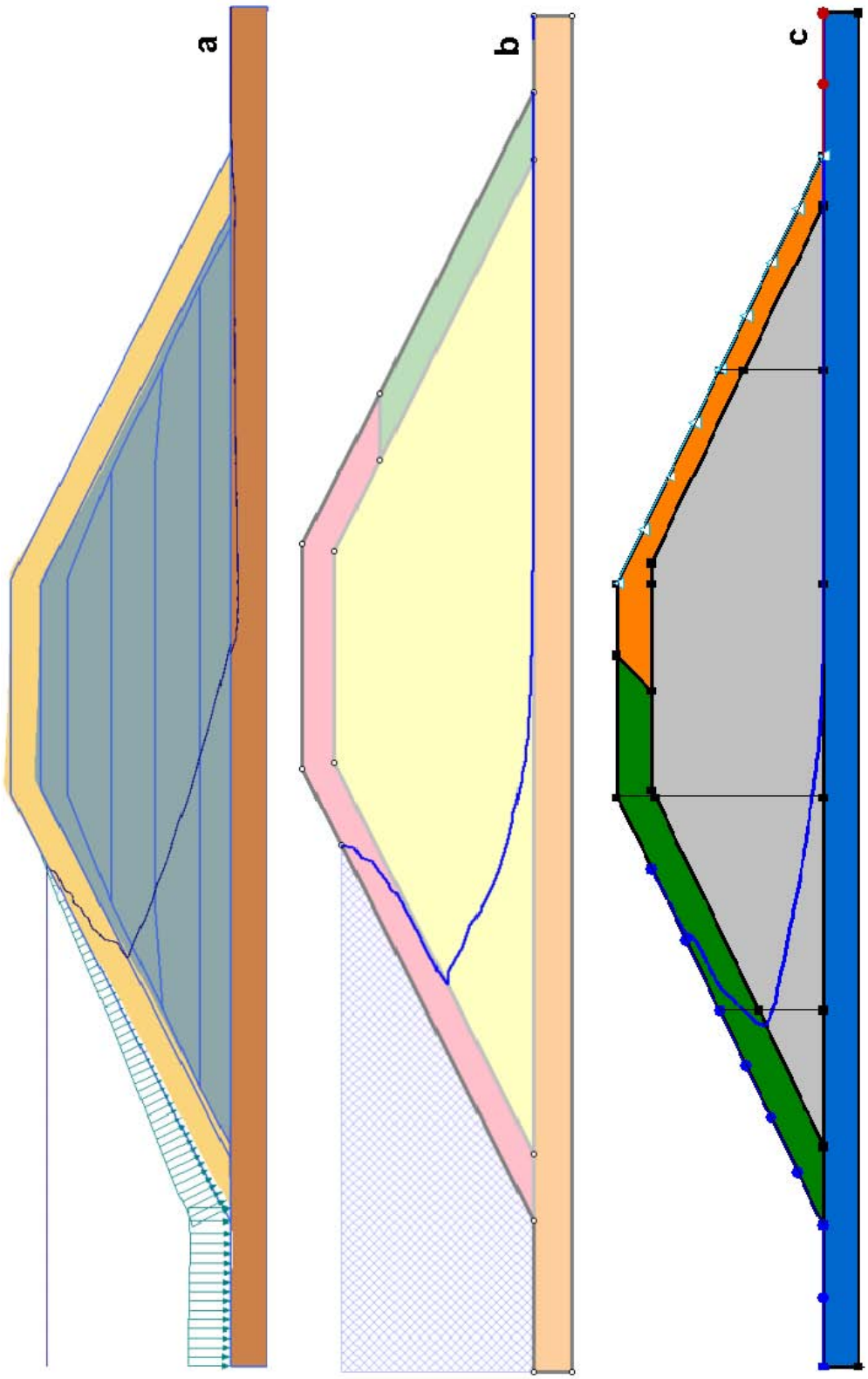

Figure 121: Comparison between Plaxis® (a), Slide® (b), GeoStudio™ (c) models after 5 days of filling of the reservoir

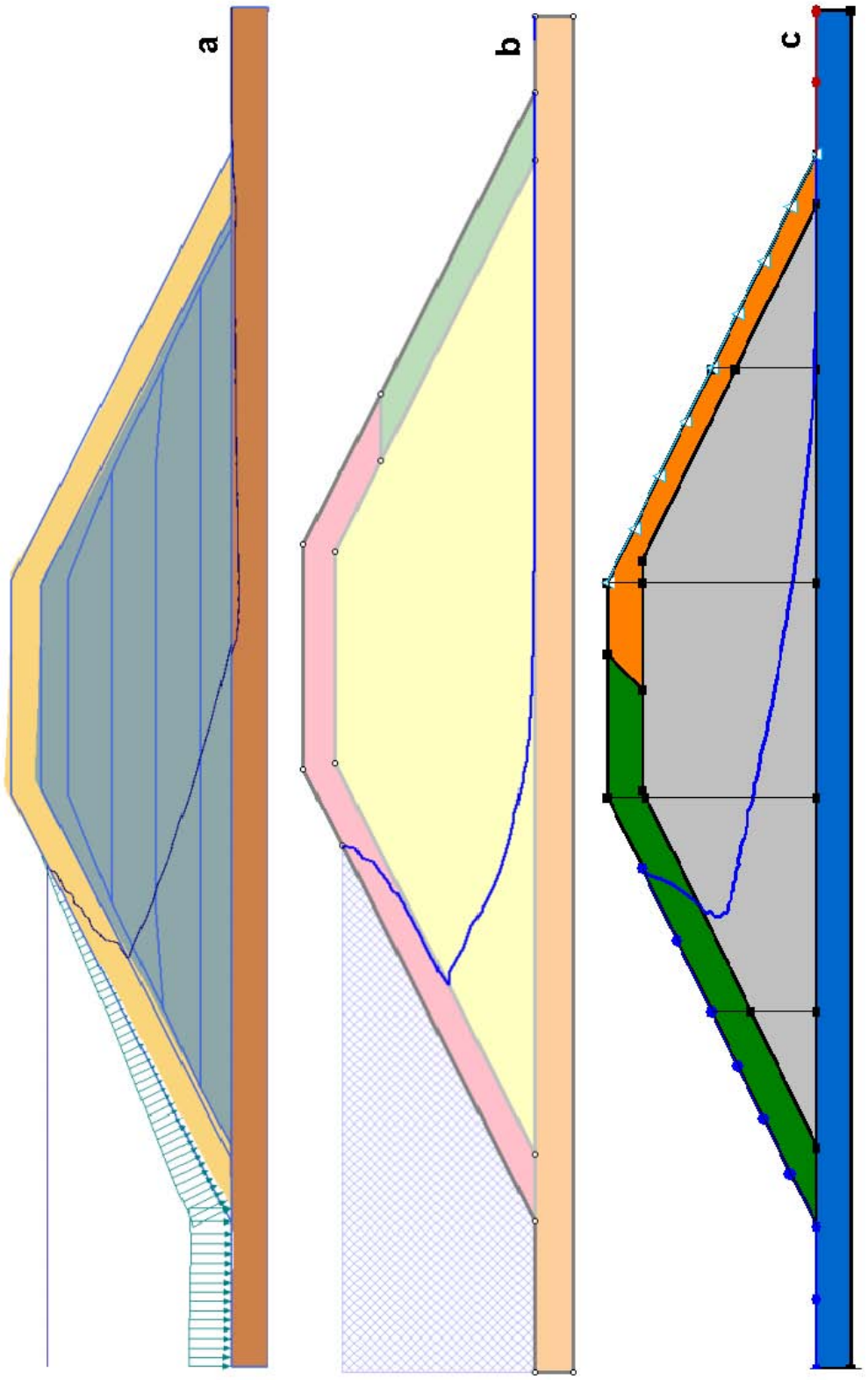

Figure 122: Comparison between Plaxis® (a), Slide® (b), GeoStudio™ (c) models after 7 days of full reservoir

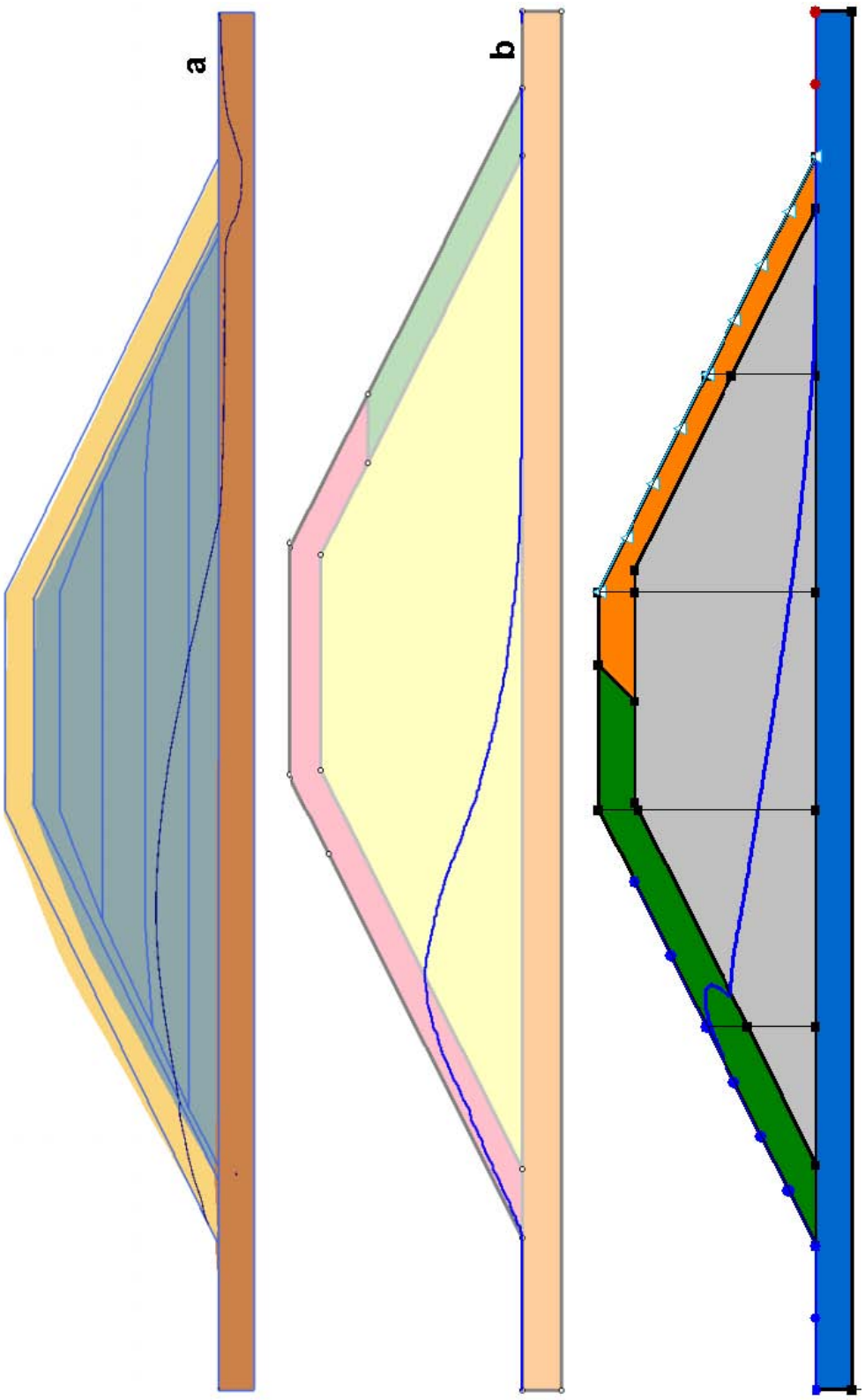

Figure 123: Comparison between Plaxis® (a), Slide® (b), GeoStudio™ (c) models after drawdown

Field tests

The dike was subjected to many experiments to evaluate many parameters of the dike's materials. The parameter studied in the following experiment is the permeability.

The permeability test is performed by keeping water level raised up on the seepage side for a certain number of days. Afterwards, to verify the stability of the dike, the water is drawn down rapidly. After pumping out, the water content and its distribution inside the dike are observed for following days.

Measurements

Four electronic piezometers had been installed in the dike's core. Two piezometers are placed on the edges of the dike's crown, while the other two are located in the middle of the dike's slope, and the edge of the slope intersects the piezometer at 1,5 meter of height.

The devices measure water pressure in each cross-section, once every hour. Non-linearity of the sensors, as well as temperature dependencies, are mathematically compensated.

The data from piezometers are sent by GSM signal to the monitoring station, localized near the dike. The computer, using special software, processes the measurement data and sends it to the receiver. Complete results are sent every 12 hours in a form of a text file.

In this thesis, only the one set of data for each day of the experiment are presented.

Collecting all data, the actual height of the water table in piezometers can be calculated from Pascal's law, which states that, when there is an increase in pressure at any point in a confined fluid, there is an equal increase at every other point in the container.

$$\frac{F_1}{A_1} = \frac{F_2}{A_2}$$

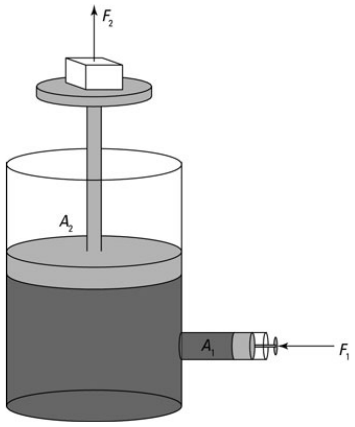

Figure 124: Pascal's law schema

This law can also be written as:

$$p_2 - p_1 = \gamma_w(h_2 - h_1)$$

where:

$p_2 \left[{kN}/{m^2}\right]$ = water pressure in the piezometer ;

$p_1 \left[{kN}/{m^2}\right] = p_{atm}$ = atmospheric pressure;

$\gamma_w \left[{kN}/{m^3}\right]$ = water unit weight;

$h_2\,[m]$ = researched water height;

$h_1[m]$ = water height at atmospheric pressure.

At height of +/- 0,00 m the pressure is equal to atmospheric pressure, so the Pascal's principle can be transform into following form:

$$h = \frac{p - p_{atm}}{100\gamma_w}$$

Seepage experiments

The first seepage experiment was started on 3rd July 2013, at 8.00 a.m.

Initially, the reservoir was filled in 24 hours; when the water reached the maximum level (2,5 m), it stopped to be pumped in. After flooding the seepage side of the dike, the water was not refilled throughout the experiment, so the water table was slowly falling down through the passing time. On the fifth day the water was pumped out during few hours. Water conditions, inside the dike's core, were finally observed for following 7 days.

Figure 125 shows how changed the water level in the reservoir during the experiment.

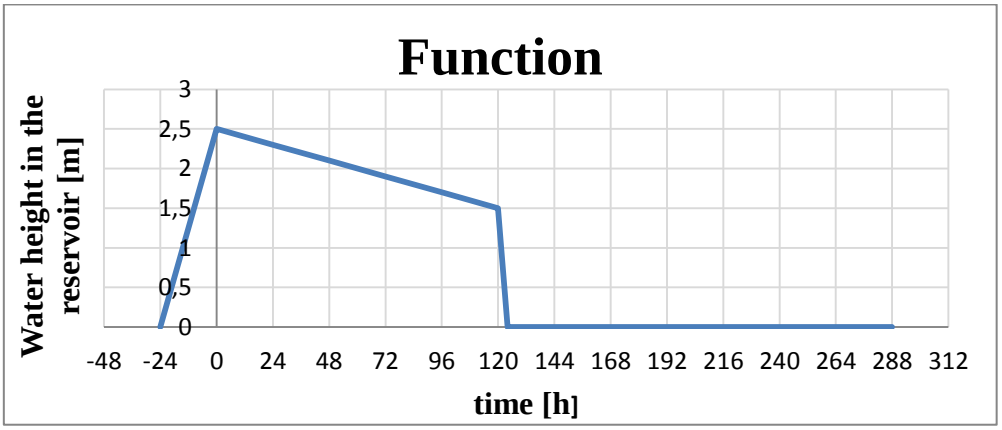

Figure 125: Head vs time function

The level of the water initially increases in 24 hours, then it slowly decreases 0,2 m every day for 5 days, and finally it drops quickly in 4 hours. After emptying the reservoir, the level of the water remains equal to 0.0 m throughout the 7 days long period of observation.

Table 23 shows the water level in each piezometer for the first experiment. These data have been collected by the polish student Mr. Tomczak.

Table 23: Measured water heights in piezometers for the first experiment

Time from experiment start	Date	Water height in piezometer 1	Water height in piezometer 2	Water height in piezometer 3	Water height in piezometer 4
[h]	[-]	[m]	[m]	[m]	[m]
-16	2,07,13	0,088	0,116	0,138	0,062
8	3,07,13	2,265	0,837	0,338	0,16
32	4,07,13	2,08	1,641	1,017	0,159
56	5,07,13	1,858	1,577	1,109	0,377
80	6,07,13	1,644	1,424	1,078	0,52
104	7,07,13	1,456	1,28	1,003	0,537
128	8,07,13	0,681	0,895	0,77	0,466
152	9,07,13	0,397	0,553	0,532	0,357
176	10,07,13	0,225	0,336	0,364	0,278
200	11,07,13	0,155	0,177	0,22	0,205
224	12,07,13	0,152	0,114	0,131	0,183
248	13,07,13	0,153	0,114	0,101	0,183
272	14,07,13	0,152	0,117	0,104	0,186
296	15,07,13	0,151	0,115	0,102	0,186

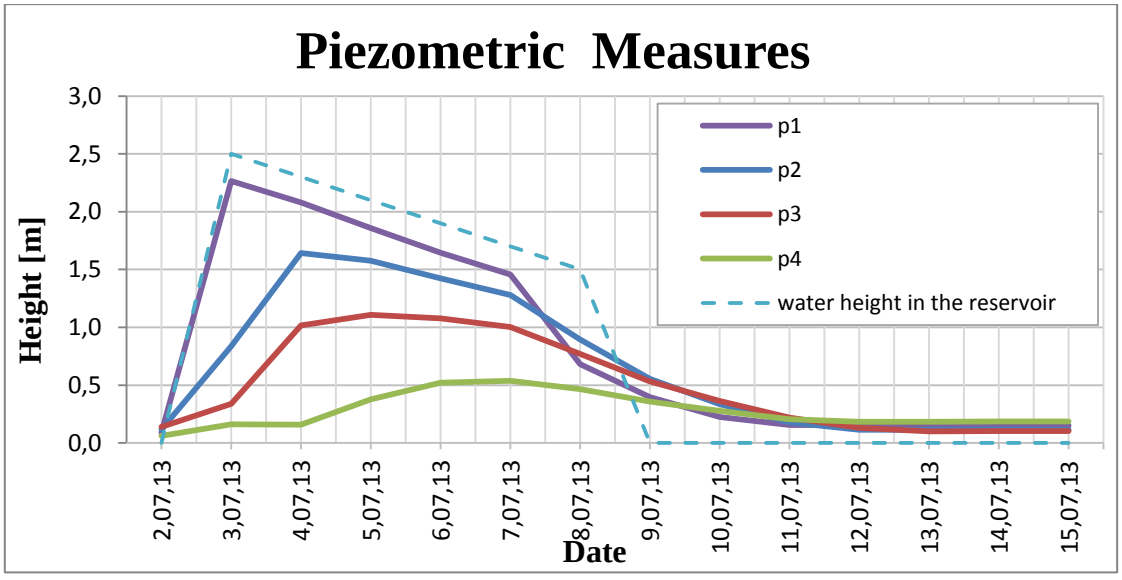

Figure 126: Trend of the saturation level of the piezometers for first experiment

The previous field test was repeated few days later: it was started again on 24th July 2013, at 9 a.m., 9 days after the end of the first one.

At the beginning of this experiment, there were some little differences in the water heights in the piezometer compared to the ones of the previous experiment, as it is possible to see in Table 24.

Table 24: Measured water heights in piezometers for the second experiment

Time from experiment start	Date	Water height in piezometer 1	Water height in piezometer 2	Water height in piezometer 3	Water height in piezometer 4
[h]	[-]	[m]	[m]	[m]	[m]
-16	2,07,13	0,146	0,107	0,09	0,164
8	3,07,13	2,44	0,953	0,446	0,164
32	4,07,13	2,285	1,875	1,243	0,277
56	5,07,13	2,094	1,834	1,395	0,604
80	6,07,13	1,911	1,71	1,372	0,69
104	7,07,13	1,734	1,57	1,276	0,659
128	8,07,13	1,571	1,427	1,167	0,608
152	9,07,13	0,721	0,97	0,885	0,503
176	10,07,13	0,42	0,597	0,586	0,378
200	11,07,13	0,242	0,352	0,377	0,282
224	12,07,13	0,156	0,124	0,132	0,188
248	13,07,13	0,156	0,124	0,132	0,188
272	14,07,13	0,154	0,121	0,103	0,185
296	15,07,13	0,155	0,122	0,105	0,186

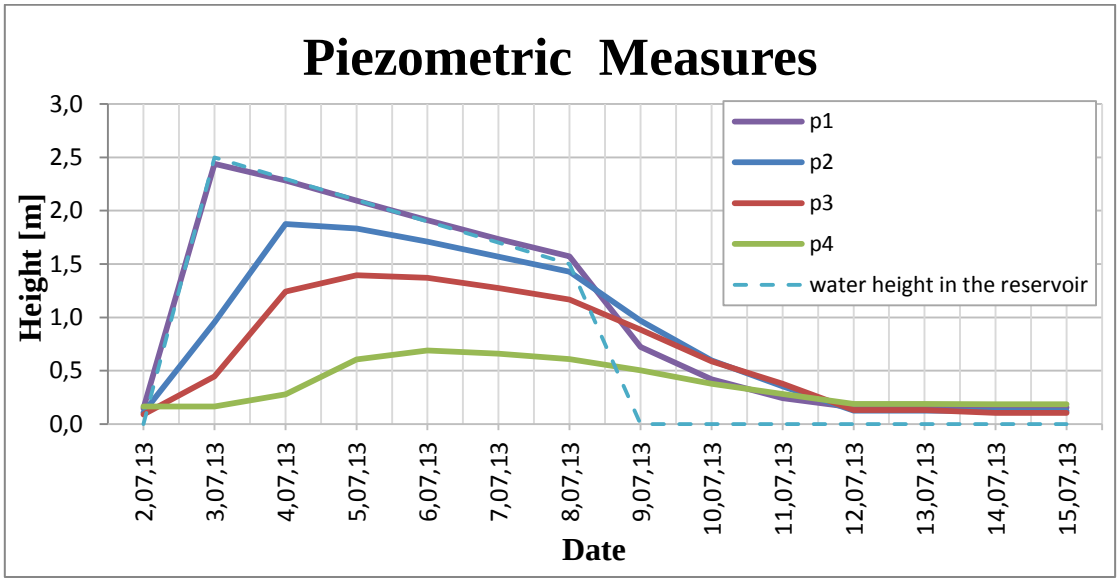

Figure 127: Trend of the saturation level of the piezometers for second experiment

Both figures show similar piezometric heights. The main difference between the two experiments is the maximum water level observed in all piezometers (higher in the second test).

The piezometers p1, p2, p3 begin to saturate after couple of hours from the start of experiment. The piezometer p4 is reached by water after 27 hours, while it needed 39 hours to saturate in the first experiment. The different conditions of saturation of this piezometer are shown in the graph below (Figure 128). These differences show changes in water filtration coefficient in the dike induced by the first test.

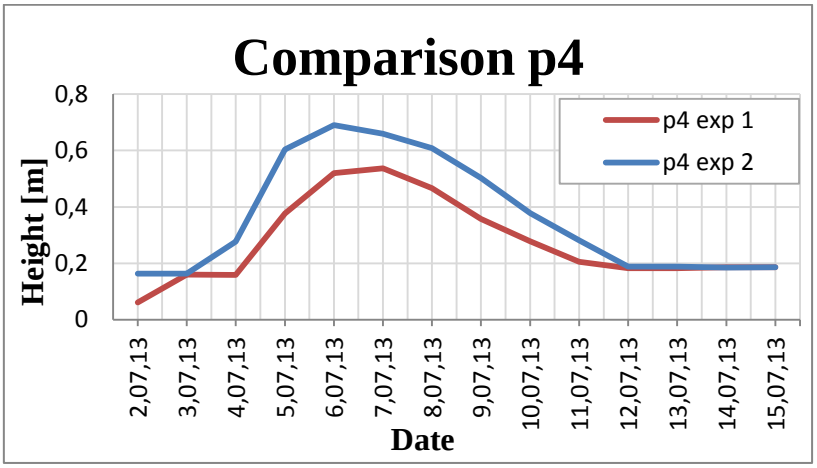

Figure 128: Different saturation conditions for piezometer p4

In the second test, the dredged material shows bigger saturation capacity, as the piezometers show higher water table level compared to the one in first analysis. This means that the water flow through the dike in the two experiments is relatively different.

FEM analysis

Groundwater analysis

The first field measure is reproduced using *GeoStudio™ 2007* software. A transient analysis is performed to simulate the seepage through the dike and evaluate the water height in the piezometers, comparing it to the values got from the field test.

In finite element model, the soil is assumed to be in dry state, before the beginning of the test. The data measured by Mr. Tomczak have to be modified to be compared with the ones obtained from the FEM analysis: the initial value at empty reservoir should be 0,0 m, so it is necessary to compensate the piezometric heights for this effect. The corrected data are gathered in Table 25.

Table 25: Collected measured water heights in piezometers for the first experiment

Time from experiment start	Date	Water height in piezometer 1	Water height in piezometer 2	Water height in piezometer 3	Water height in piezometer 4
[h]	[-]	[m]	[m]	[m]	[m]
-16	2,07,13	0	0	0	0
8	3,07,13	2,177	0,721	0,200	0,098
32	4,07,13	1,992	1,525	0,879	0,097
56	5,07,13	1,770	1,461	0,971	0,315
80	6,07,13	1,556	1,308	0,940	0,458
104	7,07,13	1,368	1,164	0,865	0,475
128	8,07,13	0,593	0,779	0,632	0,404
152	9,07,13	0,309	0,437	0,394	0,295
176	10,07,13	0,137	0,22	0,226	0,216
200	11,07,13	0,067	0,061	0,082	0,143
224	12,07,13	0,064	0	0	0,121
248	13,07,13	0,065	0	0	0,121
272	14,07,13	0,064	0	0	0,124
296	15,07,13	0,063	0	0	0,124

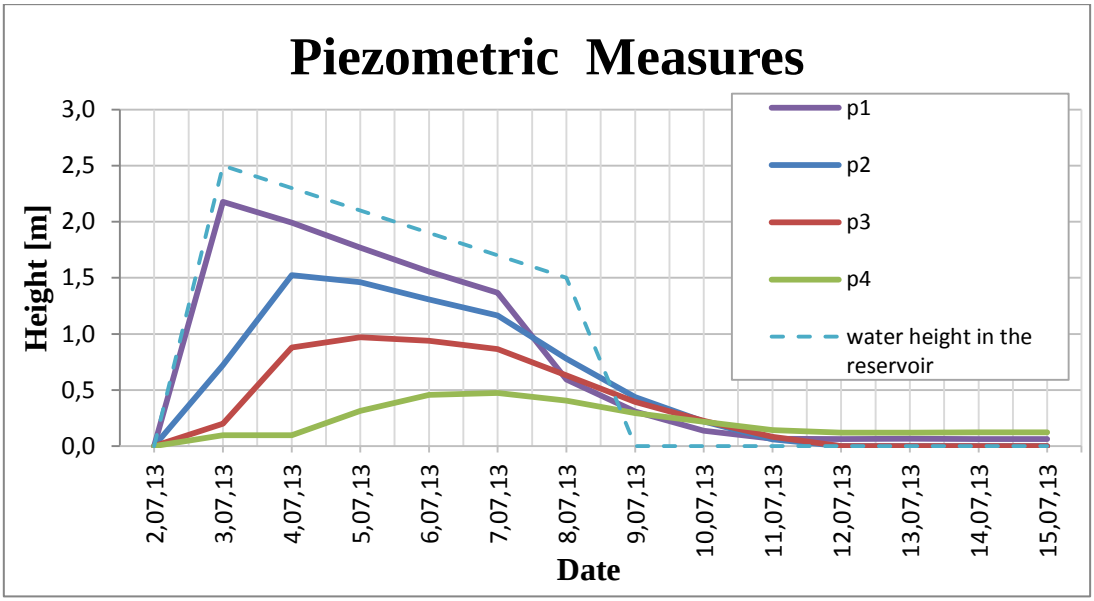

Figure 129: Trend of the corrected water level in the piezometers

The model is the same as the one used in the previous analysis, but in this case the mesh is modified so that where there is a piezometer, there are the nodes of the mesh, too. The piezometers are modelled as a vertical line, as it is shown in Figure 130.

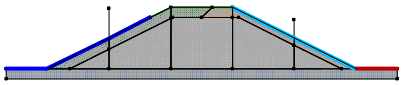

Figure 130: Model for piezometric analysis

The boundary conditions utilized are *Total Head* in riverside slope to simulate the trend of the ponded water in the reservoir, *Total Flux (Q=0)* in downstream side and Pressure Head (P=0).

The results of the water height in piezometers obtained from the simulation are collected in the Table 26.

Table 26: Water heights in piezometers from GeoStudio™ analysis for the first experiment

Time from experiment start	Date	Water height in piezometer 1	Water height in piezometer 2	Water height in piezometer 3	Water height in piezometer 4
[h]	[-]	[m]	[m]	[m]	[m]
-16	2,07,13	0	0	0	0
8	3,07,13	0,717	0,019	0	0
32	4,07,13	0,934	0,134	0	0
56	5,07,13	0,999	0,242	0,001	0
80	6,07,13	0,998	0,316	0,007	0
104	7,07,13	0,956	0,363	0,026	0
128	8,07,13	0,787	0,367	0,043	0
152	9,07,13	0,688	0,356	0,06	0
176	10,07,13	0,637	0,348	0,075	0
200	11,07,13	0,604	0,342	0,085	0,001
224	12,07,13	0,577	0,337	0,093	0,001
248	13,07,13	0,556	0,332	0,101	0,002
272	14,07,13	0,584	0,328	0,107	0,003
296	15,07,13	0,523	0,324	0,112	0,004

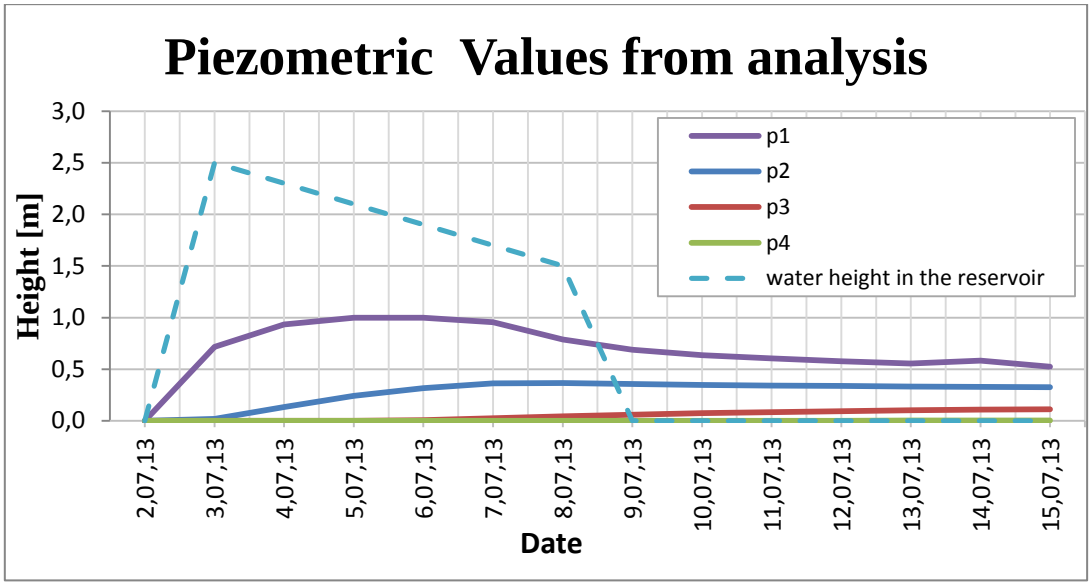

Figure 131: Trend of water in piezometers from analysis with GeoStudio™ 2007

Analyzing the data in the previous paragraphs it is clear that the dam's finite element modeling is not relevant: the piezometric behavior appears substantially different.

This can be due to the fact that the permeability in close area of standpipes can be much higher than the one determined in laboratory's tests, because of drilling procedure and filling the space between borehole and standpipe with some coarser material. So I tried to increase the permeability coefficient of the external impervious layer and the core of the dike to see the effect of it.

The values of conductivity coefficients that allow to achieve similar results to those measured in field tests are: $k_s = 4\,e^{-6}\ [^m/_s]$ for both tephra-sand mixture and clay; $k_s = 2\,e^{-6}\ [^m/_s]$ for the core. In this condition the external layer becomes more permeable than the core, and this is not consistent with the initial assumption.

In my opinion, the differences between the FEM analysis results and the field test results can be caused by:

- damaging of the piezometer during the installation;
- relevant alteration of the external layer during installation of piezometers;
- the fact that the FEM software considers the external layers more impervious that the real one: in the real test dike the shell layer is not delaying the water penetration.

The results of the modified analysis are collected in Table 27.

Table 27: Results of the analysis with modified Ks

Time from experiment start	Date	Water height in piezometer 1	Water height in piezometer 2	Water height in piezometer 3	Water height in piezometer 4
[h]	[-]	[m]	[m]	[m]	[m]
-16	2,07,13	0	0	0	0
8	3,07,13	2,146	1,379	0,821	0,413
32	4,07,13	2,010	1,509	0,986	0,523
56	5,07,13	1,857	1,439	0,985	0,546
80	6,07,13	1,652	1,345	0,964	0,551
104	7,07,13	1,469	1,237	0,908	0,544
128	8,07,13	0,968	0,870	0,672	0,434
152	9,07,13	0,749	0,677	0,549	0,370
176	10,07,13	0,612	0,559	0,466	0,320
200	11,07,13	0,520	0,480	0,404	0,281
224	12,07,13	0,454	0,421	0,358	0,249
248	13,07,13	0,405	0,380	0,324	0,226
272	14,07,13	0,367	0,347	0,299	0,210
296	15,07,13	0,336	0,321	0,278	0,195

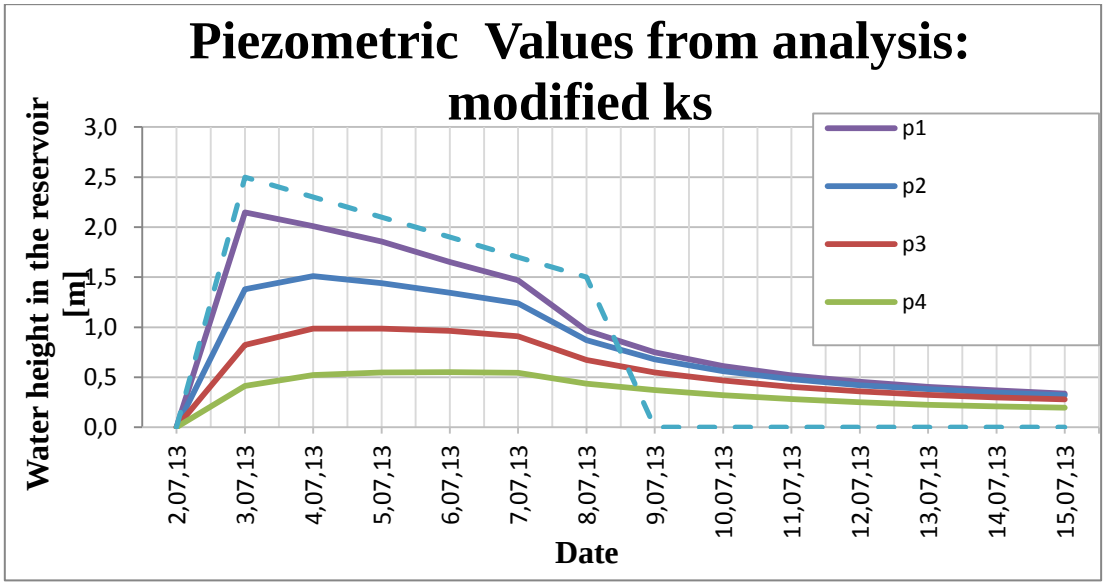

Figure 132: Trend of water in piezometers from modified analysis with GeoStudio™ 2007

The Figure 132 shows how the results are similar to the one measured, regarding the maximum value, but, again, there is an insufficient correspondence between FEM model and data collected: in the analysis the pressure in piezometers p1, p2 and p3 takes more time to dissipate, so after 7 days there are 0,3 m of water in the piezometers, even if the measured values are around 0,0 m.

The effects of the involved variables are evaluated and I have concluded that only the presence of a drain at the upstream side's toe can ensure the measured water head.

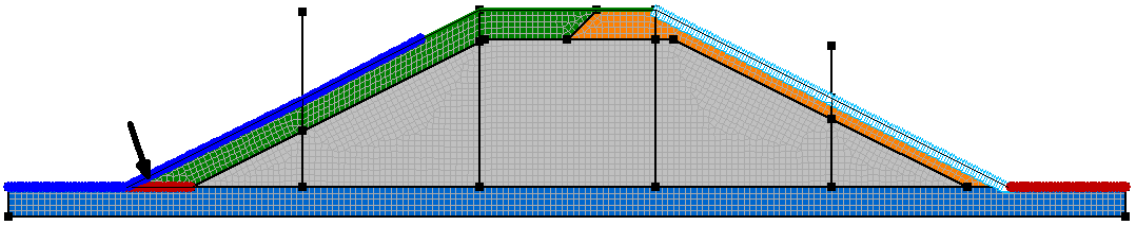

Figure 133: Insertion of drain

The FEM analysis was repeated after introduce a horizontal drain in the dike's toe on riverside. The presence of the drain is simulated with the *Pressure Zero* boundary conditions. In this way the results become similar to the measured values. This confirms the hypothesis that a non-mentioned drain was installed in the embankment's toe.

The Table 28 shows the results:

Table 28: Results of the analysis with modified Ks and drain

Time from experiment start	Date	Water height in piezometer 1	Water height in piezometer 2	Water height in piezometer 3	Water height in piezometer 4
[h]	[-]	[m]	[m]	[m]	[m]
-16	2,07,13	0	0	0	0
8	3,07,13	2,146	1,392	0,824	0,410
32	4,07,13	1,957	1,446	0,927	0,493
56	5,07,13	1,790	1,408	0,967	0,538
80	6,07,13	1,614	1,328	0,951	0,547
104	7,07,13	1,431	1,209	0,886	0,533
128	8,07,13	0,618	0,644	0,526	0,358
152	9,07,13	0,297	0,330	0,308	0,263
176	10,07,13	0,179	0,200	0,203	0,194
200	11,07,13	0,139	0,147	0,151	0,156
224	12,07,13	0,124	0,126	0,130	0,139
248	13,07,13	0,118	0,116	0,120	0,130
272	14,07,13	0,112	0,108	0,111	0,123
296	15,07,13	0,336	0,321	0,278	0,195

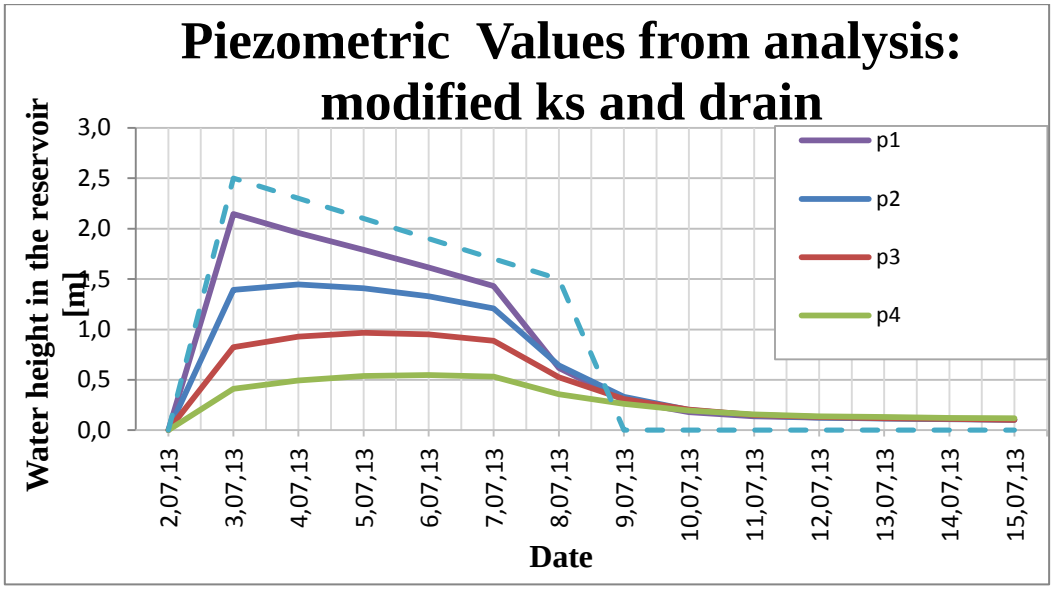

Figure 134: Trend of water in piezometers from modified analysis with drain with GeoStudio™ 2007

The Figure 135-Figure 138 show the trend of measured water height and results from FEM analysis, with or without drain, for each piezometer. The figures confirm that the presence of a drain leads to results similar to the ones obtained by fields test.

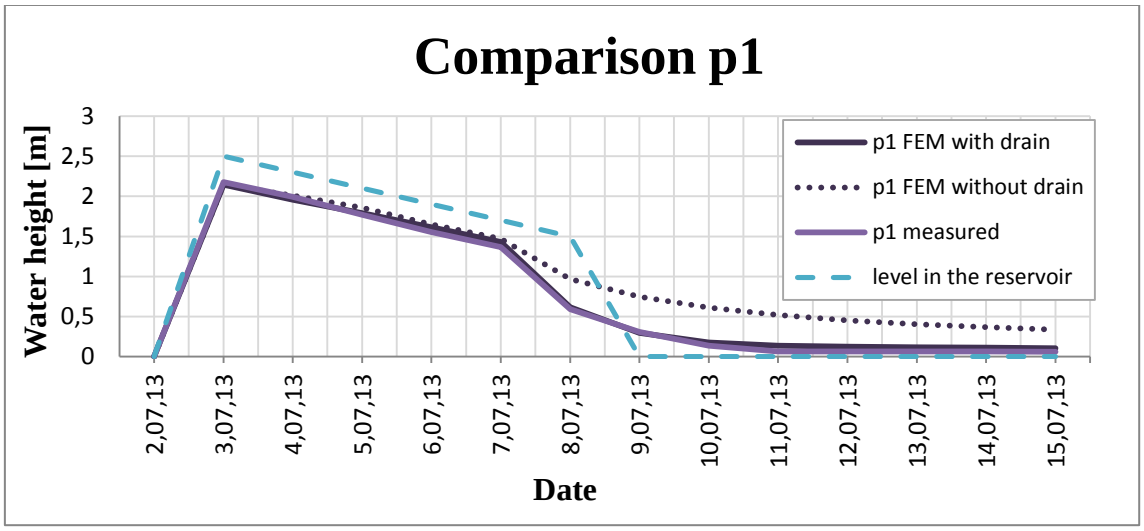

Figure 135: Comparison between measured data and results from FEM analysis for piezometer 1

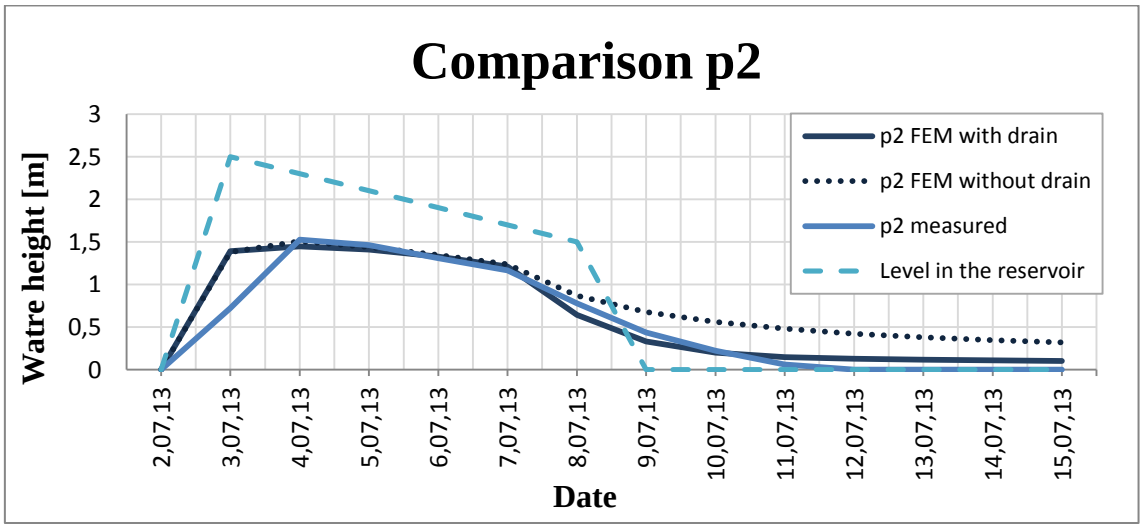

Figure 136: Comparison between measured data and results from FEM analysis for piezometer 2

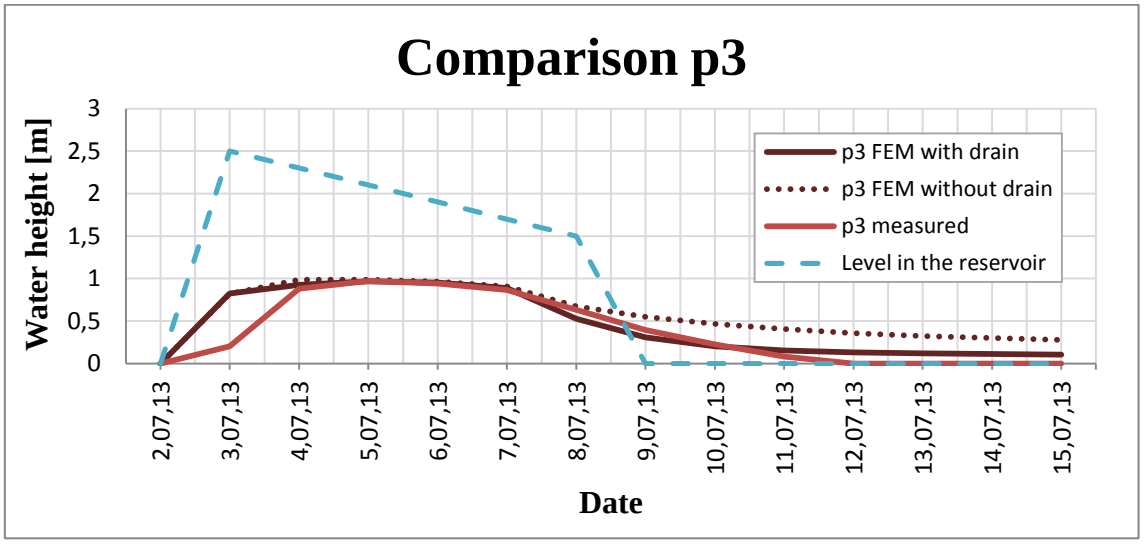

Figure 137: Comparison between measured data and results from FEM analysis for piezometer 3

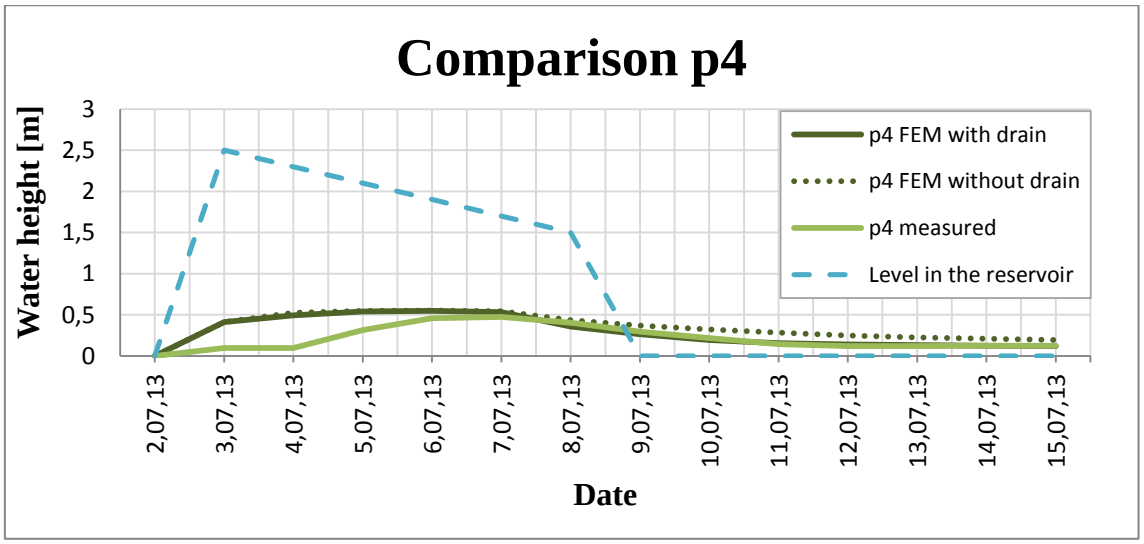

Figure 138: Comparison between measured data and results from FEM analysis for piezometer 4

The results from FEM software are finally similar to the ones got in the field test, but the model is now completely inconsistent if compared to the initial one. It is possible to conclude that the seepage tests, executed on the test dike in Trzcinisko are not convergent with the finite element models created using the mechanical properties of the samples taken from the test dike.

Slope Stability

The results of the first field test are used as input parameters to run the slope stability analysis.

This study is conducted by steps: first the stability of the embankment at empty reservoir is examined, than the stability at fully supplied level. The emptying of the reservoir is analyze as a slow and rapid drawdown in dependence of the speedy of the emptying itself. The aim of this study is to evaluate the change of the safety factor (FS) as the piezometric level in the embankment changes. Since pore water pressures have a dominant influence on the factor of safety of slopes, remedial action should be taken if the factor of safety, based on the measured values, is considered to be too low.

Because of the first piezometer is installed in the dike's upstream slope, it can be used as a watermark on the seepage side: the pore water pressure measured in this piezometer during the first experiment is assumed to represent the level of the water in the reservoir. This simplification is not precisely correct, but the difference in the two water levels is relatively small, so this assumption does not lead to big mistakes in FEM analysis.

The first slope stability analysis conducted in the upstream slope, concerns the critical stage of the embankment at the end of construction, with empty reservoir. For FEM analysis the same model and the same discretization and mesh described previously are employed. The boundary conditions are *Total Head* equal to 0 to simulate the empty reservoir at upstream side, *Pressure Head* on the ground on the opposite side and finally *Total Flux* in downstream side slope.

To find the critical surface with *GeoStudio™ 2007*, I allow every kind of slip surface, in order to establish the critical one also if it was a composite surface. The method used to determine the safety factor is the one proposed by Morgestern and Price (*Morgerstern N. R. and Price V. E.,* 1965).

After running the analysis, a safety factor equal of 4,609 is obtained, which is much major of FS establishes for limit equilibrium, so the slope stability at this stage is ensured.

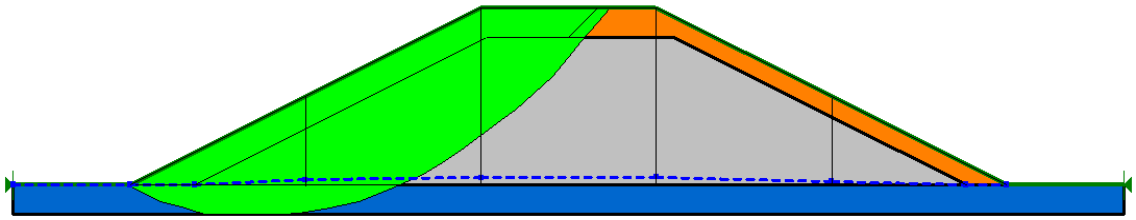

Figure 139: FS= 4.609 for water conditions at 02/07/2013

The second day of the experiment the water level in the reservoir reaches the maximum value (2,265 m), and the analysis at fully supplied water level was conducted. The safety factor obtained is 6,592. It is so big because of the stabilizing effect of the water at the slope surface. With full reservoir, the failure of the embankment does not occur in upstream side: if a failure happens, this is due to internal erosion and breakage of downstream toe caused by pore-water pressures.

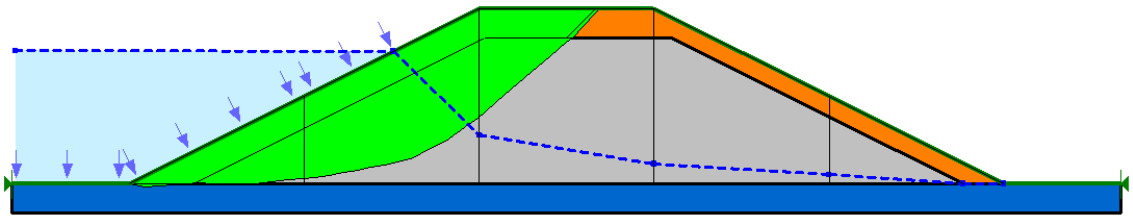

Figure 140: FS= 6.592 for water conditions at 03/07/2013

After reaching the maximum water height in the reservoir, the water table, is slowly falling down through the passing time because water wasn't refilled, and I assume that the water level decreases 0,2 m every day for 5 days.

This is a situation of slow drawdown, in which the reservoir pool is drawn down as fast as the pore water can spillage, so no excessive pore water pressures result. In the slow drawdown situation the water level within the slope is assumed to equalize the reservoir level at any time.

The same model is used to run the FEM analysis, and the safety factor is evaluated using again the Morgerstern and Price method for each day.

The results are shown from Figure 141 to Figure 144 The safety factor decreases as the water level decreases, because of the lack of stabilizing effect of the water on upstream side, and the increase of shear stresses.

Any case, the factor of safety is high enough not to fear slope instability.

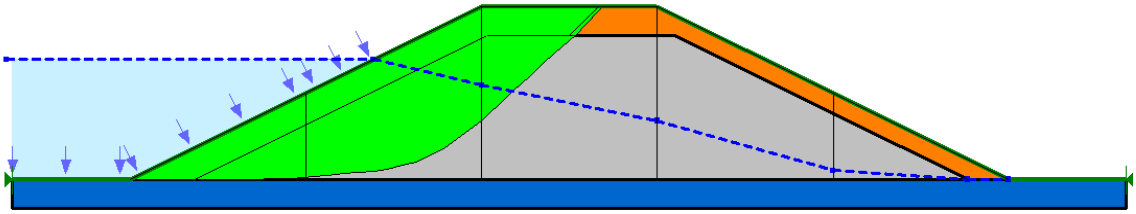

Figure 141: FS= 5.698 for water conditions at 04/07/2013

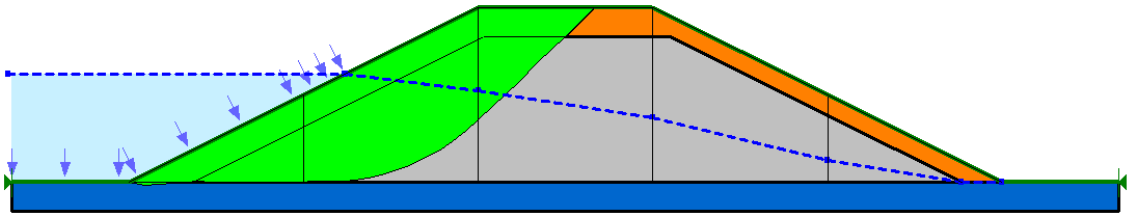

Figure 142: FS= 5.196 for water conditions at 05/07/2013

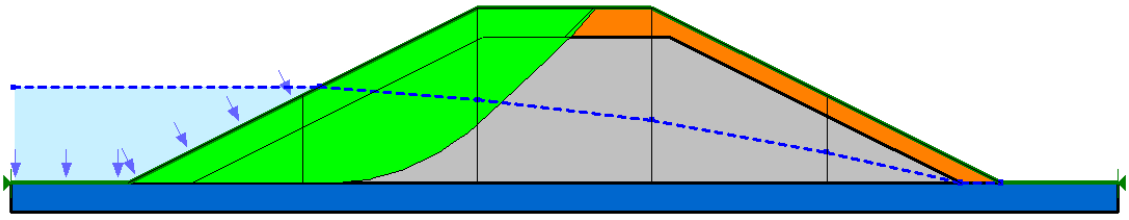

Figure 143: FS= 4.890 for water conditions at 06/07/2013

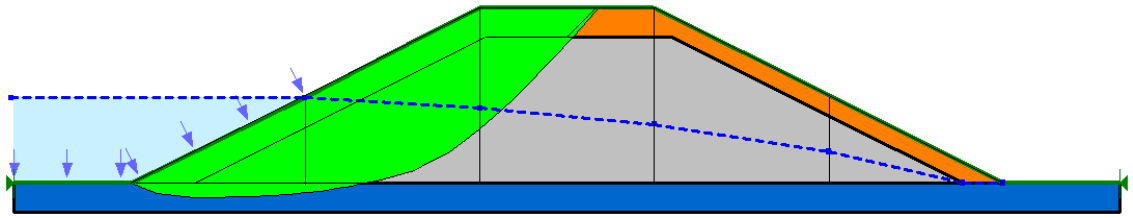

Figure 144: FS=5.169 for water conditions at 07/07/2013

After 5 days from the beginning of the experiment the water is pumped out in few hours (I assumed a 4-hours long pumping out period). The water level adjacent to the slope drops rapidly relative to the time required for water pressures to dissipate in the slope, so excessive pore water pressure has been generated. The total stresses in the slope were reduced, while the shear stresses increased.

Since the rapid drawdown is one of the most dangerous conditions for the upstream slope, it is necessary to study the slope stability of earth fill dams during drawdown.

The FEM analysis with *GeoStudio™ 2007* software was carried out using the same model described before. The level of the water in the reservoir is assumed to pass instantaneously from 1,456 m to 0 m; afterward the trend of the piezometric line is evaluated.

In this case the slope stability was still ensured, but the safety factor reached its minimum value in the analysis (Figure 145).

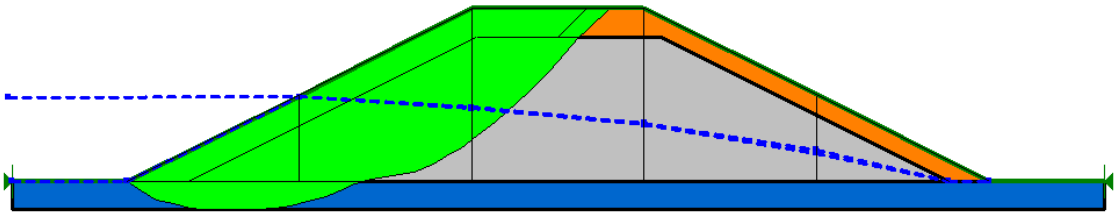

Figure 145: FS=2.243 for water conditions at 08/07/2013 at drawdown

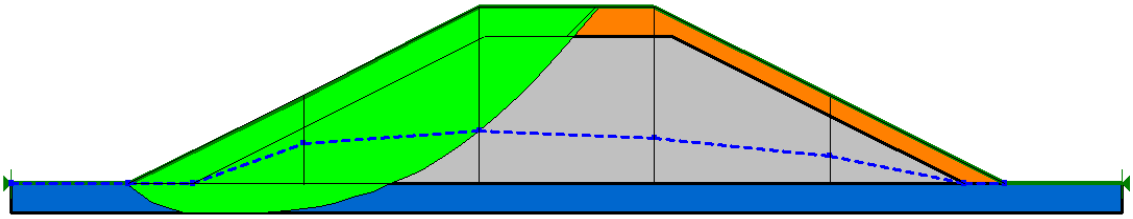

Figure 146: FS=4.247 for water conditions at 08/07/2013 after drawdown

After the rapid drawdown, the level of the water in the embankment decreases slowly, because of the low permeability of the external layer, so another slow drawdown analysis is carried out.

In this condition the safety factors increased again, because this situation did not determine failure in the dike's slope.

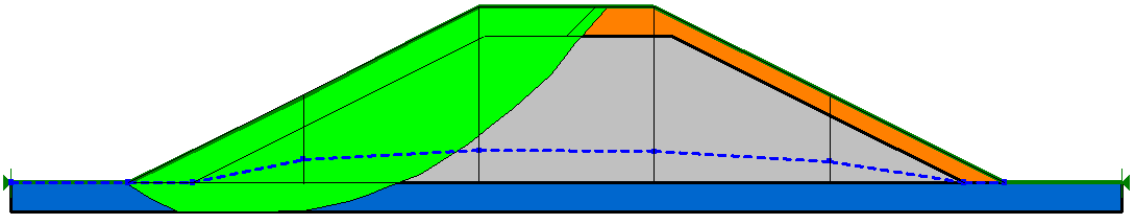

Figure 147: FS= 4.420 for water conditions at 09/07/2013

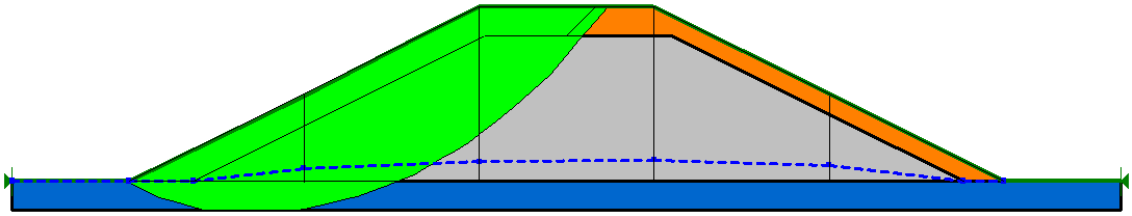

Figure 148: FS= 4.554 for water conditions at 10/07/2013

The Table 29 and the graph below (Figure 149) show factors of safety obtained for each day of the experiment. It increases during filling the reservoir, it decreases during the

emptying of the reservoir, and reaches its minimum during rapid drawdown afterward it increases again once that the pore-water pressures in the embankment is dissipated, reaching a value almost constant after 10 days; therefore, I stopped the analysis at 10th July.

Table 29: FS obtained in the first experiment

Time from experiment start	Date	Water height in the reservoir	FS (Morgerstern-Price)
[h]	[-]	[m]	[-]
-16	2,07,13	0	4,609
8	3,07,13	2,5	6,592
32	4,07,13	2,3	5,698
56	5,07,13	2,1	5,196
80	6,07,13	1,9	4,890
104	7,07,13	1,7	4,850
128	8,07,13	1,5	4,247
128	8,07,13	0	2,243
152	9,07,13	0	4,420
176	10,07,13	0	4,554

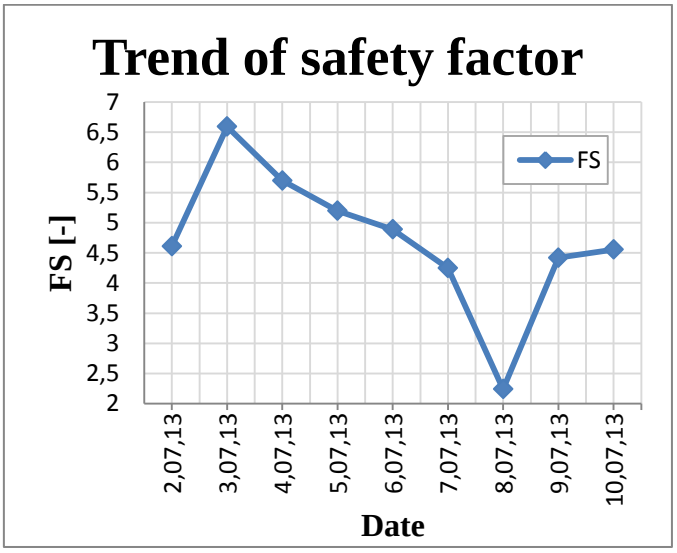

Figure 149: Trend of the safety factor during the first experiment

By using the piezometric line obtained from the first experiment as input data in the slope stability analysis, we obtained FS>2. Although the seepage analysis is not convergent with the results from field test, nevertheless the slope stability is verify.

Conclusion

The material removed from the bottom of lakes, rivers and harbors is called dredged material. Most dredging is done to maintain or deepen navigation channels for the safe passage of boats and ships.

The mouth of Vistula River, is located near Gdansk, in Poland. This river is navigable and the sediments need to be removed, in order to preserve the depth of the estuary for navigation.

Due to the increasing shortage of clay and mild and the negative effect that their extraction from natural deposits causes on the environment, these materials are replaced with coal ashes.

The dredged material excavated from the mouth of Vistula, mixed with bottom ashes, has been reused to build the dike's core in Trzcinisko.

This Master Thesis aim is to model the test dike and to conduce a FEM analysis, in order to evaluate the seepage through the embankment and its global stability. In this way, the possibility of employing the sand-ash mixture in dike's construction is evaluated, comparing the results of the analysis with the values measured during a field test.

The piezometric heights, determined with numerical analyses using the data collected from laboratory tests on soil samples taken from the dike, are different from the measured values. There exist many possible reasons for the divergence between finite element method results and field test values. The principal are collected below.

- The samples can be not representative of the real situation of the humidity conditions in the embankment. The test dike was built in summer 2012, during severe rainfall, so probably the water content in the dike at that moment was higher respect the one found during the experiments (Summer 2013).

- The FEM software assumes a dry soil before the beginning of the test. But, as seen before, it is possible to find different humidity and water content conditions in the levee, depending on meteorology conditions. Since the seepage is strictly influenced from the initial soil water content, the results can be as much different from the expected ones.

- In FEM models, the tephra and sand mixture layer is considered very impervious, so the hydraulic load is dissipated mostly in this layer. In the real situation this effect is not so evident and this material allows the entrance of the water.

- The laboratory data, determined in an external laboratory in Germany, were prepared for 6 suction pressures: (0,3 kPa, 2 kPa, 6 kPa, 13 kPa, 30 kPa, 60 kPa). The number of samples is not enough to describe precisely the retention curve shape at low pressure heads. This fact can lead to imprecise results.

- In winter in the north of Poland, temperature reaches very low vales (-15°C). Due to temperatures below 0 degrees, ice lens may form. This phenomenon can lead to formation of cracks inside the soil's structure and may change the moisture content inside the dike. Unpredicted water flow may be induced by changes in soil structure during winter.

By adopting the results obtained from the first field test, a slope stability analysis is conducted. The FS obtained are major than 2, so the embankment stability is verified.

The research conducted within this thesis indicated that the application of totally new material into common use needs to be done with proper care and sensitivity, because it could show in the reality, a very different behavior compared to the one hypothesized by processing laboratory tests.

Further studies will be necessary to evaluate the changes in the mechanical properties in time, due to the presence of a material with pozzolanic properties.

The number of samples in these analyses must be adequate to describe the water content in different water content conditions, in order to be able to define the water retention a curve and the conductivity function correctly.

If the further analysis will lead to positive results, the employment of dredged materials and fly ashes in the construction of dikes can catch on, with economic and environmental benefits.

Figure index

FIGURE 1: GDANSK, POLAND CLIMATE GRAPH (ALTITUDE 12M)....13
FIGURE 2: DIVISION OF VISTULA BASIN INTO 3 SUBCATCHMENTS (SOURCE IMGW-PIB)....14
FIGURE 3: THE CATCHMENT OF THE LOWER VISTULA....15
FIGURE 4: NATURAL CAUSES OF FLOODS....16
FIGURE 5: TYPICAL EMBANKMENT....17
FIGURE 6: DIFFERENT KINDS OF EMBANKMENT....19
FIGURE 7: DREDGED MATERIAL PUMPED ONTO A SPOIL FIELD....21
FIGURE 8: ROSTOCK DEPOSITION SIDE....22
FIGURE 9: DREDGDIKES PROJECT LOGO....22
FIGURE 10: TEST DIKE LOCALIZATION....24
FIGURE 11: TEST DIKES AND SHEET-PILE WALL....25
FIGURE 12: GEOMETRY....25
FIGURE 13: POSITIONS OF MOISTURE PROBES AND PIEZOMETERS....26
FIGURE 14: GEOMETRY AND THICKNESS OF MATERIALS....27
FIGURE 15: MATERIALS....27
FIGURE 16: GRADING CURVE OF BOTTOM ASH....30
FIGURE 17: FLOWCHART FOR CLASSIFYING COAL ASHES....32
FIGURE 18: GRADING CURVE OF DREDGED MATERIAL (SAND)....34
FIGURE 19: PROCTOR COMPACTION TEST: MAXIMUM DRY DENSITY....35
FIGURE 20: PROCTOR COMPACTION TEST: OPTIMUM WATER CONTENT....36
FIGURE 21: OEDOMETRIC TEST....37
FIGURE 22: DIRECT SHEAR TEST: ANGLE OF INTERNAL FRICTION....38
FIGURE 23: DIRECT SHEAR TEST: COHESION....38
FIGURE 24: SHEAR TEST FOR 70/30 MIXTURE....39
FIGURE 25: OEDOMETRIC TESTS FOR 70/30 MIXTURE....40
FIGURE 26: MOHR'S CIRCLE OF STRESS USED TO DERIVE EQUATIONS FOR MOHR-COULOMB DIAGRAM....42
FIGURE 27: MOHR-COULOMB STRENGTH FUNCTION FOR ASH -SAND MIX....43
FIGURE 28: MODEL FOR GROUNDWATER ANALYSIS ON SLIDE 5:0....46
FIGURE 29: MESH DISCRETIZATION OF THE MODEL....46
FIGURE 30: BOUNDARY CONDITIONS....47

FIGURE 31: GROUNDWATER ANALYSIS: PRESSURE HEAD (A) AND TOTAL HEAD (B) RESULTS. SLOPE 1:2 49
FIGURE 32: DIKE'S SECTION, SHAFFERNAK SCHEMA 50
FIGURE 33: GRADIENT AT DOWNSTREAM SIDE'S TOE 53
FIGURE 34: PORE-WATER PRESSURE AT CORE-EXTERNAL LAYER INTERFACE 54
FIGURE 35: CHANGE OF SLOPES 54
FIGURE 36: CHANGE OF WATER EXIT HEIGHT FOR DIFFERENT SLOPES 55
FIGURE 37: DIFFERENT THICKNESS 56
FIGURE 38: CHANGE OF WATER EXIT HEIGHT FOR DIFFERENT THICKNESSES 57
FIGURE 39: DIFFERENT WATER HEIGHTS FOR DIFFERENT HYDRAULIC CONDUCTIVITY 58
FIGURE 40: COMPARISON OF DIFFERENT HYDRAULIC CONDUCTIVITY 59
FIGURE 41: TOE DRAIN IN THE EMBANKMENT 59
FIGURE 42: MODELING OF THE DRAIN. MESHING AND BOUNDARY CONDITIONS 60
FIGURE 43: GROUNDWATER ANALYSIS WITH TOE-DRAIN 61
FIGURE 44: METHOD OF SLICES 63
FIGURE 45: FREE BODY DIAGRAM AND FORCE POLYGON FOR THE ORDINARY METHOD 65
FIGURE 46: FREE BODY DIAGRAM AND FORCE POLYGON FOR BISHOP'S SIMPLIFIED METHOD 66
FIGURE 47: FREE BODY DIAGRAM AND FORCE POLYGON FOR JANBU'S SIMPLIFIED METHOD 67
FIGURE 48: FREE BODY DIAGRAM AND FORCE POLYGON FOR SPENCER'S METHOD 67
FIGURE 49: FREE BODY DIAGRAM AND FORCE POLYGON FOR MORGENSTERN AND PRICE'S METHOD 68
FIGURE 50: HALF-SINE FUNCTION 68
FIGURE 51: MODEL FOR SLOPE-STABILITY ANALYSIS (SLIDE 5.0) 71
FIGURE 53: SLOPE STABILITY ANALYSIS (SLOPE 1:2) 72
FIGURE 53: QUERY SLICE DATA 73
FIGURE 54: MINIMUM SURFACES (SLOPE 1:2) 73
FIGURE 55: COMPARISON BETWEEN FS 75
FIGURE 56: FS FOR DIFFERENT COHESION VALUES 76
FIGURE 57: FS FOR DIFFERENT ANGLES OF FRICTION 77
FIGURE 58: VOLUMETRIC WATER CONTENT FUNCTION 82
FIGURE 59: VWC FUNCTION 83
FIGURE 60: VWC FOR SAND-ASH MIXTURE 84
FIGURE 61: VWC FOR CLAY 85
FIGURE 62: VWC FOR SAND-TEPHRA MIXTURE 86
FIGURE 63: VWC FOR LOAM 86
FIGURE 64: HYDRAULIC CONDUCTIVITY FUNCTION 88
FIGURE 65: CONDUCTIVITY FUNCTION FOR ASH-SAND MIXTURE 91
FIGURE 66: HYDRAULIC CONDUCTIVITY CURVE FOR SAND-ASH MIXTURE 92

FIGURE 67: HYDRAULIC CONDUCTIVITY CURVE FOR CLAY 92
FIGURE 68: HYDRAULIC CONDUCTIVITY CURVE FOR TEPHRA-SAND MIXTURE 93
FIGURE 69: HYDRAULIC CONDUCTIVITY CURVE FOR LOAM 93
FIGURE 70: COMPARISON BETWEEN HYDRAULIC CONDUCTIVITY OF DIFFERENT MATERIALS 94
FIGURE 71: RESULTS OF STEADY-STATE ANALYSIS (10 CM) 95
FIGURE 72: HYDRAULIC BOUNDARY FUNCTION. FILL OF THE RESERVOIR 96
FIGURE 73: WATER TABLE AFTER 24 HOURS (FILLED RESERVOIR) 97
FIGURE 74: WATER TABLE AFTER 14 DAYS (FILLED RESERVOIR) 97
FIGURE 75: WATER TABLE AFTER 20 DAYS: PHREATIC SURFACE AT DOWNSTREAM SIDE 98
FIGURE 76: WATER HEIGHT AFTER 50 DAYS 98
FIGURE 77: EXTERNAL LAYER MADE UP WITH CLAY 100
FIGURE 78: DIFFERENT IMPERVIOUS MATERIAL'S CONDUCTIVITY FUNCTION 101
FIGURE 79: TRANSIENT ANALYSIS WITH A DRAIN 102
FIGURE 80: HYDRAULIC BOUNDARY FUNCTION. DRAWDOWN AFTER 7 DAYS 103
FIGURE 81: WETTING UP AND DOWN. FIRST MONITORING PLAN 104
FIGURE 82: COMPARISON BETWEEN FUNCTION OF FIRST AND SECOND MONITORING PLAN 105
FIGURE 83: WETTING UP AND DOWN. SECOND MONITORING PLAN 106
FIGURE 84: GDANSK, POLAND CLIMATE GRAPH (ALTITUDE 12M) 107
FIGURE 85: WATER LEVEL IN THE EMBANKMENT AFTER 24 HOURS OF RAINFALL 108
FIGURE 86: PIEZOMETRIC LEVEL AFTER FILLING THE RESERVOIR 109
FIGURE 87: PIEZOMETRIC LEVEL DURING BOTH RAINFALL AND FILLING OF THE RESERVOIR 111
FIGURE 88: WATER LEVEL AFTER 7 DAYS 112
FIGURE 89: STRESS CONDITIONS RESULTING FROM RAPID DRAWDOWN 113
FIGURE 90: INITIAL CONDITIONS DERIVED FROM STEADY STATE ANALYSIS 114
FIGURE 91: HYDRAULIC BOUNDARY FUNCTION FOR SLOW DRAWDOWN 115
FIGURE 92: SLOW DRAWDOWN DURING EMPTYING OF THE RESERVOIR 117
FIGURE 93: PHREATIC SURFACE AFTER 40 DAYS (30 DAYS OF EMPTY RESERVOIR) 118
FIGURE 95: FS=7,264 AT STEADY STATE CONDITIONS 119
FIGURE 95: FS= 6,781AFTER 10 HOURS 121
FIGURE 96: FS=6,341 AFTER 24 HOURS 121
FIGURE 97: FS= 5,735 AFTER 2 DAYS 122
FIGURE 98: FS=4,862 AFTER 3 DAYS 122
FIGURE 99: FS= 4,676AFTER 5 DAYS 123
FIGURE 100: FS=4,194 AFTER 8 DAYS 123
FIGURE 101: FS= 4,267 AFTER 10 DAYS 124
FIGURE 102: FS=4,441 AFTER 20 DAYS 124

FIGURE 103: FS= 4,441AFTER 30 DAYS....125
FIGURE 104: FS=4,446 AFTER 40 DAYS....125
FIGURE 105: TREND OF FS DURING THE EMPTYING OF THE RESERVOIR IN SLOW DRAWDOWN....127
FIGURE 106: HYDRAULIC BOUNDARY FUNCTION FOR RAPID DRAWDOWN....128
FIGURE 107: RAPID DRAWDOWN DURING EMPTYING OF THE RESERVOIR....129
FIGURE 108: PIEZOMETRIC LINE AFTER 40 DAYS....129
FIGURE 109: FS=5.051 AFTER 1 HOUR....131
FIGURE 110: FS= 4.511 AFTER 2 HOURS....131
FIGURE 111: FS= 4.050 AFTER 3 HOURS....132
FIGURE 112: FS= 4.685 AFTER 4 HOURS....132
FIGURE 113: TREND OF FS DURING RAPID DRAWDOWN....134
FIGURE 114: PROFILE USED AND ASSUMED PIEZOMETRIC LINE AFTER INSTANTANEOUS DRAWDOWN....135
FIGURE 115: CRITICAL SLIP SURFACE AND FS=2,048 AFTER INSTANTANEOUS DRAWDOWN....135
FIGURE 116: SEEPAGE FLOW 1 HOUR AFTER RAPID DRAWDOWN....136
FIGURE 117: SEEPAGE FLOW AFTER ONE DAY....136
FIGURE 118: SEEPAGE FLOW AFTER 20 DAYS....136
FIGURE 119: TREND OF FS DURING INSTANTANEOUS DRAWDOWN....137
FIGURE 120: HEIGHT IN THE RESERVOIR FOR BOTH THE SIMULATIONS....139
FIGURE 121: COMPARISON BETWEEN PLAXIS® (A), SLIDE® (B), GEOSTUDIO™ (C) MODELS AFTER 5 DAYS OF FILLING OF THE RESERVOIR....140
FIGURE 122: COMPARISON BETWEEN PLAXIS® (A), SLIDE® (B), GEOSTUDIO™ (C) MODELS AFTER 7 DAYS OF FULL RESERVOIR....141
FIGURE 123: COMPARISON BETWEEN PLAXIS® (A), SLIDE® (B), GEOSTUDIO™ (C) MODELS AFTER DRAWDOWN....142
FIGURE 124: PASCAL'S LAW SCHEMA....144
FIGURE 125: HEAD VS TIME FUNCTION....145
FIGURE 126: TREND OF THE SATURATION LEVEL OF THE PIEZOMETERS FOR FIRST EXPERIMENT....146
FIGURE 127: TREND OF THE SATURATION LEVEL OF THE PIEZOMETERS FOR SECOND EXPERIMENT....148
FIGURE 128: DIFFERENT SATURATION CONDITIONS FOR PIEZOMETER P4....149
FIGURE 129: TREND OF THE CORRECTED WATER LEVEL IN THE PIEZOMETERS....150
FIGURE 130: MODEL FOR PIEZOMETRIC ANALYSIS....151
FIGURE 131: TREND OF WATER IN PIEZOMETERS FROM ANALYSIS WITH GEOSTUDIO™ 2007....152
FIGURE 132: TREND OF WATER IN PIEZOMETERS FROM MODIFIED ANALYSIS WITH GEOSTUDIO™ 2007....154
FIGURE 133: INSERTION OF DRAIN....155
FIGURE 134: TREND OF WATER IN PIEZOMETERS FROM MODIFIED ANALYSIS WITH DRAIN WITH GEOSTUDIO™ 2007....156
FIGURE 135: COMPARISON BETWEEN MEASURED DATA AND RESULTS FROM FEM ANALYSIS FOR PIEZOMETER 1....157
FIGURE 136: COMPARISON BETWEEN MEASURED DATA AND RESULTS FROM FEM ANALYSIS FOR PIEZOMETER 2....157

FIGURE 137: COMPARISON BETWEEN MEASURED DATA AND RESULTS FROM FEM ANALYSIS FOR PIEZOMETER 3 158
FIGURE 138: COMPARISON BETWEEN MEASURED DATA AND RESULTS FROM FEM ANALYSIS FOR PIEZOMETER 4 158
FIGURE 139: FS= 4.609 FOR WATER CONDITIONS AT 02/07/2013 160
FIGURE 140: FS= 6.592 FOR WATER CONDITIONS AT 03/07/2013 160
FIGURE 141: FS= 5.698 FOR WATER CONDITIONS AT 04/07/2013 161
FIGURE 142: FS= 5.196 FOR WATER CONDITIONS AT 05/07/2013 161
FIGURE 143: FS= 4.890 FOR WATER CONDITIONS AT 06/07/2013 161
FIGURE 144: FS=5.169 FOR WATER CONDITIONS AT 07/07/2013 162
FIGURE 145: FS=2.243 FOR WATER CONDITIONS AT 08/07/2013 AT DRAWDOWN 162
FIGURE 146: FS=4.247 FOR WATER CONDITIONS AT 08/07/2013 AFTER DRAWDOWN 163
FIGURE 147: FS= 4.420 FOR WATER CONDITIONS AT 09/07/2013 163
FIGURE 148: FS= 4.554 FOR WATER CONDITIONS AT 10/07/2013 163
FIGURE 149: TREND OF THE SAFETY FACTOR DURING THE FIRST EXPERIMENT 165

Table Index

TABLE 1: ENVIRONMENTAL AVERAGE PARAMETERS IN GDANSK 12
TABLE 2: CHEMICAL COMPOSITION OF COAL ASHES AND SOILS 29
TABLE 3: COAL ASH CLASSIFICATION SYSTEM 33
TABLE 4: BENEFICIAL ENGINEERING PROPERTIES OF COAL ASHES 34
TABLE 5: PROPERTIES OF THE MATERIALS 41
TABLE 6: WATER EXIT HEIGHTS FOR DIFFERENT SLOPES 55
TABLE 7: WATER EXIT HEIGHTS FOR DIFFERENT THICKNESSES 56
TABLE 8: WATER LEVELS FOR DIFFERENT RIVERSIDE MATERIAL 57
TABLE 9: WATER LEVELS FOR DIFFERENT CORE'S MATERIAL 58
TABLE 10: SATISFIED EQUATION OF STATIC 70
TABLE 11: INTERSLICE FORCE CHARACTERISTICS AND RELATIONSHIPS 70
TABLE 12: FS FROM DIFFERENT METHODS (SLOPE 1:2) 71
TABLE 13: FS FROM DIFFERENT METHODS AND SLOPES 74
TABLE 14: FS FOR DIFFERENT MATERIALS 74
TABLE 15: FS FOR DIFFERENT COHESION 76
TABLE 16: FS FOR DIFFERENT FRICTION ANGLE 76
TABLE 17: VOLUMETRIC WATER CONTENT FOR DIFFERENT WATER PRESSURE 83
TABLE 18: FITTED PARAMETERS 90
TABLE 19: CALCULATED RELATIVE PERMEABILITY OF THE SOIL 91
TABLE 20: TREND OF FS IN SLOW DRAWDOWN ANALYSIS 126
TABLE 21: TREND OF FS IN RAPID DRAWDOWN ANALYSIS 133
TABLE 22: TREND OF FS IN INSTANTANEOUS DRAWDOWN ANALYSIS 137
TABLE 23: MEASURED WATER HEIGHTS IN PIEZOMETERS FOR THE FIRST EXPERIMENT 146
TABLE 24: MEASURED WATER HEIGHTS IN PIEZOMETERS FOR THE SECOND EXPERIMENT 147
TABLE 25: COLLECTED MEASURED WATER HEIGHTS IN PIEZOMETERS FOR THE FIRST EXPERIMENT 150
TABLE 26: WATER HEIGHTS IN PIEZOMETERS FROM GEOSTUDIO™ ANALYSIS FOR THE FIRST EXPERIMENT 152
TABLE 27: RESULTS OF THE ANALYSIS WITH MODIFIED KS 154
TABLE 28: RESULTS OF THE ANALYSIS WITH MODIFIED KS AND DRAIN 156
TABLE 29: FS OBTAINED IN THE FIRST EXPERIMENT 164

References

Bałachowski L., Sikora Z., (2013). *Ash-dredged material mixtures - application in dike construction.* Lulea University of Technology, Department of Geotechnics, Geology and Maritime Engineering Gdańsk University of Technology (PL).

Bishop, A. W. (1955). *The use of the slip circle in the stability analysis of slopes.* Geotechnique, 5,pp.7-17.

Brooks R.H. and Corey A.T., (1964). *Hydraulic Properties of Porous Media*. Hydrology Papers, No. 3, Colorado State U., Fort Collins, Colorado

Burdine, N.T., (1953). *Relative permeability calculations from pore-size distribution data.* Petr. Trans., Amer. Inst. Mining Metall. Eng. 198: 71-77.

Casagrande, R. C. Hirschfeld, S. J. Poulos (2007). *Embankment dam engineering*. Ia University of Michigan, Wiley, 1973

Casagrande A. (1937). *Seepage through dams.* J. New England Water Works, 51, pp 295-336.

Corey, J.C., (195)7. *Measurement of Water and Air Permeability in Unsaturated Soil.* Soil Science of America, Vol. 21.

Duncan, J.M.,Wright S.G. and Wong, K.S.(1990). *Slope Stability during Rapid Drawdown*. Proceedings of H. Bolton Seed Memorial Symposium. Vol. 2.

Fellenius W. (1936). *Calculation of the stability of earth dams*. Proceedings of the Second Congress on Large Dams, 4, pp.445-at 463.

D. G. Fredlund and J. Krahn (1977*).* *Comparison of slope stability methods of analysis*. University of Saskatchewan, Saskatoon, Sask., Canada 57N 0W0

Fredlund M., Lu H.H., Feng T.n, (2011). *Combined Seepage and Slope Stability Analysis of Rapid Drawdown Scenarios for Levee Design*. Geo-Frontiers Congress, Dallas, Texas, United States, March 13-16, 2011.

Fredlund, D. G. (l974). *Slope stability analysis.* User's Manual CD-4, Department of Civil Engineering, University of Saskatchewan, Saskatoon, Sask.

Freeze R.A., Cherry J.A., (1979). *Groundwater*. Prentice Hall, Englewood Cliffs, N.J.

GEO-SLOPE International Ltd (2008). *Seepage Modeling with SEEP/W 2007. An Engineering Methodology*. GEO-SLOPE International Ltd 1400, 633 – 6th Ave SW Calgary, Alberta, Canada T2P 2Y5.

GEO-SLOPE International Ltd (2008). *Stability Modeling with SLOPE/W 2007 Version. An Engineering Methodology*.GEO-SLOPE International Ltd 1400, 633 – 6th Ave SW Calgary, Alberta, Canada T2P 2Y5.

Green, R.E. and Corey, J.C., (197)1. *Calculation of Hydraulic Conductivity: A Further Evaluation of Some Predictive Methods*. Soil Science Society of America Proceedings, Vol. 35, pp. 3-8.

Hutchison W.R. (1983) *Earth Dam Seepage Analysis with a Programmable Calculator.* A Thesis Submitted to the Faculty of the Department of Hydrology and Water Resources For the Degree of Master of Science with a Major in Hydrology In the Graduate College The University of Arizona.

Janbu N., Bjerrum L, and Kjaernsli B. (1956). *Stabilitetsberegning for fyllinger skjaeringer og naturlige skraninger*. Norwegian Geotechnical Publication No.16, Oslo, Norway

Kenneth Gavin, Jianfeng Xue (2007). *A simple method to analyze infiltration into unsaturated soil slopes.* School of Architecture, Landscape and Civil Engineering, Earlsfort Terrace, University College Dublin, Dublin 2, Ireland

Krahn J., Price , V. E., and Morgerstern N. R. (1971). *Slope stability computer program for Morgenstern-Price method of analysis*. User's Manual No. 14, University of Alberta. Edmonton, Alta.

Lambe, T.W. and Whitman, R.V.,(1969). *Soil Mechanics.* John Wiley and Sons, pp. 359-365.

Majewski W. (2013). *Sustainable development of the Lower Vistula*. Institute of Meteorology and Water Management, National Research Institute, Podleśna Street 61, 01-673 Warszawa.

Milton E. Harr (1962). *Groundwater and Seepage.* Mc Graw-Hill.

Morgerstern N. R. and Price V. E. (1965). *The analysis of the stability of general slip surfaces.* Geotechnique,15, pp. 70-93.

Mualem, Y., (1976). *A new model for predicting the hydraulic conductivity of unsaturated porous media.* Water Resour. Res. 12: 513–522.

Nga C. W. W., Shi Q. (1997) *A Numerical Investigation of the Stability of Unsaturated Soil Slopes Subjected to Transient Seepage.* Department of Civil & Structural Engineering, the Hong Kong University of Science & Technology,Clear Water Bay, Kowloon, Hong KongbArup Geotechnics (Hong Kong), 56/F, Hopewell Centre, 183 Queen's Road East, Hong Kong

Prakash K., Sridharan A. (2004-2005). *A geotechnical classification system for coal ashes.* Proceedings of the Institution of Civil Engineers Geotechnical Engineering 159 April 2006 Issue GE2 Pages 91–98 Paper 13943

Rocscience, 'Slide 5.0 manual'

Sharma V.K., Priya T. Disaster Prevention and Management. *ISSN: 0965-3562*

Siddappa Gopi and. Shanthakumar M.C (2014). *International Conference on Geological and Civil Engineering.* P E S College of Engineering, Mandya IPCBEE vol.62 (2014) © (2014) IACSIT Press, Singapore DOI: 10.7763/IPCBEE. 2014. V62. 12

Sinha B.N. (2008). *Advance Methods of Slope-Stability Analysis for Earth Embankment with Seismic and Water Forces*. General Manager, Intercontinental Consultants & Technocrats Pvt. Ltd.**,** A-8, Green Park, New Delhi, India.

GEO-SLOPE International Ltd *SLOPE/W Example File: Rapid Drawdown with Effective Stress*. GEO-SLOPE International Ltd, Calgary, Alberta, Canada

Spercer E. (1967). *A method of analysis of the stability of embankments assuming parallel interslice forces.* Geotechnique, 17, pp. ll-26

Swanson, D. (199)1. *The Effects of Loading on the Moisture Characteristic and Permeability-Suction Relationships for Unsaturated Soils. B.Sc.* Thesis, Department of Civil Engineering, University of Saskatchewan, Saskatoon, Canada.

Timothy D. Stark T.D., Navid Jafari S.M., Leopold A.(2012). *Effect of Soil Compressibility on Transient Seepage Analyses.* ASCE Journal of Geotechnical and

Geoenvironmental Engineering.

Tomczak K. (2013). *Groundwater flow through the test dike constructed with dredged materials.* Inzynierii Ladowej I Srodowiska, Gdansk.

Tran X. Tho (2004). *Stability problems of an earthfill dam in rapid drawdown condition.*

Tran X. Tho (2001-2004). *Stability problems of earthfill dams*. Doctoral Dissertation, Slovak University of Technology, Bratislava, Slovak Republic, (in progress).

US Army Corps of Engineers (2003). *Appendix G - Procedures and Examples for Rapid Drawdown*. Engineering Manual, EM1110-2-1902. Department of the U.S Army Corps of Engineers. Washington (DC).

US Army Corps of Engineers, (2003). *Engineering and design manual- slope stability*, Engineer Manual EM 1110-2-1902, Department of the Army, Corps of Engineers, Washington (DC).

US Army Corps of Engineers, (2003). *Engineering and design manual - General design and considerations for earth and rock-fill dams*, EM 110-2-2300, Department of the Army, Corps of Engineers, Washington (DC).

USACE (2003). *Slope Stability*, EM 1110-2-1902, Washington, DC

VandenBerge Daniel R., P.E., S.M.A.S.C.E. (2012). *Application of Finite Element Method to Rapid Drawdown Analysis.* Geotechnical Engineering Program, Charles E. Via Jr. Department of Civil & Environmental Engineering

Van Genuchten M.Th., (1980). *A Closed-form Equation for Predicting the Hydraulic Conuctivity of Unsaturated Soil.* October, Madison, USA Reprinted by Soil Science Society of America Journal, vol. 44.

Van Genuchten M.Th., Leij F.J., Yates S.R. (1991). *The RETC Code for Quantifying the Hydraulic Functions of Unsaturated Soils.* U.S. Salinity Laboratory, U.S. Department of Agriculture, Agricultural Research Service Riverside, California 9250

S. M. Ali Zomorodian, S. Mehdi Abodollahzadeh (2010). *Effect of Horizontal Drains on Upstream Slope Stability During Rapid Drawdown Condition.* Shiraz University, Shiraz, Iran. International Journal of Geology

http://downloads.geoslope.com/geostudioresources/2007/examples/Rapid%20drawdown%20with%20effective%20stress.pdf

http://environment.uwe.ac.uk/geocal/SoilMech/classification/soilclas.htm

http://www.epa.gov/region02/water/dredge/

http://www.epa.gov/region02/water/dredge/intro.htm#Regulatory%20Responsibilities%20and%20Authorities

http://eprints.utm.my/8451/1/8451.pdf

http://www.fce.vutbr.cz/veda/dk2004texty/pdf/02_Konstrukce%20a%20pozemni%20stavby/2_06_Geotechnika/Tho_X_Tran.pdf

http://www.gdansk.climatemps.com/

http://www.imgw.pl/index.php?option=com_content&view=article&id=147&Itemid=180&lang=en

http://www.mhwm.pl/

http://www.pogodynka.pl/

http://www.soilvision.com/downloads/docs/pdf/research/Vietnam.pdf

http://volcanoes.usgs.gov/hazards/tephra/

http://www.zb.eco.pl/gb/24/flood.htm